Title

Mechanistic Insights and Therapeutic Approaches for Plakophilin-2 Driven Arrhythmogenic Right Ventricular Cardiomyopathy

Author

Bradford, William Henry

Publication Date

2021

Peer reviewed|Thesis/dissertation

UNIVERSITY OF CALIFORNIA SAN DIEGO

Mechanistic Insights and Therapeutic Approaches for Plakophilin-2 Driven Arrhythmogenic Right Ventricular Cardiomyopathy

A dissertation submitted in partial satisfaction of the requirements for the degree Doctor of Philosophy

in

Biomedical Sciences

by

William Bradford

Committee in charge:

Professor Farah Sheikh, Chair
Professor Ju Chen
Professor Sylvia Evans
Professor Robert Ross
Professor Gene Yeo

2021

The dissertation of William Bradford is approved, and it is acceptable in quality and form for publication on microfilm and electronically.

University of California San Diego

2021

DEDICATION

To my wife Haley, who has been a constant source of love, encouragement, and support. She has provided invaluable reminders to enjoy life amidst the challenges of this journey. To my parents Robert and Ann, and my sister Allee who have always encouraged me to pursue my passion and taught me the value in working to help others. To my amazing friends and community, who have provided unwavering friendship filled with lots of laughs. None of this would be possible without these people.

TABLE OF CONTENTS

LIST OF ABBREVIATIONS

AAV	Adeno-associated virus
ALP	Alkaline phosphatase
ALT	Alanine aminotransferase
ANF	Atrial natriuretic factor
ANOVA	Analysis of variance
ARVC	Arrhythmogenic Right Ventricular Cardiomyopathy
BGH-pA	Bovine growth hormone polyadenylation
BNP	B-type natriuretic factor
BW	Body weight
CM	Cardiomyocyte
CMV	Cytomegalovirus
Col1a1	Collagen type 1 alpha 1
Col3a1	Collagen type 3 alpha 1
CRISPR	Clustered regularly interspaced short palindromic repeats
crRNA	CRISPR RNA
CSN6	Constitutive photomorphogenesis 9 signalosome subunit 6
cTnT	Cardiac troponin T
Ctrl	Wild-type control
CX43	Connexin 43
DES	Desmin
DSC2	Desmocollin-2
DSG2	Desmoglein-2

DSP	Desmoplakin
ECG	Electrocardiogram
EDV	End diastolic volume
EF	Ejection fraction
ESV	End systolic volume
GAPDH	Glyceraldehyde 3-phosphate dehydrogenase
GC	Genome copy
GFP	Green fluorescent protein
gnomAD	Genome aggregation database
GOF	Gain of function
HW	Heart weight
ICD	Implantable cardioverter-defibrillator
iPSC	Induced pluripotent stem cell
JUP	Plakoglobin
KCl	Potassium chloride
KO	Knockout
LOF	Loss of function
LV	Left ventricle
MOI	Multiplicity of infection
MRI	Magnetic resonance imaging
mRNA	Messenger RNA
MUT	Mutant

Nav1.5	Pore forming alpha subunit of cardiac voltage-dependent Na^+ channel
N-Cad	N-Cadherin
P1	Postnatal day 1
PBS	Phosphate-buffered saline
PLN	Phospholamban
PKP2	Plakophilin-2
PKP2 Het	PKP2 heterozygous mutant mouse
PKP2 Hom	PKP2 homozygous mutant mouse
PTC	Premature termination codon
PVC	Premature ventricular contraction
qRT-PCR	Quantitative reverse transcriptase-polymerase chain reaction
RF	Radiofrequency
RT-PCR	Reverse transcriptase-polymerase chain reaction
RV	Right ventricle
SAX	Short axis
SCD	Sudden cardiac death
sgRNA	Single guide RNA
SMA	Spinal muscular atrophy
SMN1	Survival motor neuron 1
snRNP	Small nuclear ribonucleoprotein
ssODN	Single strand oligodeoxynucleotide
TE	Echo time
TEM	Transmission electron microscopy

TR	Repetition time
WPRE	Woodchuck hepatitis virus posttranscriptional regulatory element
WT	Wild-type
ZO-1	Zonula occludens-1

LIST OF TABLES AND FIGURES

ACKNOWLEDGEMENTS

I would like to thank my mentor Dr. Farah Sheikh for being an amazing role model in driving innovative and translational research. Every day I show up to lab I believe we are working towards advancing science to help patients with a devastating genetic disease. I am incredibly appreciative of the trust and independence I received to pursue the research I will present in my dissertation. I would also like to acknowledge past and current lab members that provided friendship and support: Dr. Yan Liang, Dr. Jing Zhang, Dr. Jie Wang, Dr. Kyohei Fujita, Nirsoh Mataraarachchi, and Aryanne Do. I would like to additionally thank collaborators on this project including Dr. Stephan Lange, Nancy Dalton, Yusu Gu, and Dr. Kirk L. Peterson.

Chapters 3-5 in part are currently being prepared for submission for publication of this material. Bradford, William H; Liang, Yan; Mataraarachchi, Nirosh; Zhang, Jing; Do, Aryanne; Gu, Yusu; Scheinman, Melvin; Peterson, Kirk L; Sheikh, Farah. The dissertation author was the primary investigator and author of this material.

VITA

2013 Bachelor of Sciences, University of California Berkeley

2013-2016 Research Assistant, University of California San Diego

2021 Doctor of Philosophy, University of California San Diego

PUBLICATIONS

Zhang J*, Liang Y*, **Bradford WH***, Sheikh F. Desmosomes: emerging pathways and non-canonical functions in cardiac arrhythmias and disease. Biophys Rev. 2021. In press. **(*Co-first author)**

Liang Y, Lyon RC, Pellman J, **Bradford WH**, Lange S, Bogomolovas J, Dalton ND, Gu Y, Bobar M, Lee MH, Iwakuma T, Nigam V, Asimaki A, Scheinman M, Peterson KL, Sheikh F. Desmosomal COP9 regulates proteome degradation in arrhythmogenic right ventricular dysplasia/cardiomyopathy. J Clin Invest. 2021; 137689. PMID: 33857019

Yeang C, Hasanally D, Que X, Hung MY, Stamenkovic A, Chan D, Chaudhary R, Margulets V, Edel AL, Hoshijima M, Gu Y, **Bradford W**, Dalton N, Miu P, Cheung DY, Jassal DS, Pierce GN, Peterson KL, Kirshenbaum LA, Witztum JL, Tsimikas S, Ravandi A. Reduction of myocardial ischaemia-reperfusion injury by inactivating oxidized phospholipids. Cardiovasc Res. 2019; 115(1):179-189. PMID: 29850765

Liang Y*****, **Bradford WH***, Zhang J*, Sheikh F. Four and a half LIM domain protein signaling and cardiomyopathy. Biophys Rev. 2018; 10(4):1073-85. **(*Co-first author)** PMID: 29926425

Stroud MJ, Fang X, Zhang J, Guimaraes-Camboa N, Veevers J, Dalton ND, Gu Y, **Bradford WH**, Peterson KL, Evans SM, Gerace L, Chen J. Luma is not essential for murine cardiac development and function. Cardiovasc Res. 2018; 114(3):378-88. PMID: 29040414

Bradford WH, Omens JH, Sheikh F. Vinculin at the heart of aging. Ann Transl Med. 2017; 5(3):62. PMID: 28251141

Hashem SI, Murphy AN, Divakaruni AS, Klos ML, Nelson BC, Gault EC, Rowland TJ, Perry CN, Gu Y, Dalton ND, **Bradford WH**, Devaney EJ, Peterson KL, Jones KL, Taylor MRG, Chen J, Chi NC, Adler ED. Impaired mitophagy facilitates mitochondrial damage in Danon disease. J Mol Cell Cardiol. 2017; 108:86-94. PMID: 28526246

Zhang Z, Mu Y, Veevers J, Peter AK, Manso AM, **Bradford WH**, Dalton ND, Peterson KL, Knowlton KU, Ross RS, Zhou X, Chen J. Postnatal Loss of Kindlin-2 Leads to Progressive Heart Failure. Circ Heart Fail. 2016; 9(8). PMID: 27502369

Peter AK*, **Bradford WH***, Dalton ND, Gu Y, Chao CJ, Peterson KL, Knowlton KU. Increased Echogenicity and Radiodense Foci on Echocardiogram and MicroCT in Murine Myocarditis. PLoS One. 2016; 11(8): e0159971. **(*Co-first author)** PMID: 27486657

Lao DH, Esparza MC, Bremner SN, Banerjee I, Zhang J, Veevers J, **Bradford WH**, Gu Y, Dalton ND, Knowlton KU, Peterson KL, Lieber RL, Chen J. Lmo7 is dispensable for skeletal muscle and cardiac function. Am J Physiol Cell Physiol. 2015;309(7):C470-9. PMID: 26157009

Zhang Z, Stroud MJ, Zhang J, Fang X, Ouyang K, Kimura K, Mu Y, Dalton ND, Gu Y, **Bradford WH**, Peterson KL, Cheng H, Zhou X, Chen J. Normalization of Naxos plakoglobin levels restores cardiac function in mice. J Clin Invest. 2015; 125(4):1708-12. PMID: 25705887

ABSTRACT OF THE DISSERTATION

Mechanistic Insights and Therapeutic Approaches for Plakophilin-2 Driven Arrhythmogenic Right Ventricular Cardiomyopathy

by

William Bradford

Doctor of Philosophy in Biomedical Sciences

University of California San Diego, 2021

Professor Farah Sheikh, Chair

Arrhythmogenic right ventricular cardiomyopathy (ARVC) is a fatal genetic cardiac disease with no available treatments. ARVC is termed a “disease of the desmosome” as 30-60% of ARVC mutations occur in genes of the desmosome, which is a critical cell-cell adhesion structure. The desmosomal component plakophilin-2 (PKP2) is the most frequently mutated gene causal for ARVC and studies highlight altered RNA splicing as a mechanism through which PKP2 patient genetics may drive ARVC. Additional work shows one third of human disease-causing mutations are a result of defects in RNA splicing, highlighting the importance

of testing the contribution of this mechanism in ARVC. However, limited models and mechanistic insights exist into how RNA splicing mutations drive ARVC pathogenesis.

I have defined disease mechanisms and developed therapeutic approaches for a novel mouse model harboring a PKP2 splice acceptor site mutation (PKP2 IVS10-1 G>C) found in multiple ARVC populations. My work highlighted the sufficiency of this mutation to trigger all classic ARVC disease features including sudden death, ventricular arrhythmias, biventricular dysfunction, and fibro-fatty replacement in PKP2 homozygous mutant (PKP2 Hom) mice. PKP2 Hom mice displayed an early disruption of the desmosome, which extended to the gap junction at the onset of disease features, highlighting a progressive breakdown of the cardiac intercalated disc in disease. RNA analysis in PKP2 Hom hearts revealed an aberrantly spliced mutant transcript and significantly reduced RNA levels, which was translated into a higher molecular weight mutant PKP2 protein at reduced levels in the absence of endogenous PKP2. *In vitro* mechanistic studies increasing wild-type or mutant PKP2 protein improved desmosomal components, suggesting PKP2 protein dose drives ARVC pathogenesis. Early *in vivo* restoration of PKP2 with an adeno-associated virus (AAV9 PKP2) was sufficient to prevent intercalated disc dissolution, which provided durable preservation of cardiac function and prevented mortality in PKP2 Hom mice. Late-stage AAV9 PKP2 treatment could similarly reassemble desmosomal proteins, while also improving cardiac mechanical function to avert PKP2 Hom mouse mortality. My studies demonstrate the sufficiency of RNA

splicing mutations to drive ARVC and provide critical mechanistic insights into disease pathogenesis, which informed the rational design of ARVC therapeutics.

Chapter 1

Introduction

1.1 Arrhythmogenic Right Ventricular Cardiomyopathy (ARVC)

1.1.1 ARVC clinical features

Arrhythmogenic right ventricular cardiomyopathy (ARVC) is an untreatable genetic-based heart disease, which was first characterized as a right ventricular cardiomyopathy; however, increasing evidence highlights left-dominant and biventricular forms of ARVC as well (Sen-Chowdhry, Morgan et al. 2010, Wang, James et al. 2019, Mattesi, Zorzi et al. 2020). The factors that drive right versus left ventricular disease selectivity remain unclear; however, one hypothesis may be linked to increased wall stress in the right versus left ventricle during physical activity (Wang, James et al. 2019). ARVC patients are classically characterized by early electrical defects that may occur in the absence of morphological disease, with a high frequency of ventricular arrhythmias, which can be exacerbated with exercise leading to sudden cardiac death (SCD) (Sen-Chowdhry, Morgan et al. 2010, Wang, James et al. 2019, Mattesi, Zorzi et al. 2020). However, structural defects are equally important as ARVC progresses from an electrical phase to a structural phase where ARVC hearts are characterized by fibro-fatty replacement of the myocardium, which leads to extensive ventricular dysfunction and failure (Sen-Chowdhry, Morgan et al. 2010, Wang, James et al. 2019, Mattesi, Zorzi et al. 2020). ARVC has a complex disease presentation impacting both electrical and mechanical cardiac function, requiring therapies that can address the full spectrum of clinical features.

1.1.2 ARVC patient genetics

ARVC occurs in 1: 2000-5000 people, though the prevalence may be higher due to poor diagnostic markers and lack of genetic testing (Marcus, Edson et al. 2013, Wang, James et al. 2019). Human genetic studies show that 30-60% of ARVC patients carry mutations in genes of the desmosome (Marcus, Edson et al. 2013), which is a cell-cell adhesion structure that is critical in tissues undergoing constant mechanical stress, such as the heart (Sheikh, Ross et al. 2009, Marcus, Edson et al. 2013, Wang, James et al. 2019). The five classic components of the desmosome include: desmoplakin (DSP), desmoglein-2 (DSG2), desmocollin-2 (DSC2), plakoglobin (JUP), and plakophilin-2 (PKP2) (Sheikh, Ross et al. 2009, Marcus, Edson et al. 2013, Wang, James et al. 2019). All desmosomal genes have been implicated in ARVC, with PKP2 representing the most frequently identified genetic cause of ARVC (20-46 % cases) (Wang, James et al. 2019). DSP (3-15 % cases) and DSG2 (3-20 % cases) represent the next most commonly identified genetic causes of ARVC (Wang, James et al. 2019). While largely driven by desmosomal gene mutations, there is evidence for additional genes that are causal for ARVC. Though representing a small portion of ARVC cases, mutations in alpha T-Catenin, transmembrane protein 43, Lamin A/C, desmin (DES), phospholamban (PLN), and titin have also been implicated in ARVC (Wang, James et al. 2019, Mattesi, Zorzi et al. 2020). ARVC mutations are typically inherited in an autosomal dominant manner, but autosomal recessive forms have been identified (Naxos disease, Carvajal syndrome) (Wang, James et al. 2019, Mattesi, Zorzi et al. 2020). Genetic studies have been informative in focusing research efforts on the cardiac desmosome as a primary trigger for ARVC.

A two hit hypothesis has been proposed to help explain variable penetrance of desmosomal mutations in ARVC patient populations (Delmar and McKenna 2010, Marcus, Edson et al. 2013). This hypothesis suggests that two “hits” are required through a combination of genetics and environment (single desmosomal gene mutation and exercise), or purely genetics (two desmosomal gene mutations) to drive ARVC disease features (Delmar and McKenna 2010). Genetic studies suggest this mechanism underlies ARVC in patients harboring PKP2 mutations as 65.7% of PKP2 ARVC patients harbor an additional desmosomal gene mutation (Marcus, Edson et al. 2013). Animal studies have shown the combination of PKP2 ARVC patient genetics and exercise can trigger ARVC disease features (Cruz, Sanz-Rosa et al. 2015, Moncayo-Arlandi, Guasch et al. 2016), however, no studies have assessed the ability of two genetic “hits” in PKP2 to drive ARVC disease pathogenesis.

1.1.3 Current ARVC treatments and clinical challenges

To date there are no effective treatments or cures for ARVC as well as no treatment modalities, screening regimens or medications specific for ARVC (Idris, Shah et al. 2018, Elias Neto, Tonet et al. 2019, Wang, James et al. 2019). Current approaches are directed at symptomatic relief and centered around lifestyle change (avoiding competitive sports that can trigger SCD), pharmacological intervention (anti-arrhythmic drugs, beta-blockers) that transition to more invasive actions, which include implantable cardioverter-defibrillators (ICDs), cardiac catheter ablation, and heart transplantation if a patient becomes unresponsive or intolerant to pharmacotherapies (Elias Neto, Tonet et al. 2019, Wang, James et al. 2019). ICDs

have frequent device/lead related complications, catheter ablations are subject to recurrence due to the generation of new arrhythmogenic foci, and heart transplantation has a 23% mortality rate 10 years post-procedure (Wang, James et al. 2019). These factors highlight the critical need to identify new therapeutic strategies that target common genetic drivers (desmosomal genes) in ARVC pathogenesis.

1.2 The cardiac intercalated disc

1.2.1 Components and function

At the cardiac intercalated disc the desmosome functions along with the fascia adherens junction and gap junction to coordinate mechanical sensing and muscle contraction (Sheikh, Ross et al. 2009). The desmosome serves to mechanically couple adjacent cells and tether the cytoskeletal intermediate filament network within cardiomyocytes, which makes it a critical feature in cardiomyocyte mechanotransduction (Sheikh, Ross et al. 2009, Lyon, Zanella et al. 2015). The desmosome is composed of extracellular transmembrane cadherins (DSG2, DSC2), which interact with the armadillo proteins (JUP, PKP2), to ultimately bind the plakin protein DSP. DSP serves as the direct linker to the intermediate filament consisting of DES (Sheikh, Ross et al. 2009, Lyon, Zanella et al. 2015).

Fascia adherens junctions, similar to desmosomes, are structural components within the cell that anchor the actin cytoskeleton network to the membrane-bound cadherins (Sheikh, Ross et al. 2009, Lyon, Zanella et al. 2015). The cardiac fascia adherens consists of the calcium-dependent transmembrane protein N-Cadherin (N-

Cad), which is linked to the intracellular catenins (alpha-catenin, beta-catenin, JUP), which are further connected to the catenin-binding proteins (mouse Xin-alpha, vinculin, alpha-actinin) (Sheikh, Ross et al. 2009, Lyon, Zanella et al. 2015). The fascia adherens junction has been shown to be integral in cardiac mechanotransduction, as well as a driver of intracellular signaling via beta-catenin (Sheikh, Ross et al. 2009, Lyon, Zanella et al. 2015).

The gap junction mediates electrical coupling between cells to coordinate muscle contraction (Zhao, Qiu et al. 2019). Gap junctions are predominantly composed of connexins, where six connexin monomers form hemichannels in the membrane. These hemichannels then connect between adjacent cells (Zhao, Qiu et al. 2019). Connexin 43 (CX43) is the main form found in the heart and at the intercalated disc, though other connexins (40, 45) play a role in cardiac conduction through the nodes, bundle of His, and Purkinje fibers (Zhao, Qiu et al. 2019). Zonula occludens-1 (ZO-1) is another protein associated with the gap junction that is integral in regulating and targeting CX43 to the intercalated disc (Zhao, Qiu et al. 2019).

1.2.2 ARVC pathogenesis at the intercalated disc

Instrumental to understanding ARVC pathogenesis in the context of human patient genetics is that a single desmosomal gene mutation has devastating “domino” effects on loss of expression of adjacent desmosomal proteins and neighboring gap junction proteins (Rampazzo, Calore et al. 2014, Wang, James et al. 2019). Although the neighboring fascia adherens junction proteins are initially spared, they can eventually be impacted in late-stages of failure (Rampazzo, Calore et al. 2014),

highlighting that ARVC is a disease of early desmosomal protein loss with consequences on multiple structures at the intercalated disc (Gerull, Heuser et al. 2004, Lyon, Mezzano et al. 2014, Rasmussen, Nissen et al. 2014). Thus, ARVC therapeutic strategies should be capable of reassembling all components of the cardiac intercalated disc complex. Targeting the desmosome would be an ideal strategy for addressing the primary driver of disease as a means to stabilize the entire intercalated disc. However, there are clear barriers to restoring the desmosomal complex, some of which include identifying single critical scaffold proteins capable of reassembling the complex and achieving appropriate functional stoichiometry of desmosomal protein complex members. To date no studies have shown the sufficiency of a single desmosomal gene to reassemble the entire cardiac intercalated disc in ARVC settings.

1.3 Role of PKP2 at the desmosome and in ARVC

1.3.1 PKP2 structure and function

PKP2 is the most frequently mutated gene causal for ARVC (Marcus, Edson et al. 2013, Wang, James et al. 2019), which suggests disruption of PKP2 function may be an important driver of ARVC in patient populations. PKP2 consists of an N-terminal head domain, followed by central armadillo repeat motifs, and a short C-terminal tail (Chen, Bonne et al. 2002, Bass-Zubek, Godsel et al. 2009). Biochemical studies with yeast two hybrid systems show that the PKP2 N-terminal head domain can directly interact with all desmosomal components including DSP, JUP, DSG2, and DSC2 (Chen, Bonne et al. 2002). Additionally, overexpression of PKP2

enhanced the staining of DSP at the cell borders of COS cells (Chen, Bonne et al. 2002). This data suggests a strong interaction between PKP2 and DSP, where PKP2 may have an important role in facilitating the proper cellular localization of DSP. While these initial studies have been instrumental in understanding PKP2 molecular function, further work is required to validate these concepts in more human relevant systems (cardiomyocytes, hearts) harboring ARVC patient genetics.

1.3.2 Limitations of current mouse models to understand PKP2 in ARVC

Mouse models have been used to better define the role of PKP2 in ARVC, however, current models are unable to fully recapitulate patient disease features. Initial studies with a global knockout (KO) of PKP2 revealed it is embryonic lethal, demonstrating a requirement of PKP2 for cardiac development (Grossmann, Grund et al. 2004). In contrast, global heterozygous KO of PKP2 does not trigger development of any ARVC disease features at baseline (Cerrone, Noorman et al. 2012). To circumvent this issue, an inducible and cardiac-specific KO of PKP2 was developed, which following PKP2 deletion in adulthood could drive mechanical dysfunction and fibrosis (Cerrone, Montnach et al. 2017). Lipid deposition was not assessed in this model. Interestingly, arrhythmias could not be observed at baseline, but could be induced with isoproterenol administration (Cerrone, Montnach et al. 2017).

To better understand PKP2 patient genetics in ARVC, additional models utilizing transgenic expression of a truncated mutant PKP2 (S329X) or viral transduction of a truncated mutant PKP2 (R735X) have been developed (Cruz, Sanz-

Rosa et al. 2015, Moncayo-Arlandi, Guasch et al. 2016). The transgenic PKP2 S329X mouse model displayed mechanical and electrical abnormalities with high transgene expression or advanced age (12 months) (Moncayo-Arlandi, Guasch et al. 2016). Viral transduction of PKP2 R735X resulted in subtle mechanical and electrical dysfunction with extensive exercise training (Cruz, Sanz-Rosa et al. 2015). Fibro-fatty replacement of myocardium was not detected in these models. Interpretations of these studies are further complicated by the fact that mutant PKP2 overexpression occurred with full levels of endogenous PKP2 protein. The lack of comprehensive models has inhibited the ability to fully understand the function of PKP2 in disease, particularly in the context of ARVC patient genetics. Thus, there is a requirement for models that endogenously harbor PKP2 patient mutations in human relevant and *in vivo* model systems to allow for appropriate timing and expression of mutant PKP2 proteins to more closely emulate human disease features and progression.

1.4 Altered RNA splicing in ARVC

1.4.1 RNA splicing

RNA splicing represents a complex and coordinated process through which intronic sequences are removed to leave only coding sequences in a mature messenger RNA (mRNA) (Herzel, Ottoz et al. 2017, Anna and Monika 2018). This mechanism is driven by the spliceosome, which is a protein-RNA complex that recognizes *cis* splicing elements on pre-mRNA (Herzel, Ottoz et al. 2017, Anna and Monika 2018). 5’ splice donor sites (GT sequence at 5’ exon-intron boundary), 3’ splice acceptor sites (AG sequence at 3’ intron-exon boundary), and branchpoint

sequences (18-40 nucleotides upstream of 3' splice acceptor site) represent the essential *cis* splicing elements on pre-mRNA. These sites are recognized by five small nuclear ribonucleoproteins (snRNPs) termed U1, U2, U4, U5, and U6. SnRNPs have complementary RNA sequences to these *cis* elements that enable specific RNA-RNA binding (Herzel, Ottoz et al. 2017, Anna and Monika 2018). Following initial snRNP binding, there is a coordinated recruitment, rearrangement, and then displacement of factors. This culminates in the excision of introns and exons being joined (Herzel, Ottoz et al. 2017, Anna and Monika 2018). Given the complexity and extensive coordination of RNA splicing, mutations impacting splicing machinery and elements are predicted to have dramatic effects in the cell and ultimately on tissue function.

1.4.2 Splice acceptor site mutations and mechanisms in disease

Defects in RNA splicing have been linked to approximately one third of all human disease-causing mutations (Lim, Ferraris et al. 2011). Mutations in critical splicing sites such as splice acceptor sites are linked to many human diseases including arthrogyrposis multiplex congenita, Charcot-Marie-Tooth disease, and Fabry disease (Attali, Warwar et al. 2009, Guernsey, Jiang et al. 2010, Watanabe, Hanawa et al. 2013, Anna and Monika 2018). Altered RNA splicing may be a critical mechanism through which patient genetics drive ARVC, as studies have implicated mutations in splice acceptor sites as being causal for disease (Gerull, Heuser et al. 2004, Groeneweg, Ummels et al. 2014). Analysis of Genome Aggregation Database (gnomAD) and ClinVar database revealed that splice acceptor site mutations are

found within all five human desmosomal genes (PKP2, DSP, JUP, DSG2, DSC2), many of which are classified as pathogenic for ARVC (**Table 1**; (Lek, Karczewski et al. 2016)), suggesting that disruption of normal RNA splicing may be a critical mechanism driving ARVC. Splice acceptor site mutations trigger aberrantly spliced transcripts through various potential mechanisms including utilization of a cryptic intronic splice site, exon skipping, or utilization of a cryptic exonic splice site; resulting in diverse effects on protein quality and levels but limited studies have tested the impact of RNA splicing mutations on these parameters (Attali, Warwar et al. 2009, Guernsey, Jiang et al. 2010, Watanabe, Hanawa et al. 2013, Groeneweg, Ummels et al. 2014). These diverse outcomes highlight the need to generate relevant models harboring ARVC patient genetics to determine the functional consequences of RNA splicing mutations on desmosomal gene splicing and ultimately protein quality.

1.5 Adeno-associated virus (AAV) gene therapy

The development of recombinant adeno-associated virus (AAV) vectors has significantly expanded gene therapy technology for human disease (Ishikawa, Weber et al. 2018). AAV is a single-stranded DNA virus with a 4.7kb genome, and recombinant AAVs are modified to become replication-deficient with an open cassette to insert a gene of interest for delivery (Aponte-Ubillus, Barajas et al. 2018). Tissue tropism is enabled through the discovery of unique AAV serotypes from various tissues (Srivastava 2016, Ishikawa, Weber et al. 2018). Minimal immunogenicity and non-integrating, but long-term expression of therapeutic genes are additional benefits of AAV systems (Aponte-Ubillus, Barajas et al. 2018). There

are many ongoing AAV clinical trials that have shown promising results for genetic human diseases including spinal muscular atrophy, Duchenne muscular dystrophy, retinitis pigmentosa, and hemophilia (Mendell, Al-Zaidy et al. 2021).

AAV approaches represent an appealing therapeutic option for inherited cardiomyopathies due to the availability of cardiotropic AAV9 serotypes, as well as cardiomyocyte-specific promoters that drive targeted and robust expression (Daya and Berns 2008, Zincarelli, Soltys et al. 2008, Srivastava 2016, Ishikawa, Weber et al. 2018). Preclinical animal studies have been instrumental in showing the feasibility of AAV technology to address genetic diseases with cardiac abnormalities. Recently, AAV9 has been shown to successfully prevent and alleviate electrical dysfunction in a mouse model of catecholaminergic polymorphic ventricular tachycardia (CPVT) through delivery of an inhibitory peptide to Ca^{2+}/calmodulin-dependent protein kinase II (CaMKII) (Bezzerides, Caballero et al. 2019). This study highlighted the specificity of AAV9 vectors paired with a cardiac-specific troponin T (cTNT) promoter, as well as the ability of this technology to serve as prophylaxis when administered at a neonatal stage and maintain efficacy when delivered at a late disease stage (Bezzerides, Caballero et al. 2019). Additional work has highlighted the ability of AAV9 systems to prolong survival, improve cardiac mechanical function, and reduce fibrotic remodeling through gene replacement of tafazzin in a mouse model of Barth Syndrome (Wang, Li et al. 2020). This study similarly demonstrated efficacy of this approach for both disease prevention and reversing existing disease features (Wang, Li et al. 2020). These efforts show the ability of AAV9 technology to address critical cardiac disease

features (arrhythmias, mechanical dysfunction, fibrosis), and are important examples for further efforts in genetic cardiac diseases such as ARVC.

1.6 Rationale, Hypothesis, and Specific Aims

ARVC is a genetic cardiac disease characterized by arrhythmias, ventricular dysfunction, and fibro-fatty replacement of myocardium that causes sudden death in young adults and athletes, with no available therapies (Thiene, Corrado et al. 2007, Sen-Chowdhry, Morgan et al. 2010, Mattesi, Zorzi et al. 2020). ARVC is termed a "disease of the desmosome" as 30-60% of mutations are found in desmosomal (cell-cell junction anchor) genes, with the desmosomal gene PKP2 being the most frequently mutated gene in ARVC (Sen-Chowdhry, Morgan et al. 2010, Marcus, Edson et al. 2013, Wang, James et al. 2019). Previous studies highlight altered RNA splicing as a potential mechanism through which PKP2 patient genetics drive ARVC (Gerull, Heuser et al. 2004, Groeneweg, Ummels et al. 2014). Additional studies suggest that one third of all human disease-causing mutations are a result of defects in RNA splicing (Lim, Ferraris et al. 2011, Baralle and Buratti 2017); highlighting the importance of testing this mechanism in ARVC. However, no models and limited mechanistic insights exist into how human mutations in RNA splicing impact ARVC pathogenesis, which would be essential in designing therapeutics capable of circumventing ARVC in patient settings.

To better understand the molecular mechanisms and functional impact of PKP2 splice acceptor site mutations in ARVC, our laboratory developed a novel mouse model harboring a PKP2 splice acceptor site mutation found in multiple ARVC populations (Gerull, Heuser et al. 2004, Svensson, Astrom-Aneq et al. 2016). Functional and molecular analysis of this model can determine the sufficiency of PKP2 splice acceptor site mutations to recapitulate all classic human ARVC disease

features. Furthermore, mechanistic studies can better define the relationship between splice site mutations, RNA, and protein quality/quantity. Information gained from mechanistic studies in this model system can guide the rational design and then evaluation of therapeutic approaches for ARVC.

Hypothesis: PKP2 splice acceptor site mutations are sufficient to trigger ARVC development by impacting PKP2 protein quality or quantity, and can provide critical mechanistic and therapeutic insights into how PKP2 patient genetics trigger and can be intervened with in ARVC.

Specific Aims:

1. To determine the sufficiency of PKP2 splice acceptor site mutations to drive classic ARVC disease features utilizing a novel PKP2 mutant mouse model and PKP2 mutant neonatal cardiomyocytes.
2. To determine the pathogenic mechanisms underlying PKP2 splice acceptor site mutations in ARVC utilizing a novel PKP2 mutant mouse model and PKP2 mutant neonatal cardiomyocytes.
3. To determine the impact of PKP2 restoration on ARVC progression *in vivo* through a novel PKP2 mutant mouse model.

The results of these studies are presented in chapters 3-5 and are discussed in terms of their contribution to understanding RNA splicing mutations as a trigger for ARVC,

molecular mechanisms underlying splice acceptor site mutation pathogenesis, and *in vivo* PKP2 restoration as a therapeutic approach for ARVC.

Table 1.1: Splice acceptor site mutations are identified in all desmosomal genes within ARVC populations. Compilation of splice acceptor site mutations in the five classic desmosomal genes (gnomAD) and reported associations with ARVC pathogenesis (ClinVar).

Desmosomal Gene	Variant	Pathogenic?
PKP2	c.1379-1G>A	Conflicting
	c.1511-1G>T	Yes
	c.1511-2A>T	Yes
	c.1689-1G>C	Likely
	c.2146-1G>C	Yes
	c.2490-47 (del)	Unknown
DSP	c.598-2A>C	Unknown
	c.598-2A>G	Unknown
	c.598-1G>C	Unknown
	c.1141-2A>G	Yes
	c.2131-3 (del)	Unknown
	c.2298-1G>C	Unknown
	c.3085-1G>A	Unknown
JUP	c.910-1G>C	Unknown
	c.993-1G>T	Unknown
DSG2	c.82-1G>A	Unknown
	c.379-1G>C	Unknown
	c.1424-1G>T	Unknown
	c.1652-1G>A	Likely
	c.2002-2A>G	Unknown
DSC2	c.631-2A>G	Likely
	c.1664-1G>C	Unknown

Chapter 2

Materials and Methods

2.1 Generation of experimental animals

Mouse lines harboring the PKP2 IVS9-1 G>C mutation were generated using CRISPR-Cas9 based methods that have been previously described (Ma, Chen et al. 2017). Briefly, CRISPR guide RNAs and single-strand oligodeoxynucleotide templates (ssODNs) were designed for the PKP2 IVS9-1 G>C mutation. CRISPR RNAs (crRNA) were chemically synthesized to contain the guide RNAs for PKP2 IVS9-1 G>C mutation. For PKP2 IVS9-1 G>C mutant mice, a mixture of PKP2 IVS9-1 G>C crRNA (cucacaacagauacccacauGUUUUAGAGCUAUGCUGUUUUG), ssODNs (AGAGAACTTCTCTGGTAGCAAATGTGATAGCATTTACAGGATGTGTCTCACAAC A**C**ATACCCACATTGGTGGCTCGAATGGTTGTCCAAAAGGAAAATGGTCTTCAGC ATA), trans-activating crRNA (AAACAGCAUAGCAAGUUAAAAUAAGGCUAGUCC GUUAUCAACUUGAAAAAGUGGCACCGAGUCGGUGCU), and commercially purchased Cas9 protein (New England Biolabs) was injected into pronuclei of one-cell stage zygotes from C57BL/6J mice (The Jackson Laboratory). Genomic DNA was extracted from mouse tails and genomic fragments at target sites were amplified by PCR and sequencing. Genotype positive knockin mice were backcrossed with C57BL/6J mice (The Jackson Laboratory) for at least three generations to minimize potential off-target effects. PKP2 IVS9-1 G>C heterozygous mice were crossed to generate wild-type controls, PKP2 IVS9-1 G>C Het, and PKP2 IVS9-1 G>C Hom mutant mice. All animal procedures were in full compliance with the guidelines approved by the University of California, San Diego Institutional Animal Care and Use Committee and carried out in accordance with the Guide for the Care and Use of Laboratory Animals of the National Institutes of Health.

2.2 RNA analysis

Total RNA was isolated from hearts using TRIZOL (Invitrogen) according to the manufacturer's instructions. The first-strand cDNA was generated using PrimeScript RT Reagent Kit with gDNA Eraser (Takara). RT-PCR was performed using primer sequences for PKP2 Exons 5-13 (forward = CTGAAGGCGACTACCCCAAA and reverse = TCCGGCTGTTGACAAAGTCT) with KOD Extreme Hot Start DNA Polymerase (Sigma-Aldrich). Quantitative RT-PCR was performed on heart cDNA using primer sequences for PKP2 exons 9-10 (forward = AAGGAGCAATCCACATGGCA and reverse = ACAACCATTCGAGCCACCAA), stress markers atrial natriuretic factor (ANF) (forward = GATAGATGAAGGCAGGAAGCCGC and reverse = AGGATTGGAGCCCAGAGTGGACTAGG) and B-type natriuretic factor (BNP) (forward = TGTTTCTGCTTTTCCTTTATCTGTC and reverse = CTCCGACTTTTCTCTTATCAGCTC), collagen genes collagen type 1 alpha 1 (Col1a1) (forward = TCACCAAACTCAGAAGATGTAGGA and reverse = GACCAGGAGGACCAGGAAG) and collagen type 3 alpha 1 (Col3a1) (forward = ACAGCAGTCCAACGTAGATGAAT and reverse = TCACAGATTATGTCATCGCAAAG) with Power SYBR Green PCR master mix (Applied Biosystems) and using a Bio-Rad Mastercycler. All values were normalized to GAPDH mRNA levels as indicated.

2.3 Protein analysis

2.3.1 Western blot

Total protein extracts were isolated from cardiomyocytes and ventricles as previously described (Lyon, Mezzano et al. 2014). Immunodetection of desmoplakin (mouse, 1:1000, Bio-Rad), desmoglein-2 (mouse, 1:1000, Fitzgerald), plakophilin-2 C-terminal (mouse, 1:2000, Fitzgerald), plakophilin-2 N-terminal (goat, 1:1000, Novus Bio), plakoglobin (goat, 1:1000, Sigma), N-cadherin (rabbit, 1:1000, Abcam), connexin 43 (rabbit, 1:1000, Invitrogen), FLAG (mouse, 1:500, Sigma), glyceraldehyde 3-phosphate dehydrogenase (mouse, 1:2000, Santa Cruz Biotechnology) was performed as previously described (Lyon, Mezzano et al. 2014).

2.3.2 Immunofluorescence analysis

Heart cryosections were fixed in 100% acetone at -20ºC for 8 minutes and were blocked in 5% donkey serum/ phosphate-buffered saline (PBS) before incubation with antibodies. Sections were subsequently stained with primary antibodies against plakophilin-2 (mouse, 1:10, Fitzgerald), desmoplakin (mouse, 1:100, Bio-Rad), plakoglobin (goat, 1:100, Sigma), connexin 43 (rabbit, 1:100, Invitrogen), N-cadherin (rabbit, 1:100, Abcam), FLAG (mouse, 1:100, Sigma) and secondary antibodies (1:100, Jackson ImmunoResearch Inc.). Immunofluorescence images were acquired using confocal microscopy (Leica SP8).

2.4 Histological analysis

Mouse hearts were perfused in a relaxation buffer consisting of 300 mM KCl in PBS and fixed with 4% paraformaldehyde. Fixed hearts were embedded in OCT

tissue tek (Sakura) or dehydrated and embedded in paraffin as previously described (Lyon, Mezzano et al. 2014). Sections were cut between 5 and 10 μm thickness. Whole-heart (5 μM) paraffin sections were stained with hematoxylin and eosin (Sigma-Aldrich) and Masson's trichrome (Sigma-Aldrich) according to the manufacturer's instructions. Whole-heart (10 μM) cryosections were stained with Oil Red O (Sigma–Aldrich) according to the manufacturer's instructions. Images were acquired with the Hamamatsu Nanozoomer 2.0 HT Slide Scanner.

2.5 Magnetic Resonance Imaging (MRI)

2.5.1 Acquisition

In vivo cardiac MRI was performed on a 7T horizontal bore MR scanner (Bruker). A quadrature volume coil (Bruker) was used for RF signal transmission and a two-channel surface array coil (RAPID MRI) was used for reception of the RF signal. Cardiac CINE images were acquired with an IntraGate (Bruker) retrospective gated 2D gradient echo pulse sequence (FLASH) with the following parameters: TE=3.1 ms, TR=5.6 ms, flip angle= 7º, 300-400 repetitions and 20 frames. A field of view = 2.0 cm x 1.5 cm and data matrix =256 x 192 were prescribed for a spatial resolution = 0.078 mm/pixel.

2.5.2 Segmentation and analysis

Equatorial frames containing the largest and smallest chamber diameters were selected to define the end-diastolic (ED) and end-systolic (ES) frames, respectively. For MRI image analyses, two-dimensional (2D) endocardial contours were manually

segmented and slice volumes calculated using freely available software (Medviso Segment) for each heart at ED and ES (both LV and RV). Volumes from continuous slices were summed to generate total chamber volumes at ED and ES. Ejection fractions (EF) were averaged over all continuous slices.

2.6 Surface ECG

Surface ECG was performed as previously described (Lyon, Mezzano et al. 2014). Briefly, mice were anesthetized with 5% isoflurane for 15 seconds and maintained at 1.5% isoflurane during the procedure. Needle electrodes (30 gauge) were inserted subcutaneously into right forearm and left leg. Electrical activity was recorded for 5 minutes. For analysis, composite ECG tracings were generated for 100 consecutive beats and wave parts manually identified to generate heart rates, PR intervals, and QRS intervals. For PVC analysis, ectopic beats were identified over the entire 5 minute recording. LabChart software (AD instruments) was used for electrophysiology data analysis.

2.7 Transmission electron microscopy (TEM)

Mice were perfused with a fixation buffer containing 2% paraformaldehyde and 2.5% glutaraldehyde in 0.15 M sodium cacodylate buffered to pH 7.4. Fixed hearts were excised and only right and left ventricular free walls were processed. Images were captured with a FEI Tecnai Spirit G2 BioTWIN Transmission Electron Microscope as previously described (Lyon, Mezzano et al. 2014).

2.8 Adenovirus and adeno-associated virus vector design and production

Adenovirus vectors expressing either wild-type or mutant PKP2 were designed and synthesized containing a CMV promoter, C-terminal PKP2 FLAG tag, and P2A linked GFP (Vector Builder). Adenovirus was packaged and amplified through the UCSD viral vector core. Adeno-associated virus vector expressing wild-type PKP2 was designed and synthesized containing a cardiac troponin T promoter, C-terminal PKP2 FLAG tag, Kozak sequence, WPRE, and bGH-PA (Vector Builder). Viral particles were packaged into a cardiotropic AAV9 serotype and amplified through the UCSD viral vector core.

2.9 Neonatal cardiomyocyte isolation and protein analysis

Ventricular cardiomyocytes were isolated from neonatal (1–2 days old) mouse hearts and plated on laminin as previously described (Lyon, Mezzano et al. 2014). Briefly, excised hearts were incubated in trypsin solution overnight, then cells dissociated with multiple rounds of collagenase type II incubation. Isolated cardiomyocytes were maintained in media consisting of DMEM, M199, 5% fetal bovine serum, 10% horse serum and 1% penicillin/streptomycin/glutamine. For western blot protein analyses, cardiomyocytes were collected six days after plating.

2.10 Neonatal cardiomyocyte electrophysiology measurements

Neonatal mouse cardiomyocytes were isolated as above and seeded on a laminin coated E-Plate CardioECR 48 at a density of 50,000 cells per microelectrode well. Field potential data was acquired using the xCELLigence RTCA CardioECR

Data Acquisition software (Agilent). Field potential data was collected during 30s sweeps every 15 min over the course of 2hrs. For analysis, field potential peaks were identified and then beating irregularity index was calculated as the coefficient of variation (standard deviation/mean) for all peaks within a 30s sweep.

2.11 Neonatal cardiomyocyte PKP2 protein restoration

Wild-type control and PKP2 Hom neonatal cardiomyocytes were isolated and plated at a density of 150,000 cells per well on a laminin coated 48-well plate. PKP2 Hom cells were infected 48 hours post-plating with adenoviruses expressing either wild-type PKP2 (MOI 0.34) or mutant PKP2 (MOI 1.72) for 24 hours then media was removed and cells were maintained in culture for three additional days then harvested for protein analysis.

2.12 Human and mouse PKP2 sequence alignment

Human PKP2 IVS10-1 G>C genomic locus and mouse PKP2 IVS9-1 G>C genomic locus, along with surrounding 100bp of intronic sequence and 100bp of exonic sequence were aligned using nucleotide Basic Local Alignment Search Tool (BLAST) from NCBI.

2.13 AAV injection

Early AAV injections were performed at postnatal day 2 using a 31 gauge needle and syringe to deliver $5x10^{11}$ viral particles per mouse in 50 µl of solution containing AAV9 GFP or AAV9 PKP2 via intraperitoneal injection. Late-stage AAV

injections were performed at four weeks of age using a 28 gauge needle and syringe to deliver $5x10^{11}$ viral particles per mouse in 50 µl of solution containing AAV9 GFP or AAV9 PKP2 via retro-orbital injection.

2.14 Serum liver enzyme analysis

Blood was collected from the abdominal aorta of wild-type control mice at six months of age and PKP2 Hom mice six months post-AAV9 PKP2 treatment. Blood was allowed to settle for 30 min at room temperature, then was centrifuged at 10,000g for 1 min. Serum was collected and snap frozen in liquid nitrogen. Serum alkaline phosphatase (ALP) and alanine aminotransferase (ALT) levels were assessed using a VetScan2 chemistry analyzer (Zoetis).

2.15 Statistical analysis

All data are presented as means ± standard deviation. GraphPad Prism was used for analyses and significance was evaluated by unpaired t-test and one-way or two-way ANOVA with Tukey's post-hoc multiple comparison tests. For Kaplan-Meier survival analysis, significance was assessed by the log-rank test. Categorical data was analyzed using a Fisher's exact test in RStudio software. A p value <0.05 was considered statistically significant.

Chapter 3

Characterization of a Novel Mouse Model Harboring a PKP2 Splice Acceptor Site Mutation

3.1 Generation of a novel mouse model harboring a human PKP2 splice acceptor site variant

To better understand the role of PKP2 splice acceptor site mutations in ARVC, I sought to characterize a mouse model harboring a splice site mutation found in various human ARVC populations (Gerull, Heuser et al. 2004, Syrris, Ward et al. 2006, Groeneweg, Ummels et al. 2014, Svensson, Astrom-Aneq et al. 2016). Genetic studies identified a PKP2 splice acceptor site mutation (PKP2 IVS10-1 G>C) in multiple ARVC populations where patients displayed classic ARVC disease features including SCD, arrhythmias, mechanical dysfunction, and fibro-fatty replacement of myocardium on cardiac wall biopsies (Gerull, Heuser et al. 2004, Syrris, Ward et al. 2006, Groeneweg, Ummels et al. 2014, Svensson, Astrom-Aneq et al. 2016). To investigate the impact of the PKP2 IVS10-1 G>C mutation on splicing, the Sheikh laboratory created a knockin mouse model within mouse intron 9 (mouse IVS9-1 G>C equivalent to human IVS10-1 G>C) through CRISPR-Cas9 genome editing (Fig. 3.1A). PKP2 heterozygous mutant (PKP2 Het) founder mice harboring the IVS9-1 G>C mutation were identified (Fig. 3.1B), backcrossed for three generations to remove CRISPR-Cas9 associated off-target effects and bred to homozygosity. Offspring from PKP2 heterozygous mutant breeding strategy were viable and born at Mendelian ratios (Fig. 3.1C), but PKP2 IVS9-1 G>C homozygous mutant (PKP2 Hom) mice displayed SCD beginning at four weeks of age, with a median survival of 11 weeks, and no PKP2 Hom mice surviving past 26 weeks of age (Fig. 3.1D). One death was observed out of 27 PKP2 Het mice followed until one year of age, suggesting a second allele hit may be required to both accelerate and consistently

recapitulate SCD, a hallmark of ARVC (Wang, James et al. 2019, Mattesi, Zorzi et al. 2020).

3.2 Mechanical dysfunction in PKP2 Hom mice

Given the extensive pathology in the right ventricle of ARVC patients and mouse models (Cerrone, Montnach et al. 2017, Mattesi, Zorzi et al. 2020), PKP2 IVS9-1 G>C mutant mice were subjected to cardiac MRI as it provides reliable characterization of right and left ventricle dimensions and function in the mouse compared to echocardiography (Ho and Nihoyannopoulos 2006). To quantify cardiac chamber dimensions and function, I obtained serial short axis (SAX) cine MRI views throughout the cardiac cycle. Left and right ventricle endocardial borders at end-diastole and end-systole were segmented to obtain volumes and ejection fractions (EFs). Physiological studies (MRI and surface ECG) are performed under isoflurane anesthesia, which is known to directly decrease heart rate and cardiac function (Pachon, Scharf et al. 2015). Therefore, it is critical that heart rates within anesthetized physiological studies are not different to ensure functional differences are not driven by anesthesia. No significant differences in heart rate were observed between littermate wild-type control and PKP2 Hom mice (Fig. 3.2B). However, PKP2 Hom mice displayed significantly enlarged right ventricular end-diastolic and end-systolic volumes (Fig. 3.2D-E), as well as significantly increased left ventricular end-systolic volumes (Fig. 3.2E) compared to littermate wild-type control mice. Representative four chamber and SAX views further highlight the extensive pathological remodeling in PKP2 Hom mouse hearts, particularly within the right

ventricle (Fig. 3.2A). A significant decrease in EF was also observed in both left and right ventricles in PKP2 Hom mice compared to littermate wild-type controls (Fig. 3.2C), suggestive of functional deficits. These results highlight extensive right and left ventricular remodeling and biventricular systolic dysfunction in PKP2 Hom mice.

3.3 Electrical dysfunction and arrhythmias in PKP2 Hom mice

Electrical dysfunction is a hallmark of ARVC and a major contributor to SCD in ARVC patients (Sen-Chowdhry, Morgan et al. 2010, Mattesi, Zorzi et al. 2020). I performed surface electrocardiogram (ECG) analysis at four weeks of age to gain insight into the electrical defects in PKP2 Hom mice. Analysis of composite surface ECG tracings from PKP2 Hom mice and littermate controls showed no significant differences in heart rate or PR intervals (reflective of time it takes for an electrical impulse to travel from sinoatrial node in the atria and across atrioventricular node to the ventricle) (Fig 3.3A-B). However, there was a significantly widened QRS interval (reflective of electrical impulse to travel through both the right and left ventricle) in PKP2 Hom hearts (Fig. 3.3A-B), indicative of ventricular depolarization delay, a common feature observed in ARVC patients (Thiene, Corrado et al. 2007, Sen-Chowdhry, Morgan et al. 2010, Mattesi, Zorzi et al. 2020). Ventricular depolarization abnormalities can serve as a primer for ventricular reentry, termed a premature ventricular contraction (PVC) (Lyon, Mezzano et al. 2014). Analysis of surface ECG tracings at four weeks of age (onset of sudden death) also revealed PVCs in 62.5% of PKP2 Hom mice, whereas none were observed in littermate wild-type controls

(Fig. 3.3C). These data altogether suggest that PKP2 Hom mice recapitulate electrical disease features classic to ARVC.

3.4 Fibro-fatty replacement of myocardium in PKP2 Hom mice

A key clinical feature of human ARVC is fibro-fatty replacement of myocardium (Mattesi, Zorzi et al. 2020). To assess whether PKP2 IVS9-1 G>C Hom mice recapitulate fibro-fatty replacement of myocardium, cardiac histological analysis was performed at six weeks of age. Masson's Trichrome staining marks collagen and highlighted severe fibrosis, particularly in the LV free wall and diffuse fibrosis within both left and right ventricles (Fig. 3.4A-B). Quantitative RT-PCR analysis validated findings at the histological level, as a significant increase in expression of pro-fibrotic genes, collagen type 1 alpha 1 (Col1a1) and type 3 alpha 1 (Col3a1) was observed in PKP2 Hom hearts compared to littermate wild-type controls (Fig. 3.4C). Fat deposition is an additional contributor to tissue remodeling in some human ARVC patients (Basso and Thiene 2005, Thiene, Corrado et al. 2007, Sen-Chowdhry, Morgan et al. 2010). Studies in ARVC patients and mouse models of ARVC have demonstrated a particular affinity for fat deposition to more specifically localize to the right ventricle subepicardium, which reflects a primary location for fat accumulation and critical location to understand the mechanisms of adipogenesis in ARVC (Basso and Thiene 2005, Te Riele, James et al. 2013, Lyon, Mezzano et al. 2014). Using Oil Red O staining as a marker for neutral lipids, my results show that six week old PKP2 Hom mice display lipid accumulation within the right ventricular subepicardium (Fig. 3.5), a finding which was not observed in left ventricles of PKP2 Hom mice and either

ventricles in littermate wild-type control mice (Fig. 3.5). PKP2 Hom mice display fibro-fatty replacement of myocardium, a hallmark of human ARVC.

3.5 Desmosomal and gap junction disruption at onset of SCD in PKP2 Hom mice

To determine the impact of the PKP2 IVS9-1 G>C mutation on cardiac intercalated disc protein homeostasis, western blot analysis was performed in ventricular lysates from PKP2 Hom hearts and littermate wild-type controls at four weeks of age. A higher molecular weight mutant PKP2 protein was identified in the absence of endogenous PKP2 within PKP2 Hom hearts (Fig. 3.6A). Mutant PKP2 protein was found at significantly reduced levels to wild-type PKP2 in littermate wild-type control hearts (Fig. 3.6A-B). These molecular consequences resulted in the direct loss of additional desmosomal components including DSP, DSG2, and JUP in PKP2 Hom hearts (Fig. 3.6A-B). The molecular alterations at the desmosome had direct consequences on the predominant ventricular gap junction protein, CX43, which was significantly reduced in PKP2 Hom hearts compared to controls (Fig. 3.6A-B). CX43 is thought to be a direct target of DSP, suggesting a molecular consequence from desmosomal disruption (Lyon, Mezzano et al. 2014). At this time point, levels of the fascia adherens marker N-Cad in PKP2 Hom hearts were not significantly different from littermate wild-type controls (Fig. 3.6A-B). The specificity of desmosomal and gap junction protein loss was further shown through immunofluorescence microscopy at four weeks of age, as reduced staining of desmosomal (PKP2, DSP, JUP) and gap junction proteins (CX43), but not fascia

adherens proteins (N-Cad) was observed at the cardiac intercalated disc in PKP2 Hom hearts (Fig. 3.6C).

To determine the long-term consequences of the PKP2 IVS9-1 G>C mutation on cardiac intercalated disc protein homeostasis, I performed protein analysis in PKP2 Hom mice at eight weeks of age. As observed at four weeks, there was a loss of endogenous PKP2 and appearance of a larger mutant form (at reduced levels to wild-type PKP2) in PKP2 Hom hearts (Fig. 3.7A-B). This resulted in a reduction in additional desmosomal (DSP, DSG2, JUP) and gap junction (CX43) proteins in PKP2 Hom hearts (Fig. 3.7A-B). However, at eight weeks of age, the fascia adherens protein N-Cad was also significantly reduced in PKP2 Hom hearts when compared to littermate wild-type controls (Fig. 3.7A-B). This data demonstrates the early molecular consequences of the PKP2 IVS9-1 G>C mutation on desmosome and gap junction proteins, which coincides with the onset of electrical dysfunction and SCD. The data also highlight the late molecular consequences of the PKP2 IVS9-1 G>C mutation, which reflect the progressive breakdown of the entire cardiac intercalated disc structure as observed in ARVC.

3.6 Desmosomal protein loss and degradation in PKP2 Hom hearts

Ultrastructure analysis is commonly used to provide high resolution assessment of cardiac intercalated disc integrity in ARVC mouse and patient tissues (Lyon, Mezzano et al. 2014, Rampazzo, Calore et al. 2014). Transmission electron microscopy (TEM) analysis at two weeks of age revealed electron dense desmosomes at the intercalated disc in wild-type control hearts; however,

desmosomes were at significantly reduced levels in PKP2 Hom hearts (Fig. 3.8A-B). This suggests an early loss of desmosomal numbers in PKP2 Hom hearts. Further TEM analysis at four weeks of age (onset of ARVC disease features) similarly identified desmosomes in wild-type control hearts, however, PKP2 Hom hearts displayed enlarged gaps and diffuse electron dense signal at desmosomal cell-cell contacts indicative of loss of desmosomal structure (Fig. 3.8C). An accumulation of multi-membrane vesicles was also found at the cardiac intercalated disc in PKP2 Hom hearts (Fig. 3.8C), which bears striking similarity to protein degradation accumulation found at the intercalated disc in hearts deficient of constitutive photomorphogenesis 9 signalosome subunit 6 (CSN6) (Liang, Lyon et al. 2021). CSN6 has been newly implicated in driving desmosomal protein degradation defects that underlie ARVC pathogenesis (Liang, Lyon et al. 2021). These multi-membrane vesicles were not present in littermate wild-type control hearts at four weeks of age (Fig. 3.8C), highlighting the specificity of the junctional ultrastructural defects to PKP2 Hom hearts and consequence of the PKP2 IVS9-1 G>C mutation.

3.7 PKP2 Hom neonatal mice as a platform to dissect early events underlying ARVC

3.7.1 Early desmosomal protein loss precedes overt structural disease onset in PKP2 Hom mice

To identify an early time point before the onset of disease features, analysis was performed in PKP2 Hom hearts and littermate wild-type controls at postnatal day 1 (P1). Heart weight to body weight analysis showed no significant differences in gross cardiac morphology in P1 PKP2 Hom hearts when compared to littermate wild-

type controls (Fig. 3.9A). Gene expression analysis of P1 hearts also showed no significant differences in cardiac stress markers (ANF and BNP) and fibrosis (Col1a1 and Col3a1) between wild-type control and PKP2 Hom hearts (Fig. 3.9B-C). Molecular analysis of the cardiac intercalated disc at P1 revealed a loss of endogenous PKP2 and presence of a mutant PKP2 protein in PKP2 Hom hearts (Fig. 3.9D). Mutant PKP2 protein was significantly reduced when compared to wild-type PKP2 levels in littermate wild-type control hearts (Fig. 3.9D-E). These consequences resulted in a significant reduction of additional desmosomal proteins (DSP, DSG2, JUP) (Fig. 3.9D-E), while fascia adherens (N-Cad) and gap junction (CX43) protein levels remained unchanged (Fig. 3.9D-E). These findings identify P1 as a time point where there is a molecular consequence on the desmosome in the absence of changes to the gross morphology and disease hallmarks associated with ARVC.

3.7.2 Early desmosomal protein loss and CX43 reduction coincident with baseline arrhythmias in PKP2 Hom neonatal cardiomyocytes

To more specifically determine the impact of the PKP2 IVS9-1 G>C mutation in cardiomyocytes, neonatal cardiomyocytes were isolated from PKP2 Hom P1 and littermate wild-type control hearts and assessed for molecular and electrical deficits. Desmosomal protein disruption (PKP2, DSP, DSG2, JUP) was detected in cultured PKP2 Hom neonatal cardiomyocytes (Fig. 3.10A), similar to the desmosomal protein deficits observed in P1 PKP2 Hom hearts (Fig. 3.8D-E). Interestingly, PKP2 Hom neonatal cardiomyocytes displayed reduced levels of the gap junction protein CX43, which was distinct from findings in P1 PKP2 Hom hearts where CX43 levels remain

unchanged (Fig. 3.10A). Given that prolonged *in vitro* culture of neonatal cardiomyocytes can improve cardiac intercalated disc structural maturation over time, it is possible that that reduction of CX43 from the intercalated disc in PKP2 Hom neonatal cardiomyocytes (cultured for six days) may also reflect molecular defects found in a “mature state”. To determine the electrophysiological impact of the PKP2 IVS9-1 G>C mutation *in vitro*, wild-type control and PKP2 Hom neonatal cardiomyocytes were subjected to field potential analysis through the xCELLigence RTCA CardioECR system. Field potential measurements serve as a proxy for aggregate electrical activity in cultured cardiomyocytes. Variability of field potential activity can be quantified through a field potential rhythm irregularity index, which is a measurement for the coefficient of variance within peaks of continuous field potential recordings. Representative field potential tracings from PKP2 Hom cardiomyocytes highlight large variability in intervals of field potential peaks, suggestive of arrhythmias (Fig. 3.10B). The larger values for field potential rhythm irregularity index in PKP2 Hom cardiomyocytes confirmed a significant increase in arrhythmias compared to wild-type control neonatal cardiomyocytes (Fig. 3.10C). This data demonstrates early consequences of the PKP2 IVS9-1 G>C mutation on desmosomal and gap junction protein loss, which are likely instrumental in driving baseline arrhythmias in PKP2 Hom neonatal cardiomyocytes.

Chapters 3-5 in part are currently being prepared for submission for publication of this material. Bradford, William H; Liang, Yan; Mataraarachchi, Nirosh; Zhang, Jing; Do, Aryanne; Gu, Yusu; Scheinman, Melvin; Peterson, Kirk L; Sheikh,

Farah. The dissertation author was the primary investigator and author of this material.

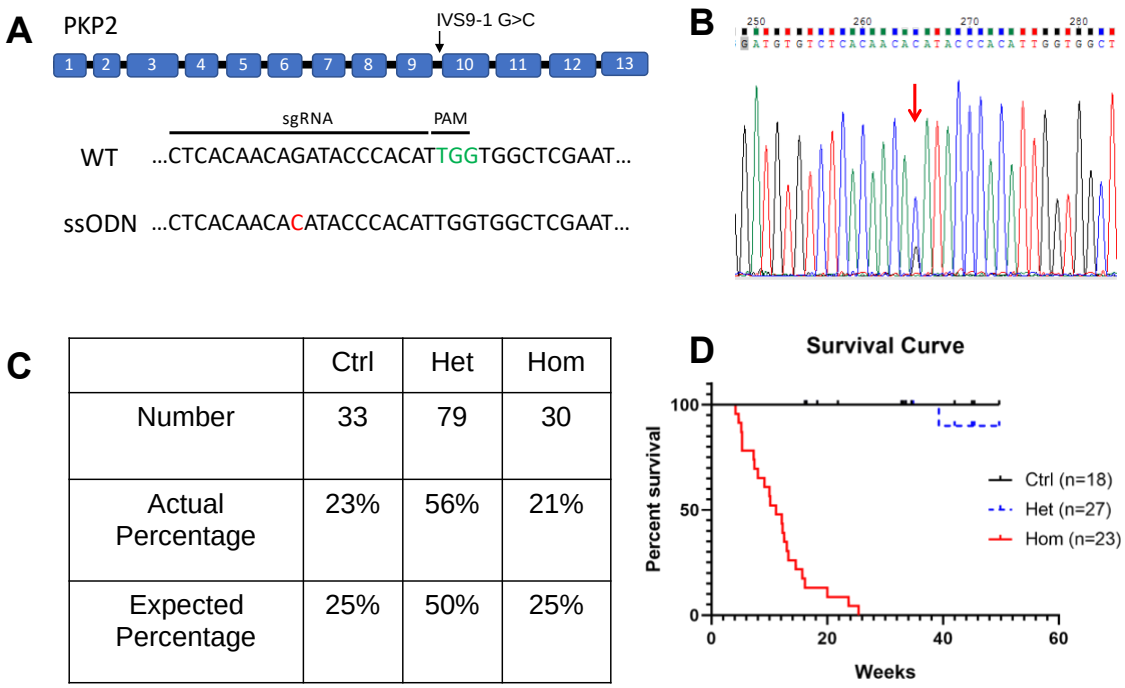

	Ctrl	Het	Hom
Number	33	79	30
Actual Percentage	23%	56%	21%
Expected Percentage	25%	50%	25%

Figure 3.1: Generation of a novel knock-in mouse model harboring a PKP2 splice acceptor site mutation. **A.** Schematic demonstrating genomic location for PKP2 IVS9-1 G>C mutation, sgRNA and PAM sequences, and ssODN with mutation template. **B.** Sanger sequencing of genomic DNA from founder PKP2 IVS9-1 G>C Het mice. **C.** Table recording Mendelian ratios of Ctrl, PKP2 Het mutant, and PKP2 Hom mutant numbers at weaning (three weeks of age). **D.** Survival curve analysis of Ctrl, PKP2 Het mutant, and PKP2 Hom mutant mice.

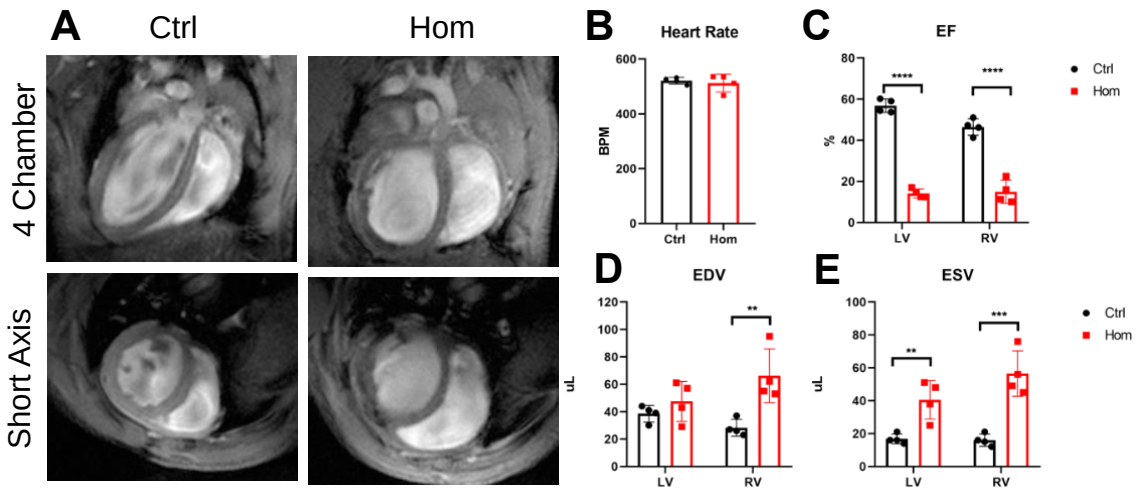

Figure 3.2: PKP2 Hom mice display biventricular mechanical dysfunction. **A.** Representative four-chamber and short axis cardiac MRI views from Ctrl and PKP2 Hom hearts at 4 weeks of age. Quantification of: **B.** heart rate, **C.** ejection fraction (EF), **D.** end diastolic volume (EDV), and **E.** end systolic volume (ESV) from cine MRI in Ctrl and PKP2 Hom hearts (n = 4 per group). Unpaired t-test for heart rate, two-way ANOVA with Tukey's multiple comparison test for additional measurements. ****, p<0.0001. ***, p<0.001. **, p<0.01.

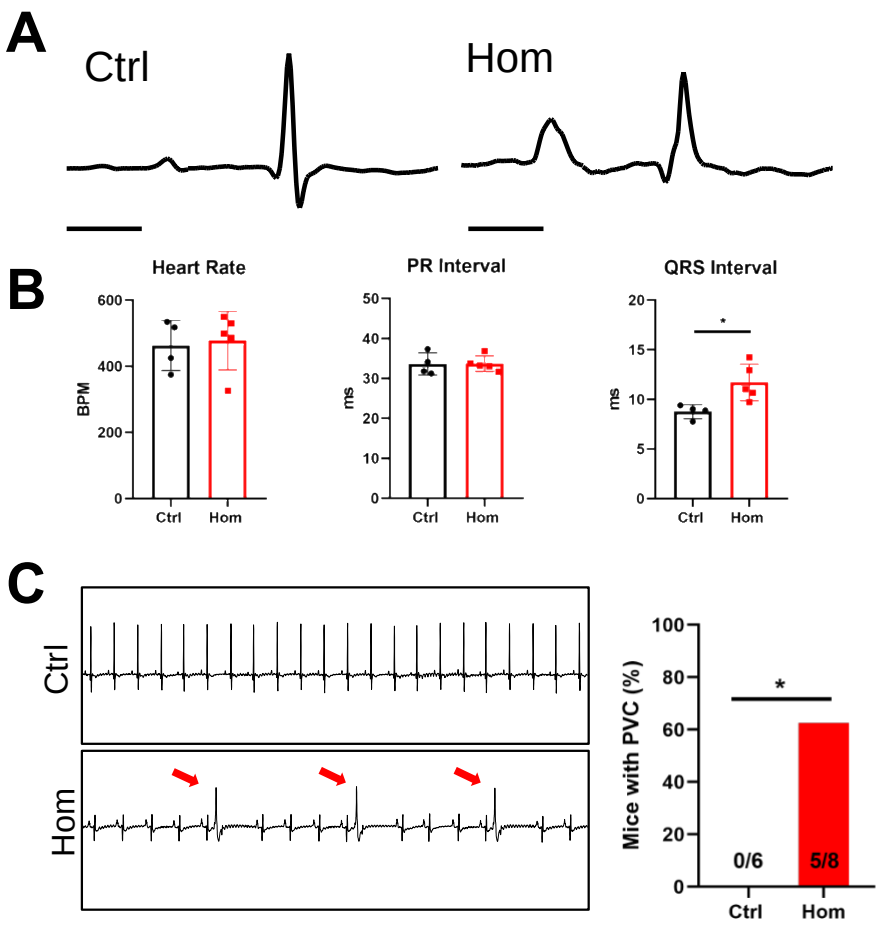

Figure 3.3: PKP2 Hom mice exhibit cardiac electrical dysfunction. A. Representative composite surface ECG tracings averaged from four beats in Ctrl and PKP2 Hom mice at four weeks of age. Scale bar = 10 ms. **B.** Quantification of heart rate, PR interval, and QRS interval from composite surface ECG tracings (n = 4-5 per group). Unpaired t-test, *, $p<0.05$. **C.** Representative ECG tracings from Ctrl and PKP2 Hom mice at four weeks of age (left) and quantification of mice demonstrating premature ventricular contractions (PVCs) (right), n = 6-8 per group. PVCs marked with red arrows. Fisher's Exact Test, *, $p<0.05$.

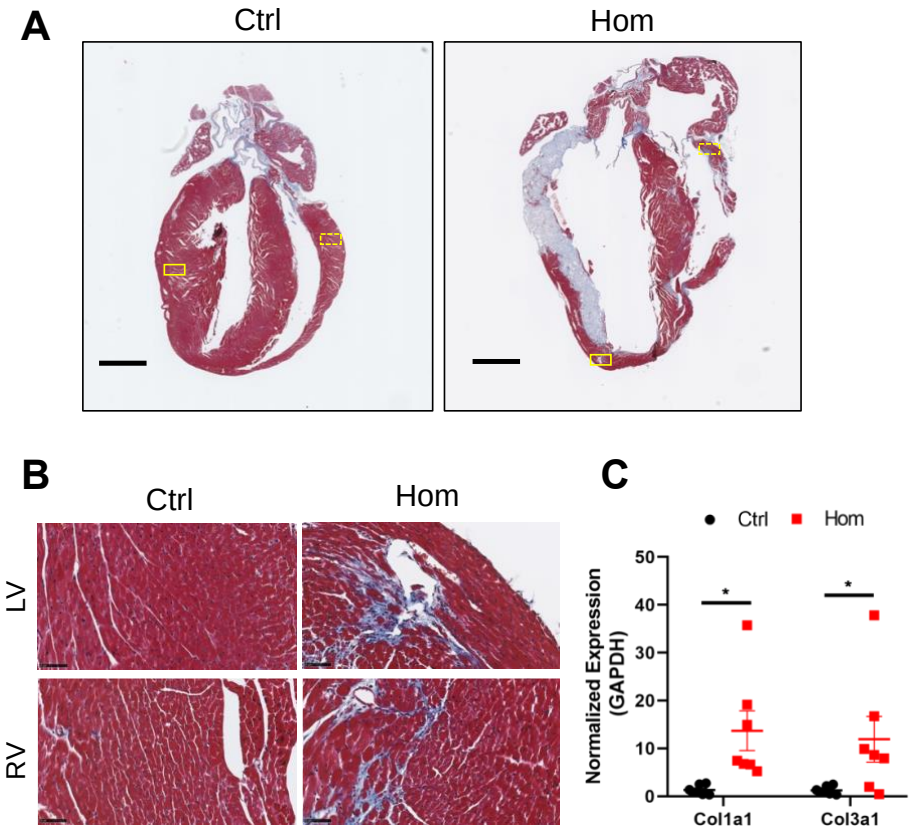

Figure 3.4: PKP2 Hom mice display fibrotic replacement of the ventricular myocardium. A. Representative cardiac sections stained with Masson's Trichrome from Ctrl and PKP2 Hom mice at 6 weeks of age. Scale bar = 1mm. **B.** Zoomed Masson's Trichrome stained sections for left ventricle (LV) taken from yellow solid box in **A** and right ventricle (RV) taken from yellow dashed box in **A**. Scale bar = 50 µm. **C.** Quantification of fibrosis with qRT-PCR for pro-fibrotic gene markers Col1a1 and Col3a1 (n = 5-7 per group). Unpaired t-test. *, $p<0.05$.

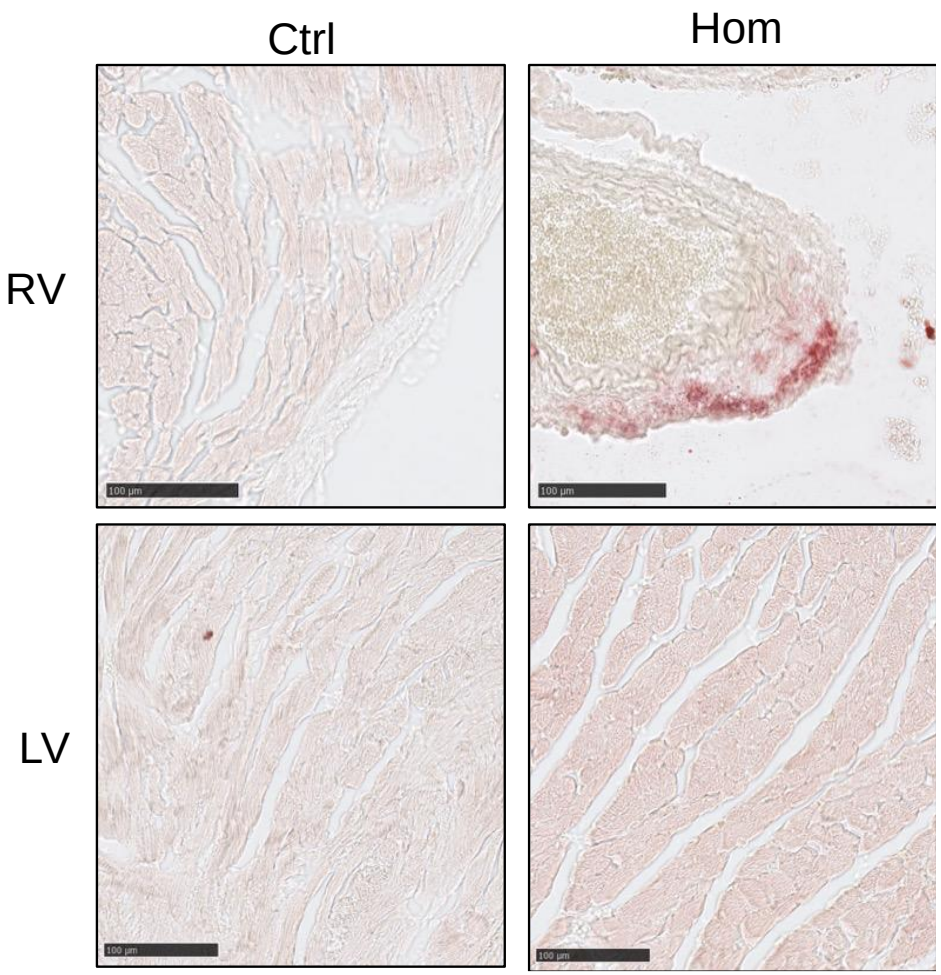

Figure 3.5: Lipid deposition in RV of PKP2 Hom hearts. Right ventricle (RV) and left ventricle (LV) sections stained with Oil Red O from Ctrl and PKP2 Hom hearts at 6 weeks of age. Scale bar = 100 µm.

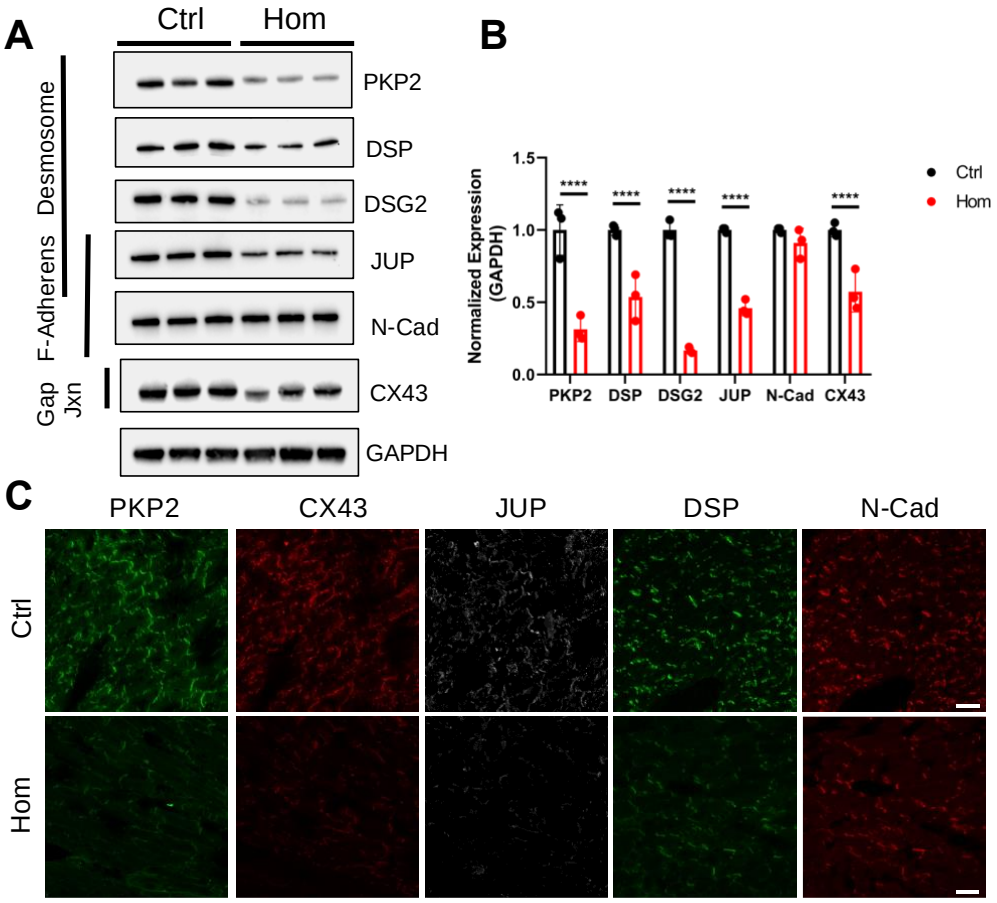

Figure 3.6: Desmosomal and gap junction disruption in PKP2 Hom hearts. A. Western blot analysis of desmosomal, fascia-adherens, and gap junction proteins at four weeks of age in Ctrl and PKP2 Hom hearts. GAPDH serves as the loading control. **B.** Quantification of protein expression in **A** normalized to GAPDH (n = 3 per group). Two-way ANOVA with Tukey's multiple comparison test. ****, $p<0.0001$. **C.** Immunofluorescence staining of desmosomal, fascia adherens, and gap junction proteins at four weeks of age in Ctrl and PKP2 Hom hearts. Scale bar = 25 µm.

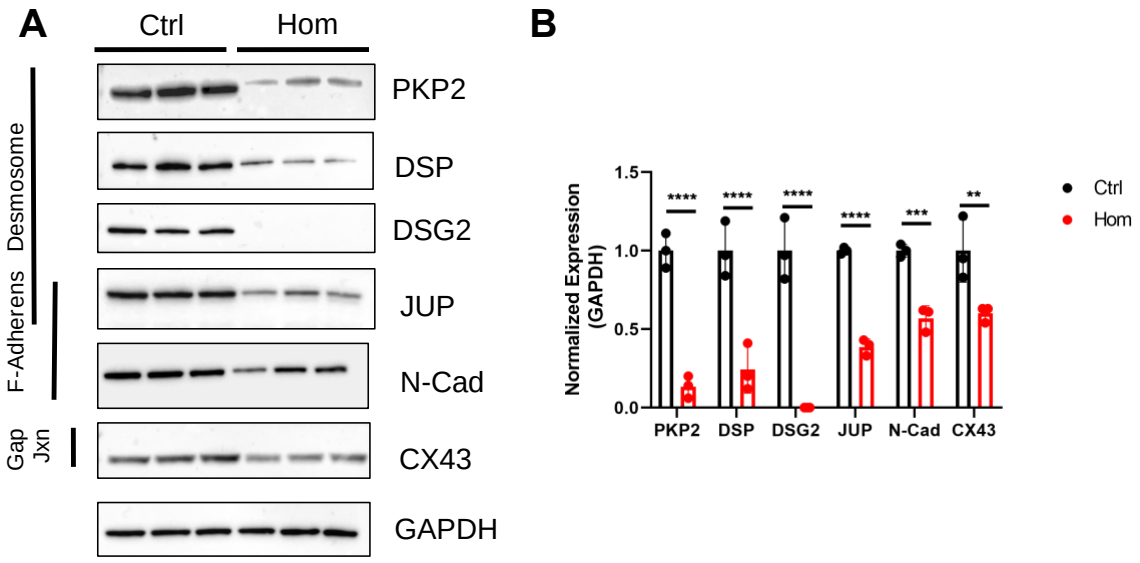

Figure 3.7: Late-stage disruption of the cardiac intercalated disc in PKP2 Hom hearts. A. Western blot analysis of desmosomal, fascia adherens, and gap junction proteins at eight weeks of age in Ctrl and PKP2 Hom hearts. GAPDH serves as the loading control. **B.** Quantification of protein expression in **A** normalized to GAPDH (n = 3 per group). Two-way ANOVA with Tukey's multiple comparison test. ****, $p<0.0001$. ***, $p<0.001$. **, $p<0.01$.

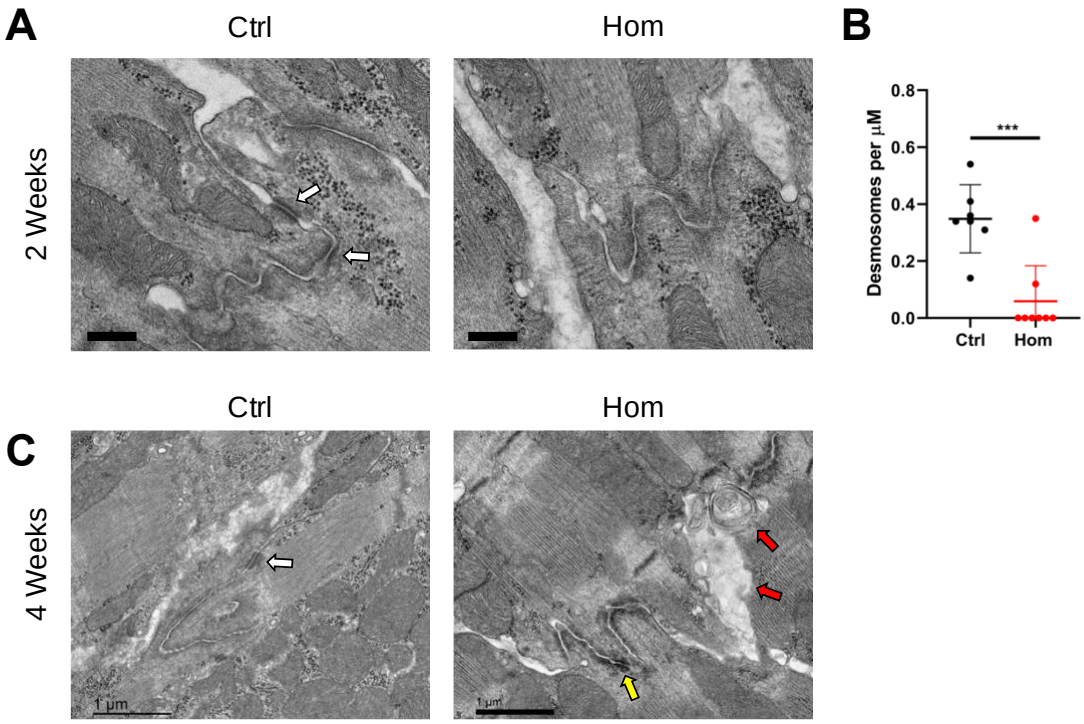

Figure 3.8: Desmosomal loss and degradation defects in PKP2 Hom hearts. A. Representative transmission electron micrographs from left ventricles of Ctrl and PKP2 Hom hearts at 2 weeks of age (n = 2 per group). White arrows denote healthy desmosomes. Scale bar = 250nm. **B.** Quantification of desmosomes per µm of membrane (n = 6-8 images per group taken from n = 2 hearts). Unpaired t-test. ***, p<0.001. **C.** Representative transmission electron micrographs from left ventricles of Ctrl and PKP2 Hom hearts at four weeks of age (n = 1-2 per group). White arrows denote healthy desmosomes. Yellow arrows denote disorganized desmosomes. Red arrows denote multi-membrane vesicles. Scale bar = 1 µm.

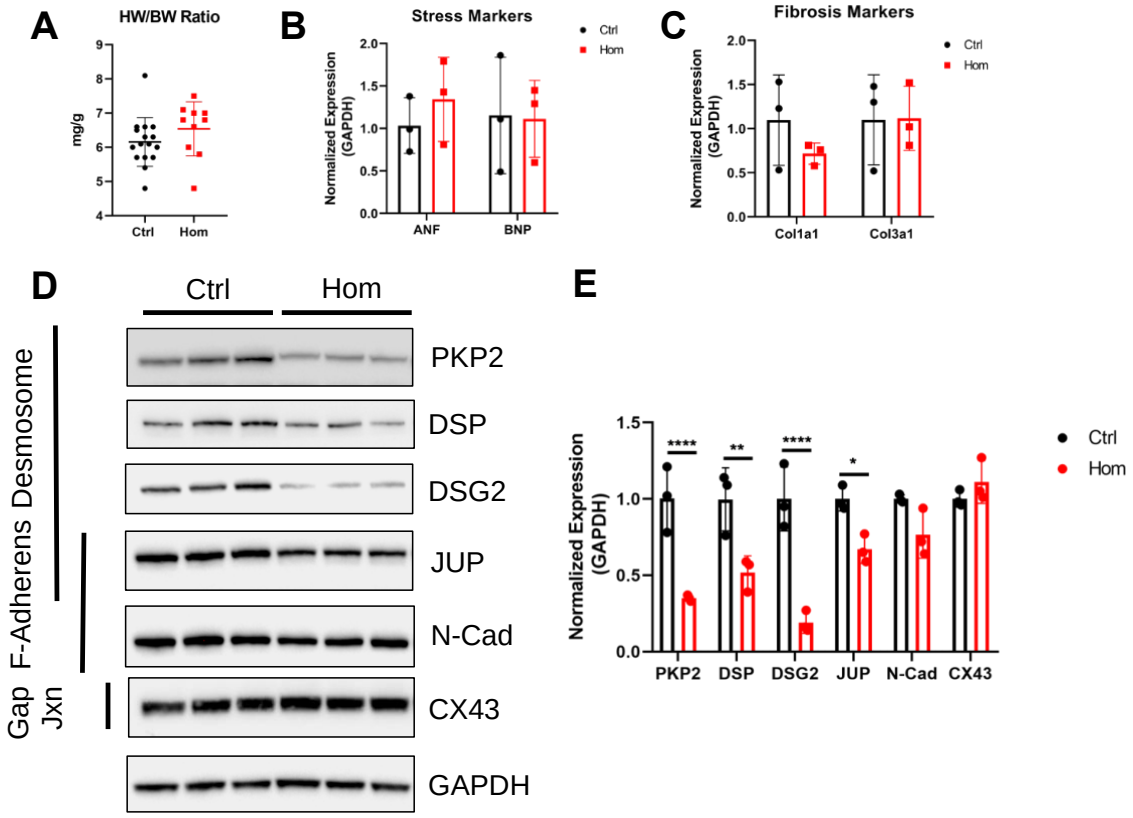

Figure 3.9: Neonatal (P1) PKP2 Hom hearts display desmosomal disruption in the absence of overt structural disease. A. Heart weight (HW) to body weight (BW) analysis in postnatal day 1 (P1) hearts from Ctrl and PKP2 Hom mice (n = 10-16 per group). Quantitative RT-PCR analysis of **B.** cardiac stress markers (ANF, BNP) and **C.** pro-fibrotic gene expression (Col1a1, Col3a1) in P1 hearts (n = 3 per group). **D.** Western blot analysis of desmosomal, fascia adherens, and gap junction proteins at P1 in Ctrl and PKP2 Hom hearts. GAPDH serves as the loading control. **E.** Quantification of protein expression in **D** normalized to GAPDH (n = 3 per group). Two-way ANOVA with Tukey's multiple comparison test. ****, $p<0.0001$. **, $p<0.01$. *, $p<0.05$.

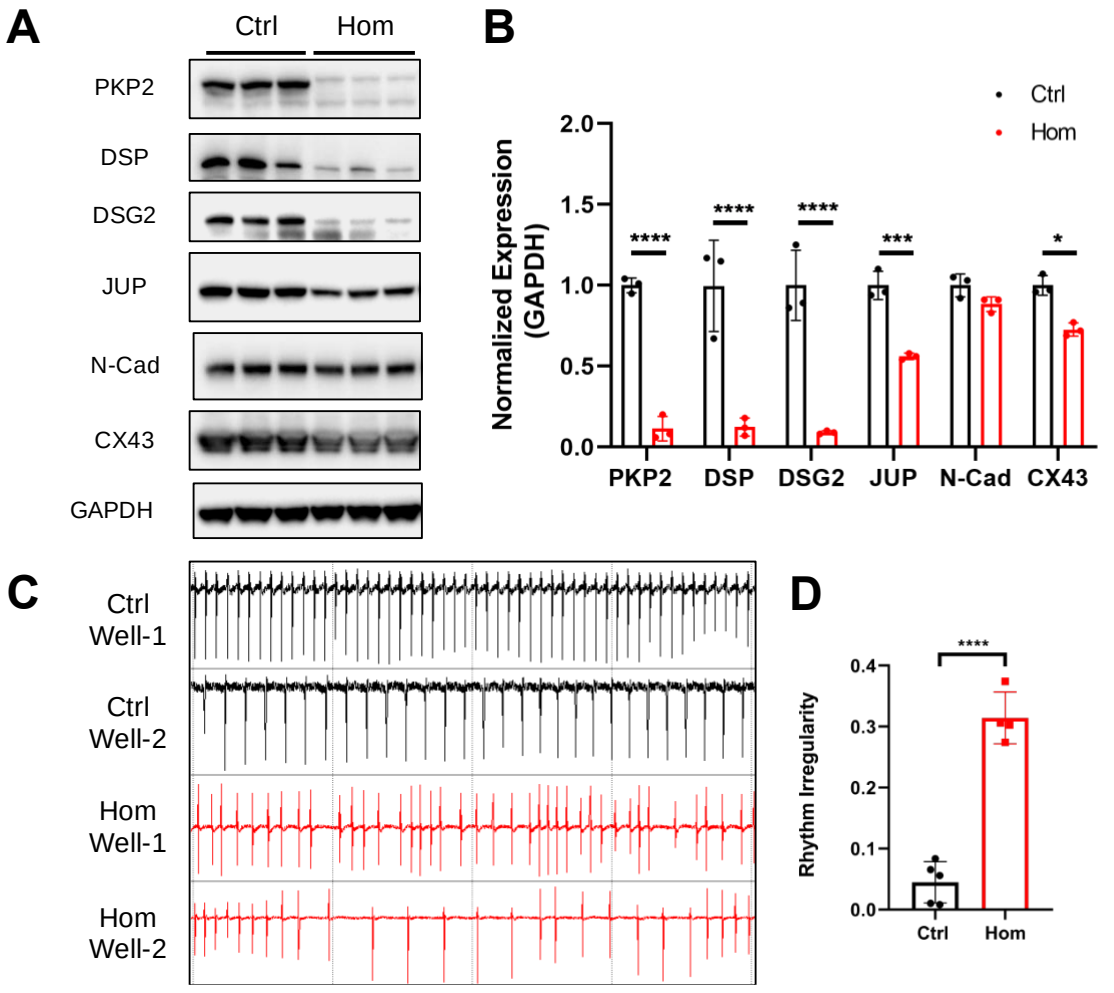

Figure 3.10: PKP2 Hom neonatal cardiomyocytes display desmosomal and gap junction deficits associated with baseline arrhythmias. A. Western blot analysis of desmosomal, fascia adherens, and gap junction proteins in neonatal cardiomyocytes from Ctrl and PKP2 Hom hearts. GAPDH serves as the loading control. **B.** Quantification of protein expression in **A** normalized to GAPDH (n = 3 per group). Two-way ANOVA with Tukey's multiple comparison test. ****, $p<0.0001$. ***, $p<0.001$. *, $p<0.05$. **C.** Representative field potential tracings from Ctrl and PKP2 Hom neonatal cardiomyocytes. **D.** Quantification of field potential rhythm irregularity index (n = 4-5 per group). Unpaired t-test. ****, $p<0.0001$.

Chapter 4

Mechanistic Insights into PKP2 Splice Acceptor Site Mutations

4.1 RNA splicing analysis in PKP2 Hom hearts

Splice acceptor site mutations result in diverse outcomes on splicing and ultimately mRNA products (Attali, Warwar et al. 2009, Guernsey, Jiang et al. 2010, Watanabe, Hanawa et al. 2013, Groeneweg, Ummels et al. 2014). To determine the impact of the PKP2 IVS9-1 G>C splice acceptor site mutation on PKP2 mRNA products, cDNA was generated from isolated ventricular RNA of littermate wild-type control and PKP2 Hom hearts at four weeks of age. RT-PCR analysis of mouse PKP2 exons 5-13 revealed a single larger product in PKP2 Hom hearts at what appeared to be reduced levels to wild-type PKP2 in control hearts (Fig. 4.1A). A more focused RT-PCR analysis of the mutation locus using PKP2 exons 9-10 similarly revealed a larger mutant product in PKP2 Hom hearts in the absence of an endogenous PKP2 product (Fig. 4.1B). Quantitative RT-PCR analysis of PKP2 exons 9-10 demonstrated a significant reduction in PKP2 transcript levels within PKP2 Hom hearts (Fig. 4.1C), suggesting that the PKP2 IVS9-1 G>C splice acceptor site mutation impacted total PKP2 RNA levels. Sanger sequencing analyses demonstrated contiguous sequences between PKP2 exons 9 and 10 in wild-type control hearts, suggestive of splicing utilizing the canonical intron 9 splice acceptor site (Fig. 4.1D). However, sequencing analyses of PKP2 Hom hearts revealed an extra 54 base pairs between exons 9 and 10 (Fig. 4.1D), suggestive of utilization of an alternative upstream splice acceptor site within intron 9 and indicative of a partial intron 9 retention. BLAST nucleotide alignment between the mouse and human PKP2 genome demonstrates a conservation of the alternative upstream splice acceptor site within the intronic region (Fig. 4.2), suggesting the possibility that the

human PKP2 IVS10-1 G>C mutation may also result in partial intron retention. These data highlight the PKP2 IVS9-1 G>C splice site mutation triggers a partial intron retention resulting in significantly reduced levels of PKP2 transcripts.

4.2 PKP2 protein analysis in PKP2 Hom hearts

To assess the impact of the PKP2 IVS9-1 G>C splice acceptor site mutation on PKP2 protein products, PKP2 Hom hearts were subjected to western blot analysis and revealed the absence of endogenous PKP2 and presence of a higher molecular weight mutant PKP2 protein, which was at significantly reduced levels when compared to wild-type PKP2 levels in wild-type control hearts (Fig. 4.3A-B). Immunofluorescence microscopy was utilized to better understand the cellular localization of mutant PKP2 protein as it is the only form found in PKP2 Hom hearts, based on western blot analyses (Fig. 4.3C). Using the intercalated disc marker N-Cad, it appears that that mutant PKP2 is localized to the intercalated disc in PKP2 Hom hearts, albeit at reduced levels when compared to wild-type control hearts (Fig. 4.3C), which is consistent with findings from western blot analysis (Fig. 4.3A-B). These data altogether demonstrate that the PKP2 IVS9-1 G>C splice acceptor site mutation results in two protein consequences, which include (i) loss of endogenous PKP2 protein and (ii) appearance/gain of a higher molecular weight mutant PKP2 protein, which appears to retain intercalated disc localization.

4.3 Manipulation of wild-type and mutant PKP2 protein levels

To determine if desmosomal disruption is driven by a gain of function (toxicity of mutant PKP2) or loss of function (dose of PKP2) mechanism, adenoviral vectors were generated expressing either wild-type (Ad PKP2 WT) or mutant PKP2 protein (Ad PKP2 MUT) to assess the impact of their restoration (levels) on desmosomal disruption in PKP2 Hom neonatal cardiomyocytes (Fig. 4.4A). As previously shown, untreated PKP2 Hom neonatal cardiomyocytes displayed a significant reduction in the desmosomal components PKP2 (endogenous), DSP, DSG2, and JUP as well as appearance of higher molecular weight PKP2, when compared to wild-type control cardiomyocytes (Fig. 4.4B-C), while fascia adherens proteins remained unchanged (Fig. 4.4B-C). However, Ad PKP2 WT treated PKP2 Hom neonatal cardiomyocytes demonstrated improvements in DSP, DSG2 and JUP expression in PKP2 Hom neonatal cardiomyocytes when compared to uninfected PKP2 Hom cardiomyocytes (Fig. 4.4B-C). Similarly, PKP2 Hom neonatal cardiomyocytes treated with Ad PKP2 MUT demonstrated improved DSP, DSG2 and JUP protein expression when compared to uninfected PKP2 Hom cardiomyocytes (Fig. 4.4B-C). Fascia adherens protein levels remained unchanged following either adenovirus treatment (Fig. 4.4B-C). Since restoration of either wild-type or mutant PKP2 protein was sufficient to increase desmosomal protein levels, these data highlight that loss of PKP2 protein dose is the driver of desmosomal disruption in PKP2 Hom neonatal cardiomyocytes. These data further set the stage to exploit PKP2 restoration strategies as a means to circumvent desmosomal disruption in ARVC settings.

Chapters 3-5 in part are currently being prepared for submission for publication of this material. Bradford, William H; Liang, Yan; Mataraarachchi, Nirosh; Zhang, Jing; Do, Aryanne; Gu, Yusu; Scheinman, Melvin; Peterson, Kirk L; Sheikh, Farah. The dissertation author was the primary investigator and author of this material.

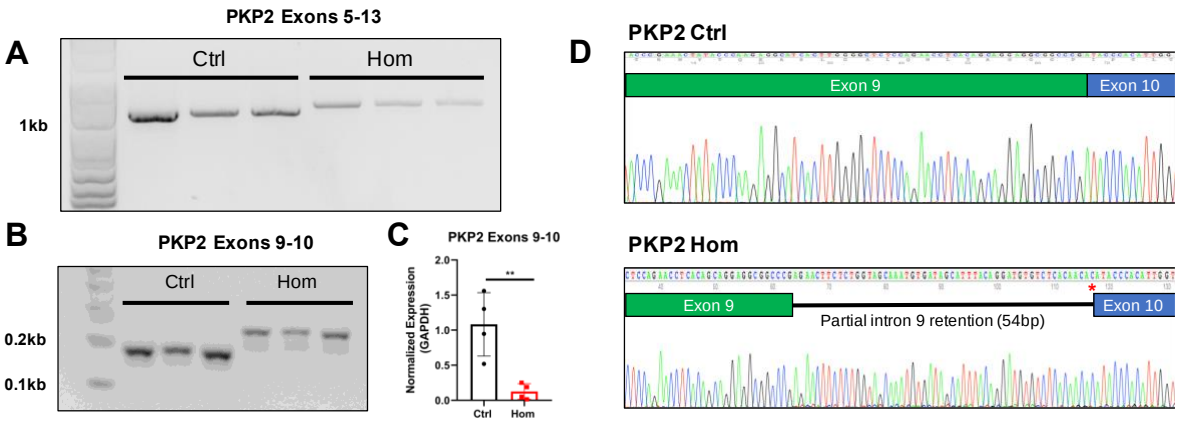

Figure 4.1: PKP2 partial intron retention and reduced transcript levels in PKP2 Hom hearts. A. RT-PCR analysis of PKP2 exons 5-13 in Ctrl and PKP2 Hom hearts at four weeks of age. **B.** RT-PCR analysis of PKP2 exons 9-10 in Ctrl and PKP2 Hom hearts at four weeks of age. **C.** qRT-PCR analysis of PKP2 exons 9-10 in Ctrl and PKP2 Hom hearts (n = 4 per group). Unpaired t-test, **, $p<0.01$. **D.** Sequencing analysis of RT-PCR products from Ctrl and PKP2 Hom hearts. * denotes mutation site.

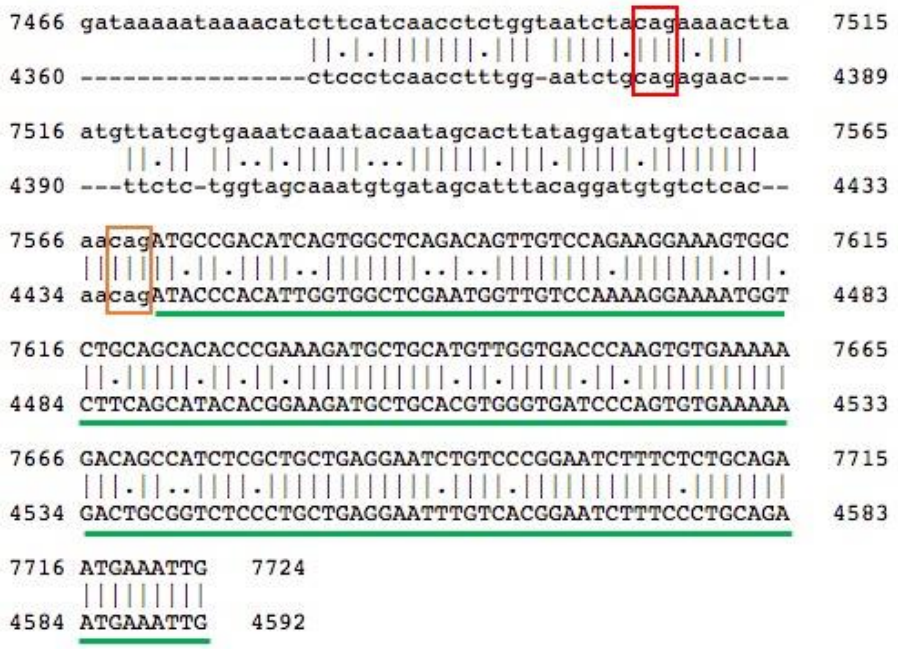

Figure 4.2: Conserved alternative upstream splice acceptor site location in PKP2 human intron 10 and its correlate mouse intron 9. Sequence alignment of human (top) and mouse (bottom) genomic DNA at PKP2 mutation locus. Green underline marks exons, orange box marks canonical splice acceptor sites, and red box marks alternative upstream splice acceptor sites within intronic sequence.

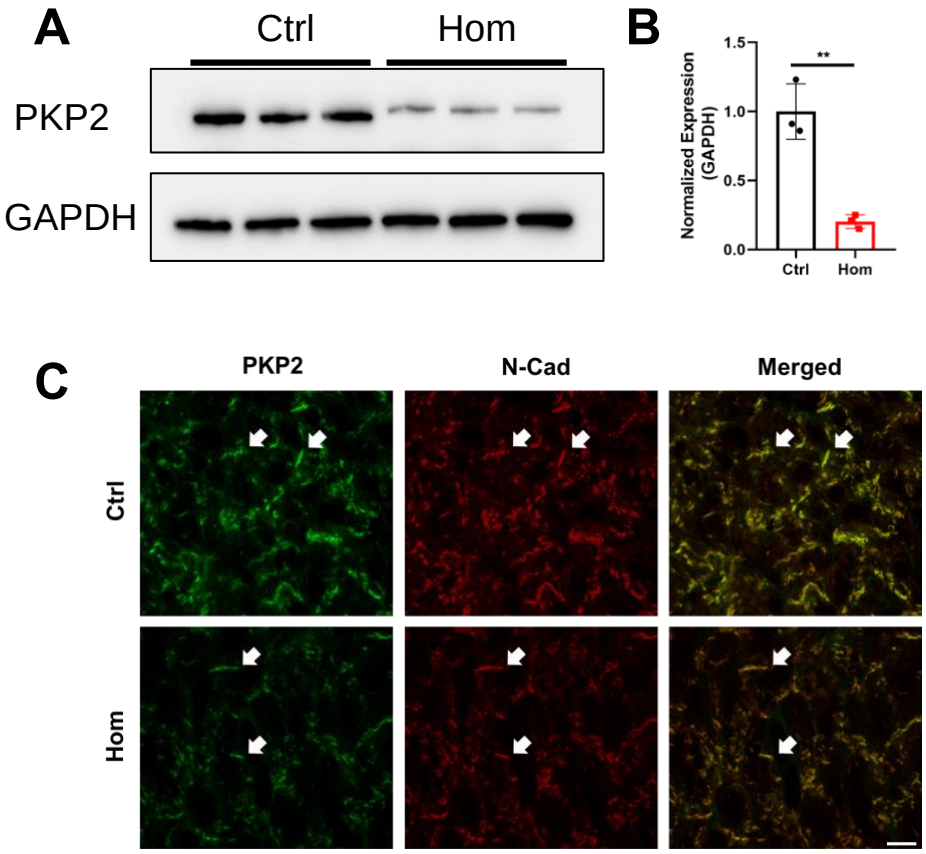

Figure 4.3: PKP2 Hom hearts exhibit reduced levels of mutant PKP2 maintained at the proper junctional localization. A. Western blot analysis of PKP2 protein in Ctrl and PKP2 Hom hearts at four weeks of age. GAPDH serves as the loading control. **B.** Quantification of protein expression in **A** normalized to GAPDH (n = 3 per group). Unpaired t-test **, $p<0.01$. **C.** Immunofluorescence staining of PKP2 (green) and N-Cad (red) in P1 Ctrl and PKP2 Hom hearts. White arrows mark PKP2 and N-Cad junctional localization. Scale bar = 8 μm.

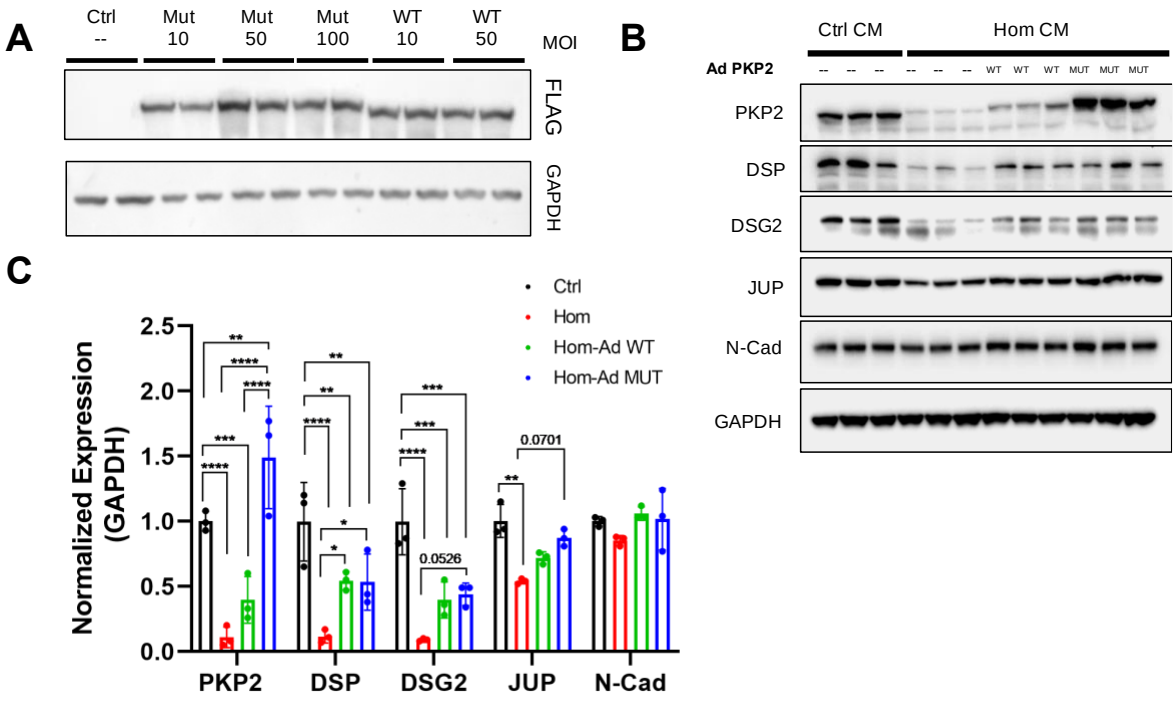

Figure 4.4: Increasing wild-type and mutant PKP2 protein levels rescues desmosomal protein loss *in vitro*. A. Western blot analysis of FLAG-tagged adenovirus vectors expressing PKP2 wild-type (Ad PKP2 WT) or PKP2 mutant (Ad PKP2 MUT) protein in wild-type neonatal cardiomyocytes at various multiplicities of infection (MOI) using FLAG antibodies. GAPDH serves as the loading control. **B.** Western blot analysis of desmosomal and fascia adherens junction proteins in Ctrl neonatal cardiomyocytes and PKP2 Hom neonatal cardiomyocytes uninfected (--), with PKP2 WT adenovirus, or PKP2 MUT adenovirus. GAPDH serves as the loading control. **C.** Quantification of protein expression in **B** normalized to GAPDH (n = 3 per group). Two-way ANOVA with Tukey's multiple comparison test. ****, p<0.0001. ***, p<0.001. **, p<0.01. *, p<0.05. Uninfected Ctrl and PKP2 Hom CM western blot data in Figure 4.4 are also presented in Figure 3.10.

Chapter 5

In Vivo Restoration of PKP2 Protein Levels and Prevention of ARVC Disease Features and Mortality

5.1 Early PKP2 administration prevents rapid ARVC onset in PKP2 Hom mice

5.1.1 AAV9-mediated delivery of PKP2 successfully localizes to the cardiac intercalated disc in adult PKP2 Hom hearts

To determine the impact of wild-type PKP2 restoration on molecular and physiological function *in vivo*, an AAV delivery strategy was employed. The AAV approach was designed with an AAV9 serotype, as this has been previously shown to display high affinity for the heart (Zincarelli, Soltys et al. 2008). A cardiac troponin T (cTnT) promoter was utilized to ensure cardiomyocyte-selective gene expression (Bezzerides, Caballero et al. 2019). A FLAG sequence was tagged to the C-terminus of wild-type PKP2 to distinguish between endogenous and transduced PKP2 (Fig. 5.1A). Additional regulatory elements were utilized including (i) a Kozak sequence to facilitate translation initiation of PKP2, (ii) Woodchuck hepatitis virus posttranscriptional regulatory element (WPRE) allows for higher titer of packaged virus and higher transgene expression, and (iii) a bovine growth hormone polyadenylation signal (BGH-pA) allows for transcription termination and mRNA polyadenylation (Fig. 5.1A) (Manso, Hashem et al. 2020). PKP2 Hom pups at postnatal day 2 were injected intraperitoneally with AAV9 PKP2 at $5x10^{11}$ gc/mouse and analyzed at four weeks of age, a time point where all ARVC disease features are present (Fig. 5.1B). AAV delivery at neonatal stages (postnatal day 2) was selected to allow for sufficient AAV expression before the rapid ARVC disease development. Virus dose was determined based on previous studies utilizing neonatal AAV injection in a mouse model of catecholaminergic polymorphic ventricular tachycardia (Bezzerides, Caballero et al. 2019). Immunofluorescence microscopy analysis

showed FLAG positive staining localized to the cardiomyocyte intercalated disc in AAV9 PKP2 treated PKP2 Hom hearts, as evidenced by co-localization with the desmosomal marker JUP within cardiomyocytes marked by alpha-actinin staining (Fig. 5.1C). This data demonstrates that exogenous PKP2 can successfully localize to the cardiomyocyte intercalated disc following AAV9 delivery.

5.1.2 PKP2 restoration prevents cardiac intercalated disc dissolution in adult PKP2 Hom mice four weeks post-AAV9 delivery

To determine the impact of wild-type PKP2 protein restoration on cardiac intercalated disc protein homeostasis, western blot analysis was performed at four weeks post-AAV9 PKP2 treatment. Neonatal administration of AAV9 PKP2 was sufficient to restore PKP2 protein to endogenous levels in adult PKP2 Hom hearts (Fig. 5.2A-B). PKP2 restoration was also sufficient to significantly increase levels of other desmosomal components (DSP, DSG2, JUP), as well as the integral gap junction component CX43 (Fig. 5.2A-B) in adult PKP2 Hom hearts. The fascia adherens marker N-Cad remained unchanged at four weeks post-AAV9 treatment in mice, similar to untreated wild-type controls, and thus levels were not impacted by AAV9 PKP2 administration (Fig. 5.2A-B). These findings were in contrast to untreated PKP2 Hom mice, which demonstrated significant desmosomal (PKP2, DSP, DSG2, JUP) dissolution and gap junction (CX43) protein reduction (Fig. 5.2A-B). These findings highlight the selective ability of PKP2 to scaffold and reassemble cardiac intercalated disc components at and beyond the cardiac desmosome.

5.1.3 PKP2 restoration prevents cardiac mechanical dysfunction in adult PKP2 Hom mice four weeks post-AAV9 delivery

To determine the functional impact of AAV9 PKP2 treatment in PKP2 Hom mice, *in vivo* cardiac MRI was employed. Previous studies highlight the ability of MRI to accurately capture the complex remodeling of both ventricles during ARVC disease progression (Lyon, Mezzano et al. 2014, Liang, Lyon et al. 2021). Four week old wild-type control, neonatal PKP2 Hom mice treated with AAV9 GFP, and neonatal PKP2 Hom mice treated with AAV9 PKP2 were subjected to MRI analysis. Endocardial borders were segmented at end-diastole and end-systole to generate chamber volumes and EFs. No significant changes in heart rates were observed in PKP2 Hom mice treated with AAV9 PKP2 when compared to PKP2 Hom mice treated with AAV9 GFP or wild-type controls (Fig. 5.3B), suggesting anesthesia does not preferentially influence cardiac function in one group. PKP2 Hom mice treated with AAV9 PKP2 displayed a preservation of end-diastolic and end-systolic volumes in both left and right ventricles similar to wild-type controls (Fig. 5.3D-E). Representative SAX MRI images further highlighted the prevention of left and right ventricular chamber dilatation in PKP2 Hom mice treated with AAV9 PKP2 (Fig. 5.3A). AAV9 PKP2 treatment also prevented cardiac dysfunction as PKP2 Hom mice exhibited left and right ventricular EFs indistinguishable from wild-type controls (Fig. 5.3C). These findings are in stark contrast to PKP2 Hom mice treated with AAV9 GFP, which developed (i) significantly increased end-diastolic volumes in the right ventricle, (ii) significantly increased end-systolic volumes in both the left and right ventricle, as well as (iii) significantly reduced EF in both left and right ventricles when

compared to both littermate wild-type controls and PKP2 Hom mice receiving AAV9 PKP2 (Fig. 5.3C-E). These data were also further reflected via SAX MRI images that highlighted pathological cardiac chamber remodeling, particularly in the right ventricle of PKP2 Hom mice treated with AAV9 GFP when compared to AAV9 PKP2 treated PKP2 Hom mice and untreated wild-type controls (Fig. 5.3A). These results show the ability of neonatal AAV9 PKP2 treatment to prevent pathological cardiac chamber dilatation and dysfunction in PKP2 Hom mice.

5.1.4 PKP2 restoration prevents cardiac electrical dysfunction in adult PKP2 Hom mice four weeks post-AAV9 delivery

To assess the impact of AAV9 PKP2 on cardiac electrical function in PKP2 Hom mice, surface ECG analysis was utilized. Composite surface ECG tracings were generated for wild-type control, PKP2 Hom mice treated with AAV9 GFP, and PKP2 Hom mice treated with AAV9 PKP2 at four weeks post-neonatal AAV9 administration (Fig. 5.4A). Heart rate and PR interval (reflective of time it takes for an electrical impulse to travel from sinoatrial node in the atria and across atrioventricular node to the ventricle) analysis revealed no differences between wild-type control, PKP2 Hom mice treated with AAV9 GFP, and PKP2 Hom mice treated with AAV9 PKP2 (Fig. 5.4B-C). However, QRS intervals in PKP2 Hom mice treated with AAV9 PKP2 were indistinguishable from wild-type controls (Fig. 5.4D), demonstrating prevention of ventricular depolarization delay in PKP2 Hom mice with AAV9 PKP2 treatment. These findings further coincided with the absence of PVCs in PKP2 Hom mice treated with AAV9 PKP2 (Fig. 5.4E-F) and were reflective of wild-type behavior as

wild-type controls do not display PVCs (Fig. 5.4E-F). These findings are in contrast to PKP2 Hom mice treated with AAV9 GFP, which (i) developed a significantly widened QRS interval indicative of ventricular depolarization delay (Fig. 5.4D) and (ii) harbored a prevalent incidence (60% of mice) of PVCs (Fig. 5.4E-F). This data indicates that neonatal administration of AAV9 PKP2 can also prevent the electrical disease (ventricular electrical abnormalities) found in adult PKP2 Hom hearts, reminiscent of ARVC.

5.1.5 PKP2 restoration prevents pathological cardiac tissue remodeling in adult PKP2 Hom mice four weeks post-AAV9 delivery

To understand the impact of AAV9 PKP2 on cardiac morphology and tissue composition in PKP2 Hom mice, gross morphological and histological analyses were utilized. Heart weight to body weight ratios in PKP2 Hom hearts treated with AAV9 PKP2 were indistinguishable from wild-type control mice (Fig. 5.5A), These findings were in contrast to PKP2 Hom hearts treated with AAV9 GFP, which displayed significantly larger heart weight to body weight ratios, indicative of pathological remodeling (Fig. 5.5A). Hematoxylin and eosin (H&E) staining of whole heart sections revealed that cardiac dimensions and cardiac muscle integrity in PKP2 Hom mice treated with AAV9 PKP2 were indistinguishable from wild-type controls (Fig. 5.5B). In contrast, PKP2 Hom mice treated with AAV9 GFP demonstrated enlarged left and right ventricular chambers and extensive hematoxylin (nuclear) staining in the left ventricle free wall, which is suggestive of cardiomyocyte necrosis and calcification based on previous studies in DSG2 deficient mouse models (Fig. 5.5B) (Kant,

Holthofer et al. 2015). Masson's Trichrome (collagen) stains revealed that cardiac sections from PKP2 Hom mice treated with AAV9 PKP2 were indistinguishable from wild-type controls, suggesting the absence of fibrosis (Fig. 5.5C). In contrast, extensive fibrotic areas were present in both left and right ventricles of PKP2 Hom mice treated with AAV9 GFP (Fig. 5.5C). Quantitative RT-PCR for fibrotic gene expression (Col1a1) also revealed a prevention of fibrotic remodeling within PKP2 Hom mice treated with AAV9 PKP2 as they were indistinguishable from wild-type controls (Fig. 5.5D). In contrast, PKP2 Hom mice treated with AAV9 GFP exhibited a significant induction of fibrotic gene expression (Fig. 5.5D). These data further highlight that AAV9 PKP2 treatment of neonatal PKP2 Hom mice can prevent pathological cardiac chamber remodeling and fibrosis in adult PKP2 Hom mice.

5.2 Neonatal PKP2 administration prevents ARVC progression and mortality in adult PKP2 Hom mice at six months of age

5.2.1 Neonatal AAV9 PKP2 treatment prevents mortality and cardiac dysfunction in adult PKP2 Hom mice at six months of age

To determine the long-term effects of neonatal AAV9 PKP2 treatment, survival analysis was assessed in wild-type control, untreated PKP2 Hom, and PKP2 Hom mice treated with AAV9 PKP2 until six months of age. Untreated PKP2 Hom mice display a median survival of 11 weeks, with none surviving to six months of age (Fig. 5.6). AAV9 PKP2 treatment of neonatal PKP2 Hom mice prevented mortality and were only sacrificed at six months of age for endpoint analysis (Fig. 5.6). These data suggest that AAV9 PKP2 can provide lifespan benefits to PKP2 Hom mice.

Cardiac mechanical function was measured via MRI at six months following neonatal AAV9 PKP2 treatment. For the six month long-term study untreated wild-type control and PKP2 Hom mice treated with AAV9 PKP2 were utilized. Historical controls using AAV9 GFP-treated PKP2 Hom mice at six weeks of age were included as a disease-relevant control group (data from Fig. 5.11E), as no untreated PKP2 Hom mice survive to six months of age. No differences in heart rates were observed between untreated wild-type control, PKP2 Hom mice treated with AAV9 PKP2, and six week old PKP2 Hom mice treated with AAV9 GFP (historical disease control) (Fig. 5.7C). MRI analysis revealed that long-term AAV9 PKP2 treatment can prevent cardiac dysfunction in PKP2 Hom mice, as left ventricular EF was indistinguishable between control and PKP2 Hom mice treated with AAV9 PKP2 (Fig. 5.7D). These data are in contrast to the historical disease control (six week old PKP2 Hom mice treated with AAV9 GFP) group that displayed significantly lower left and right ventricular EFs (Fig. 5.7D). Representative SAX images further demonstrate that left and right ventricular chamber dimensions in PKP2 Hom mice treated with AAV9 PKP2 were indistinguishable from wild-type controls (Fig. 5.7A-B). These results suggest AAV9 PKP2 can prevent long-term cardiac mechanical dysfunction in PKP2 Hom mice.

Electrical function was assessed via composite surface ECG tracing analysis of wild-type control mice and PKP2 Hom mice treated with AAV9 PKP2 for six months. No significant differences in heart rates could be observed between AAV9 PKP2 treated PKP2 Hom mice and wild-type controls (Fig. 5.8A-B). Neonatal AAV9 PKP2 treatment prevented ventricular depolarization delay (QRS interval) and the

appearance of PVCs in PKP2 Hom mice at six months after AAV9 PKP2 treatment, and thus, were indistinguishable from wild-type controls (Fig. 5.8D; Fig. 5.8E). This data highlights that early administration of AAV9 PKP2 can provide long term protection from pathogenic QRS widening (ventricular depolarization abnormality) and PVCs in adult PKP2 Hom mice.

5.2.2 Neonatal AAV9 PKP2 treatment prevents cardiac intercalated disc dissolution in adult PKP2 Hom mice at six months of age

To determine the impact of PKP2 restoration on cardiac intercalated disc protein levels, western blot analysis was performed at six months of age in untreated wild-type control and PKP2 Hom mice with neonatal treatment of AAV9 PKP2. AAV9 PKP2 treatment prevented dissolution of the cardiac intercalated disc in PKP2 Hom mice (Fig. 5.9A-B). PKP2 protein levels were significantly increased in PKP2 Hom hearts when compared to wild-type control hearts (Fig. 5.9A-B). The increase in PKP2 protein levels is likely attributed to persistent PKP2 expression from the AAV9 vector and is not anticipated to be pathogenic as mortality is prevented and cardiac function preserved in PKP2 Hom mice at this time point. This restoration prevented loss of desmosomal (DSP, DSG2, JUP), fascia adherens (N-Cad), and gap junction (CX43) proteins in PKP2 Hom hearts treated with AAV9 PKP2, as they were indistinguishable from wild-type control hearts (Fig. 5.9A-B). In contrast, untreated PKP2 Hom mice display a significant reduction in desmosomal, fascia adherens, and gap junction protein levels by eight weeks of age when compared to wild-type

controls (Fig. 3.7). These data demonstrate that PKP2 restoration can provide long-term protection to the cardiac intercalated disc in PKP2 Hom hearts.

5.2.3 Neonatal AAV9 PKP2 treatment does not impact liver enzymes in adult PKP2 Hom mice at six months of age

The liver has been reported as a significant off-target location for systemic AAV administration, which can incur damage and necrosis with high doses of AAV (Hinderer, Katz et al. 2018). Elevation of circulating blood serum liver enzymes can serve as an indication for AAV-induced liver damage, with alkaline phosphatase (ALP) and alanine transaminase (ALT) being commonly used markers (Hinderer, Katz et al. 2018) . Analysis of blood serum ALP and ALT revealed no differences between PKP2 Hom mice six months post-AAV9 PKP2 treatment and wild-type controls, with all recorded values falling within the normal limit for mice (Fig. 5.10A-B). These data demonstrate that long-term AAV9 PKP2 treatment has no overt systemic effects on liver homeostasis.

5.3 AAV9 PKP2 treatment of diseased adult PKP2 Hom mice was sufficient to improve cardiac desmosomal protein levels, improve cardiac function, and prevent mortality

To determine whether PKP2 restoration could elicit beneficial effects in a clinically relevant setting and thus, in the presence of existing ARVC disease, AAV9 PKP2 was delivered via retro-orbital injection at $5x10^{11}$ gc/mouse to PKP2 Hom mice at four weeks of age, a time point where all classic ARVC features are present (Fig.

5.11A). The retro-orbital delivery route has previously been shown to be effective for AAV9 administration in adult mice (Bezzerides, Caballero et al. 2019). Based on previous studies (Manso, Hashem et al. 2020), a low dose of AAV9 PKP2 was utilized to minimize toxicity in PKP2 Hom mice. As early as two weeks after treatment, AAV9 PKP2 was able to resurrect desmosomal protein levels (PKP2, DSP, DSG2, JUP) in PKP2 Hom hearts (Fig. 5.11B). Littermate PKP2 Hom mice receiving AAV9 GFP injection displayed desmosomal dissolution (Fig. 5.11B). No differences were observed in heart rates between PKP2 Hom mice receiving AAV9 PKP2 or AAV9 GFP (Fig. 5.11D). However, quantitative functional analysis of serial SAX MRI studies demonstrate that AAV9 PKP2 treatment can circumvent mechanical dysfunction in PKP2 Hom mice as evidenced by significant improvements in left and right ventricular EFs compared to PKP2 Hom mice treated with AAV9 GFP (Fig. 5.11E). Representative SAX cardiac MRI at both end-diastole and end-systole highlight reduced left and right ventricular chamber dilatation in PKP2 Hom mice treated with AAV9 PKP2 versus littermate PKP2 Hom mice treated with AAV9 GFP (Fig. 5.11C). In addition, late-stage AAV9 PKP2 treatment of PKP2 Hom mice prevented mortality until the five month study endpoint (four months post-AAV9 injection) (Fig. 5.12). In contrast, 80% mortality was observed in PKP2 Hom mice treated with AAV9 GFP at this end point (Fig. 5.12). These results highlight that PKP2 restoration (even after two weeks of AAV9 PKP2 administration) is sufficient to reassemble the cardiac desmosome and this translates to improved cardiac mechanical function as well as prevention of mortality in PKP2 Hom mice, even in advanced stages of ARVC.

Chapters 3-5 in part are currently being prepared for submission for publication of this material. Bradford, William H; Liang, Yan; Mataraarachchi, Nirosh; Zhang, Jing; Do, Aryanne; Gu, Yusu; Scheinman, Melvin; Peterson, Kirk L; Sheikh, Farah. The dissertation author was the primary investigator and author of this material.

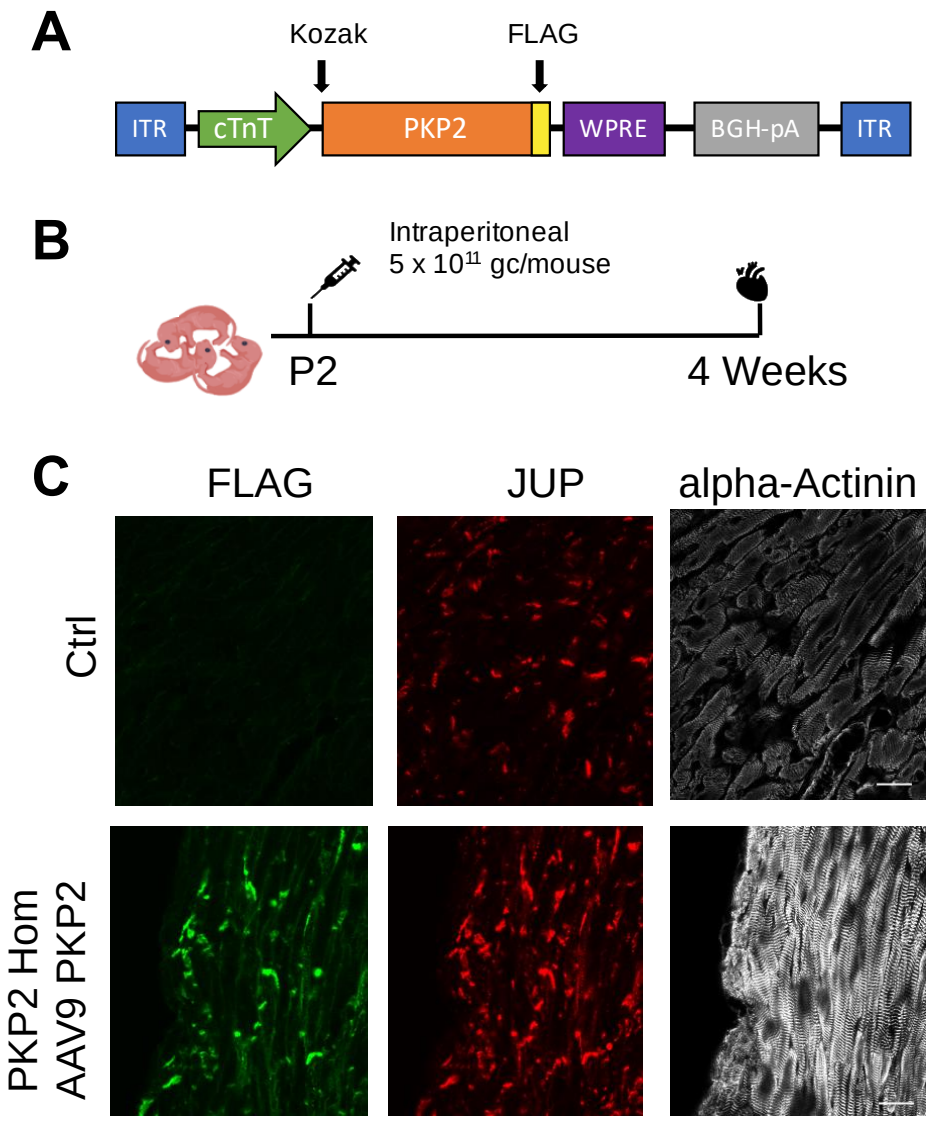

Figure 5.1: PKP2 localized to the cardiac intercalated disc following AAV9-delivery. A. Design of AAV9 PKP2 vector with inverted terminal repeats (ITR), cardiac troponin T (cTnT) promoter, Kozak sequence, PKP2 cDNA, C-terminal FLAG tag, Woodchuck hepatitis virus posttranscriptional regulatory element (WPRE), and bovine growth hormone polyadenylation signal (BGH-pA). **B.** Schemata of early neonatal delivery strategy and analysis time point. **C.** Representative immunofluorescence staining of FLAG (green), JUP (red), and alpha-actinin (white) at four weeks post-injection in uninfected wild-type control (Ctrl) and PKP2 Hom treated hearts treated with AAV9 PKP2. Scale bar = 20 µm.

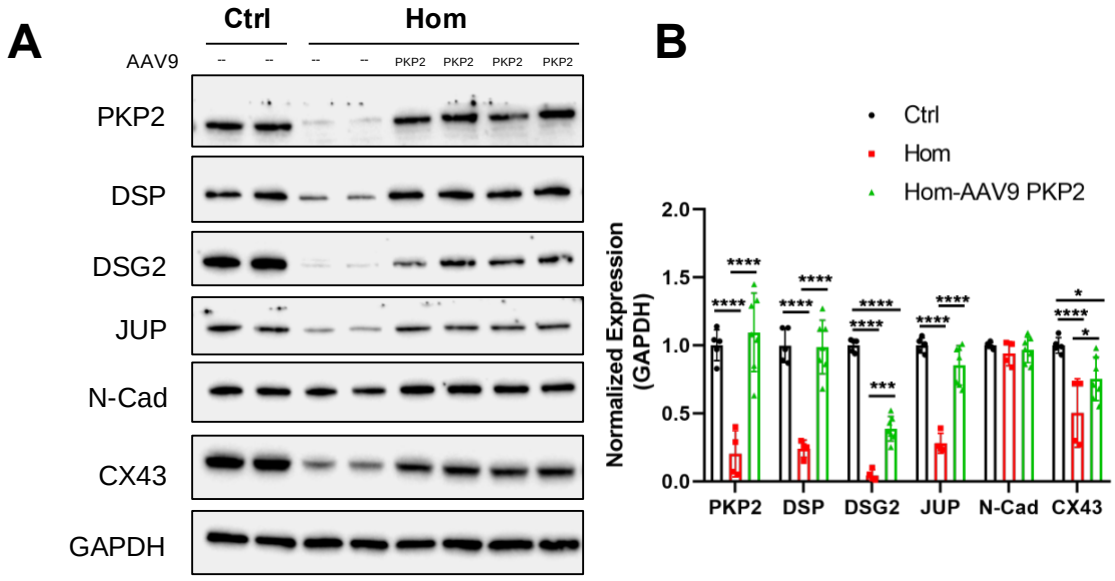

Figure 5.2: Neonatal AAV9 PKP2 administration can prevent intercalated disc protein dissolution in PKP2 Hom mouse hearts. A. Western blot analysis of desmosomal, fascia adherens, and gap junction proteins at four weeks post-injection in uninfected control (Ctrl), uninfected PKP2 Hom, and AAV9 PKP2 treated PKP2 Hom hearts. GAPDH serves as the loading control. **B.** Quantification of protein expression in **A** normalized to GAPDH (n = 4-7 per group). Two-way ANOVA with Tukey's multiple comparison test. ****, $p<0.0001$. ***, $p<0.001$. *, $p<0.05$.

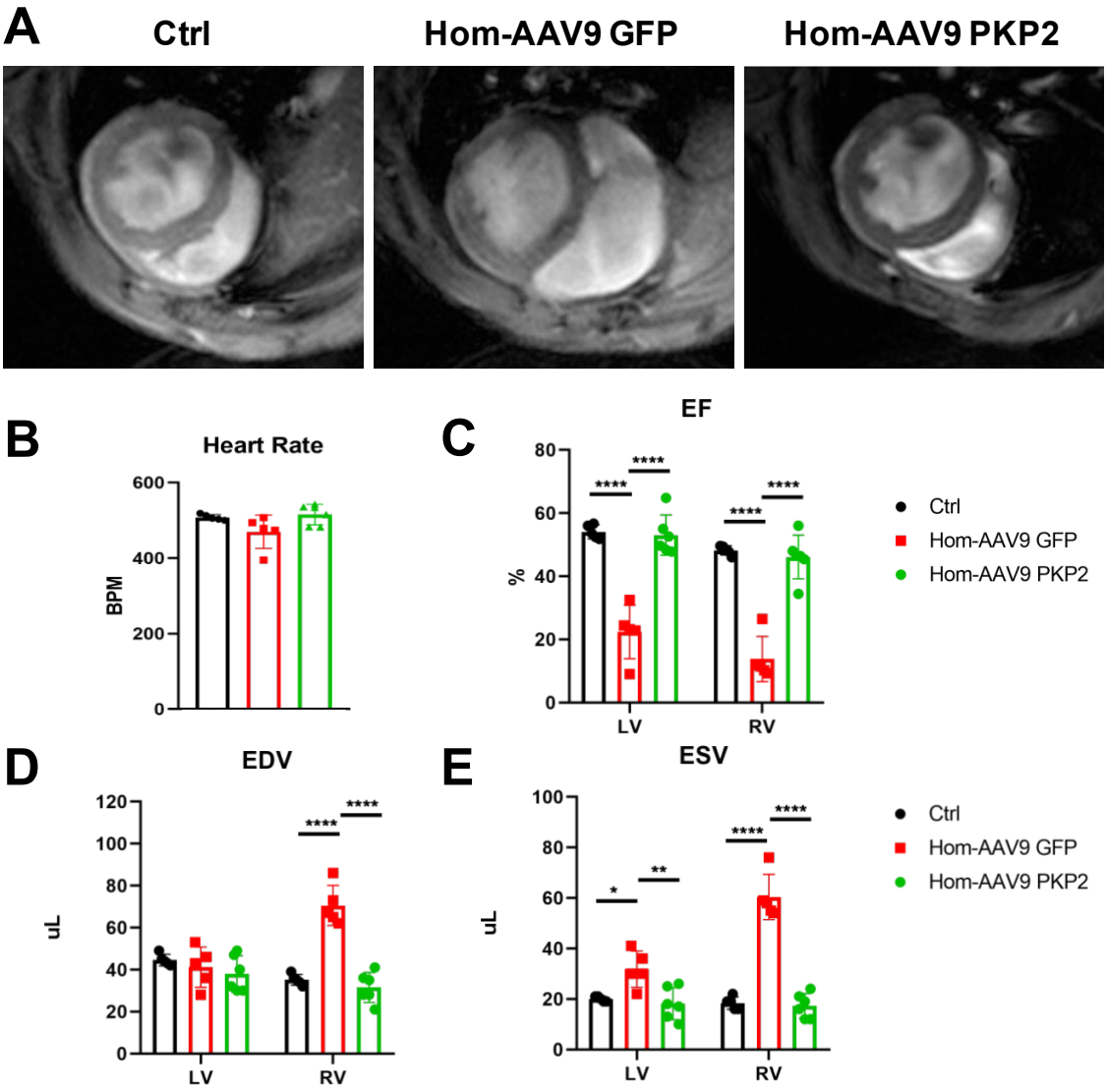

Figure 5.3: Neonatal AAV9 PKP2 administration prevents cardiac mechanical dysfunction in PKP2 Hom mouse hearts. A. Representative short-axis MRI from wild-type control (Ctrl), PKP2 Hom mice treated with AAV9 GFP, and PKP2 Hom mice treated with AAV9 PKP2. Quantification of **B.** heart rate, **C.** ejection fraction (EF), **D.** end diastolic volume (EDV), **E.** end systolic volume (ESV) (n = 5-6 per group). One-way ANOVA with Tukey's multiple comparison test for heart rate measurement. Two-way ANOVA with Tukey's multiple comparison test for additional measurements. ****, p<0.0001. **, p<0.01. *, p<0.05.

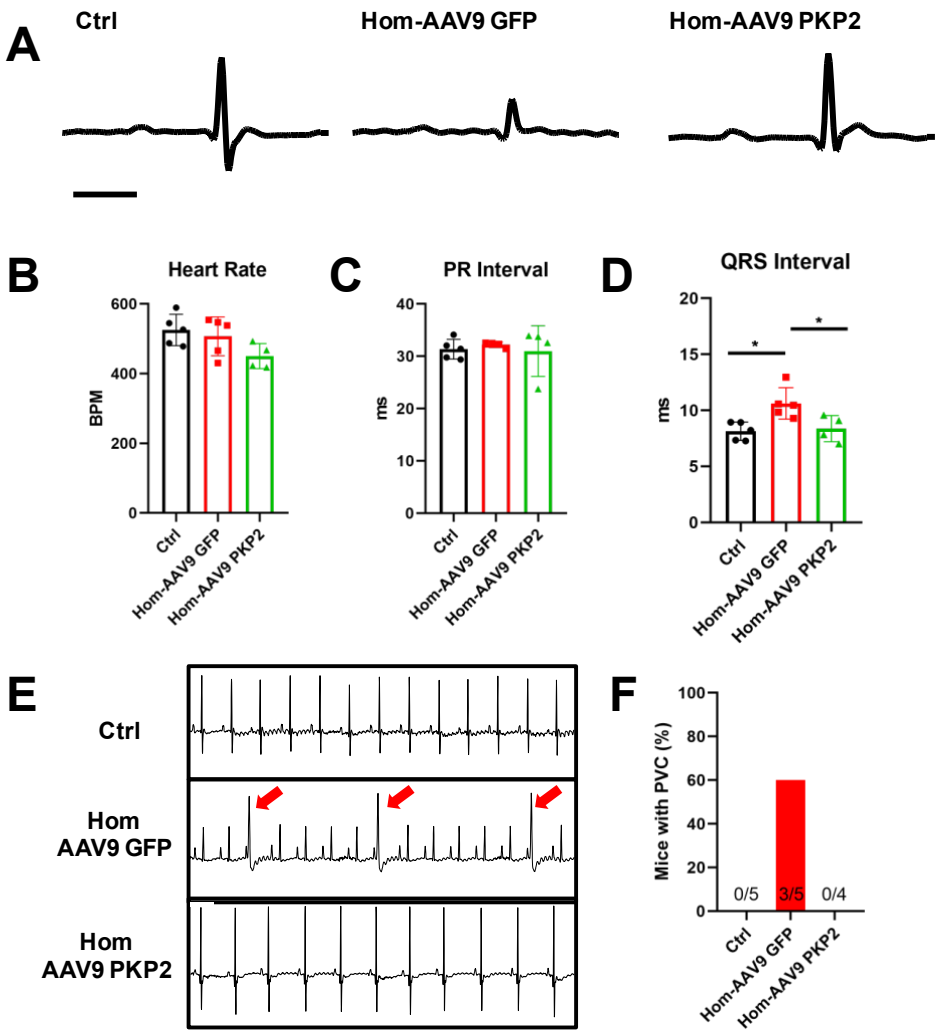

Figure 5.4: Neonatal AAV9 PKP2 administration prevents cardiac electrical dysfunction in PKP2 Hom mice. A. Representative composite surface ECG tracings averaged from four beats in wild-type control (Ctrl) and PKP2 Hom mice treated with AAV9-GFP or AAV9-PKP2 at four weeks of age. Scale bar = 10 ms. Quantification of **B.** heart rate, **C.** PR interval, and **D.** QRS interval from composite surface ECG tracings. One-way ANOVA with Tukey's multiple comparison test, *, $p<0.05$. **E.** Representative ECG tracings through time from Ctrl and PKP2 Hom mice treated with either AAV9 GFP or AAV9 PKP2 at four weeks of age. **F.** Quantification of mice demonstrating PVCs. PVCs marked with red arrows. (n = 4-5 per group).

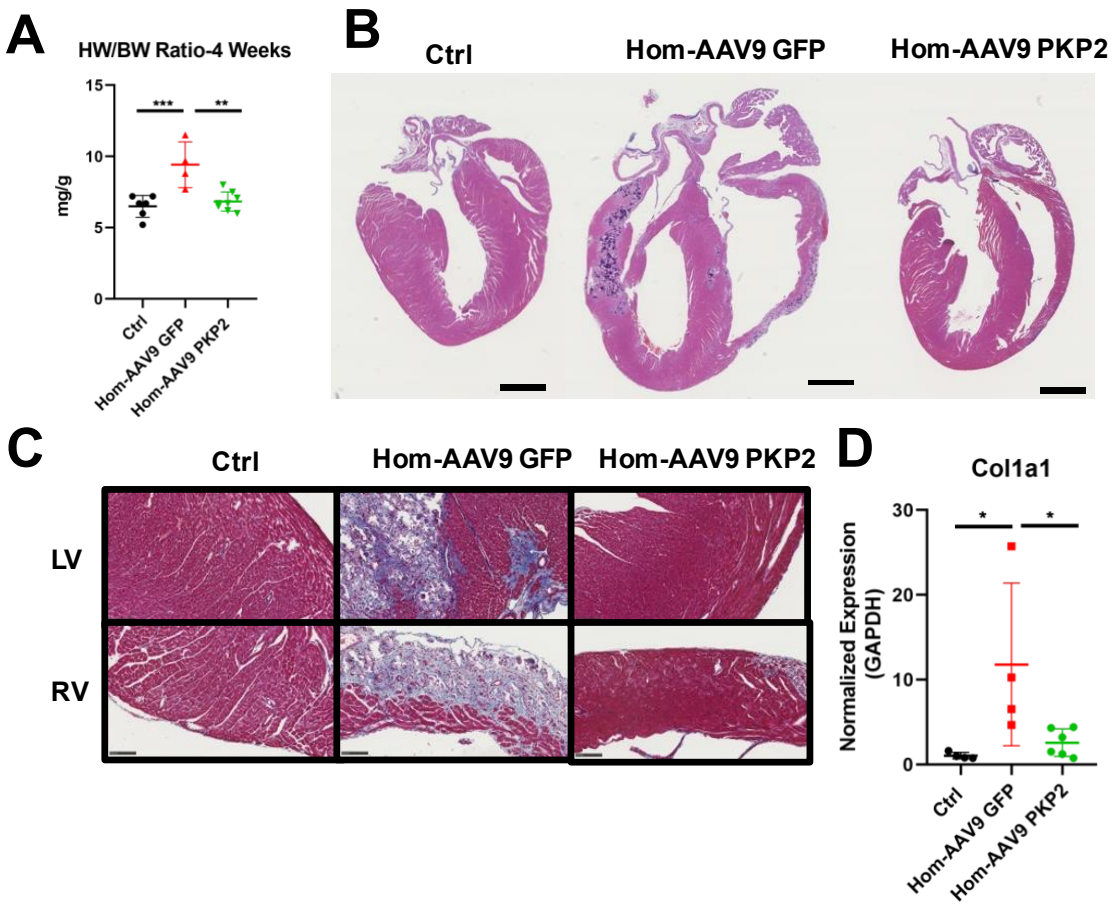

Figure 5.5: Neonatal AAV9 PKP2 administration prevents pathological cardiac tissue remodeling in PKP2 Hom mouse hearts. A. Heart weight (HW) to body weight (BW) ratios of wild-type control (Ctrl) and PKP2 Hom mice treated with AAV9-GFP or AAV9-PKP2. One-way ANOVA with Tukey's multiple comparison test. ***, $p<0.001$. **, $p<0.01$. **B.** Hematoxylin and eosin staining of cardiac sections from wild-type control (Ctrl) and PKP2 Hom mice treated with AAV9-GFP or AAV9-PKP2. Scale bar = 1mm. **C.** Masson's trichrome staining of cardiac sections from wild-type control (Ctrl) and PKP2 Hom mice treated with AAV9 GFP or AAV9 PKP2. Scale bar = 100 µm. **D.** qRT-PCR analysis of Col1a1 (collagen type 1 alpha 1) levels. (n = 4-6 per group). One-way ANOVA with Tukey's multiple comparison test. *, $p<0.05$.

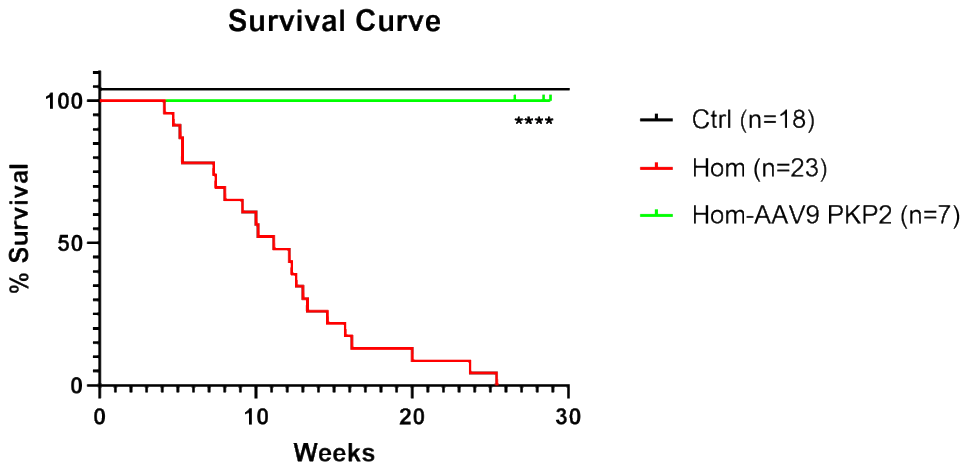

Figure 5.6: Neonatal AAV9 PKP2 administration prevents mortality of PKP2 Hom mice. Kaplan-Meier survival curves of untreated Ctrl, untreated PKP2 Hom, and PKP2 Hom treated with AAV9 PKP2. ****, $p<0.0001$. Ctrl and PKP2 Hom data in Figure 5.6 are also presented in Figure 3.1.

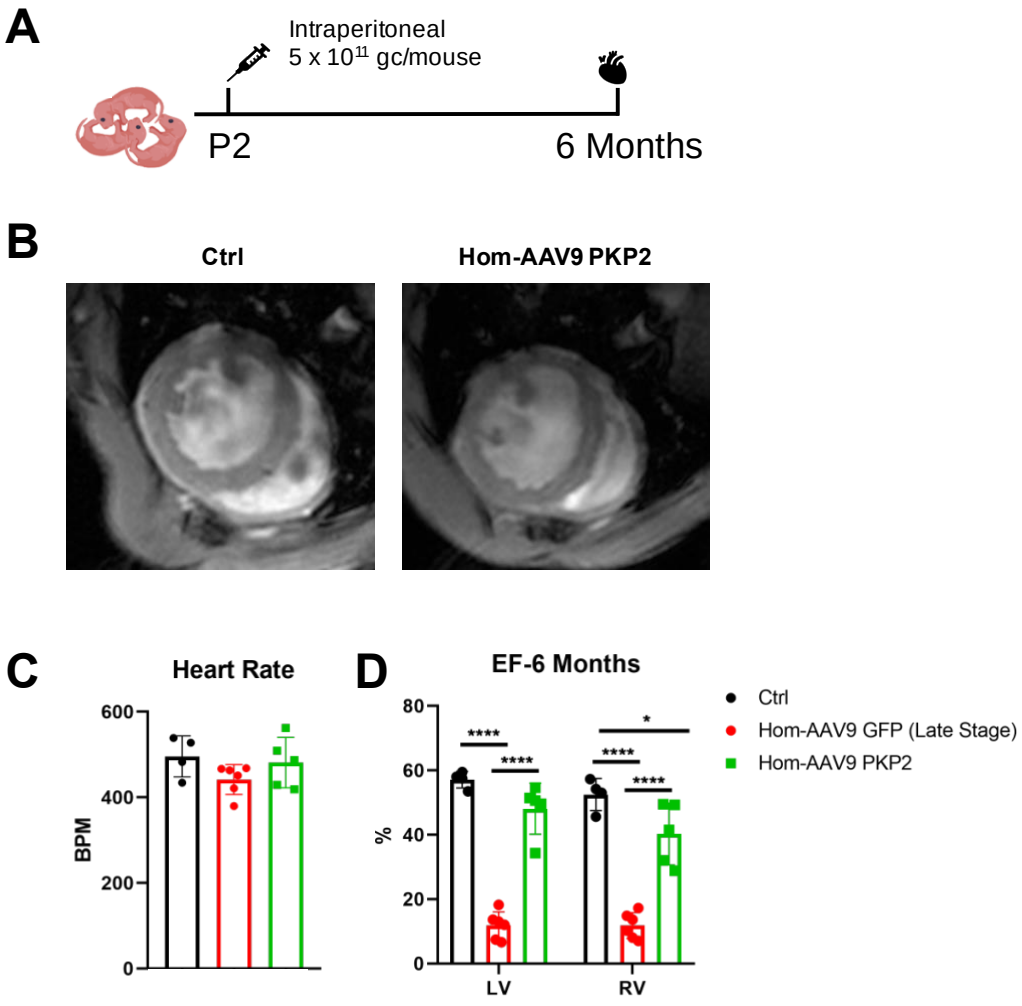

Figure 5.7: Neonatal AAV9 PKP2 treatment prevents cardiac mechanical dysfunction in PKP2 Hom mice at six months of age. A. Schemata for neonatal AAV9 delivery and long-term analysis time point. **B.** Representative short axis cardiac MRI for untreated wild-type control (Ctrl) and PKP2 Hom mice treated with AAV9 PKP2. **C.** Quantification of heart rate for untreated Ctrl, PKP2 Hom mice treated with AAV9 GFP (late-stage = 6 weeks of age), and PKP2 Hom mice treated with AAV9 PKP2. One-way ANOVA with Tukey's multiple comparison test. **D.** Quantification of ejection fraction (EF). (n = 4-6 per group). Two-way ANOVA with Tukey's multiple comparison test. ****, $p<0.0001$. *, $p<0.05$. MRI data for PKP2 Hom mice treated with AAV9 GFP in Figure 5.7 were generated and analyzed as part of late-stage AAV9 injection studies, which are presented in Figure 5.11.

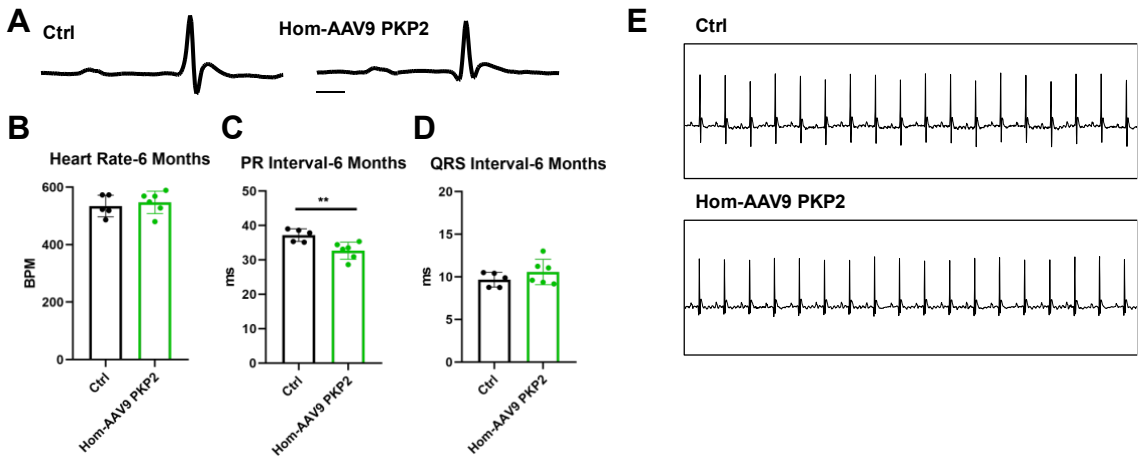

Figure 5.8: Neonatal AAV9 PKP2 treatment prevents cardiac electrical dysfunction in PKP2 Hom mice at six months of age. A. Representative composite surface ECG tracings averaged from four beats in untreated wild-type control (Ctrl) and PKP2 Hom mice treated with AAV9 PKP2. Scale bar = 10 ms. Quantification of **B.** heart rate, **C.** PR interval, and **D.** QRS interval from composite surface ECG tracings (n = 5-6 per group). Unpaired t-test, **, $p<0.01$. **E.** Representative ECG tracings from untreated Ctrl and PKP2 Hom mice treated with AAV9 PKP2 (n = 5-6 per group).

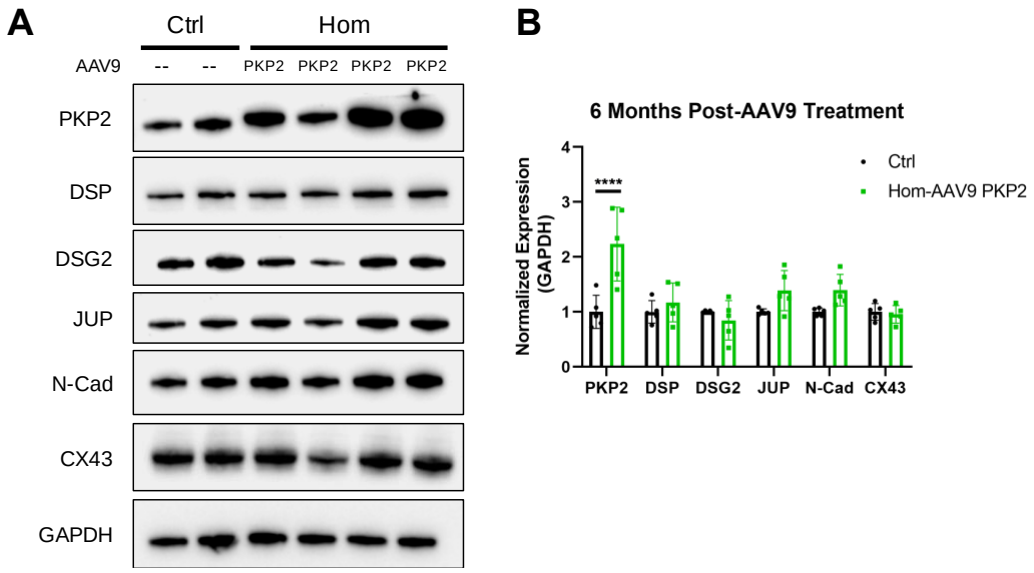

Figure 5.9: Neonatal AAV9 PKP2 treatment prevents cardiac intercalated disc dissolution at six months of age. A. Western blot analysis of desmosomal, fascia adherens, and gap junction proteins in PKP2 Hom hearts with AAV9 PKP2 and untreated wild-type control (Ctrl) hearts. GAPDH serves as the loading control. **B.** Quantification of protein expression in **A** normalized to GAPDH (n = 5 per group). Two-way ANOVA with Tukey's multiple comparison test. ****, p<0.0001.

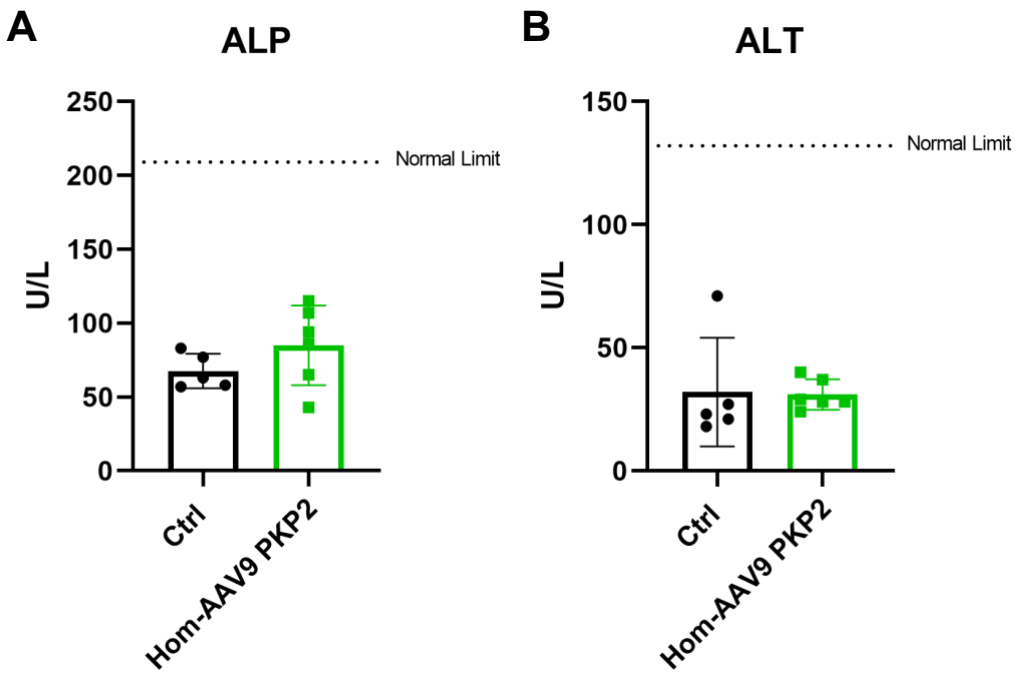

Figure 5.10: Liver enzymes are not impacted by AAV9 PKP2 treatment of PKP2 Hom mice at six months of age. Blood serum analysis for **A.** alkaline phosphatase (ALP) and **B.** alanine aminotransferase (ALT) liver enzyme levels in untreated wild-type control (Ctrl) and PKP2 Hom mice treated with AAV9 PKP2. Normal enzyme limits are indicated with dotted lines.

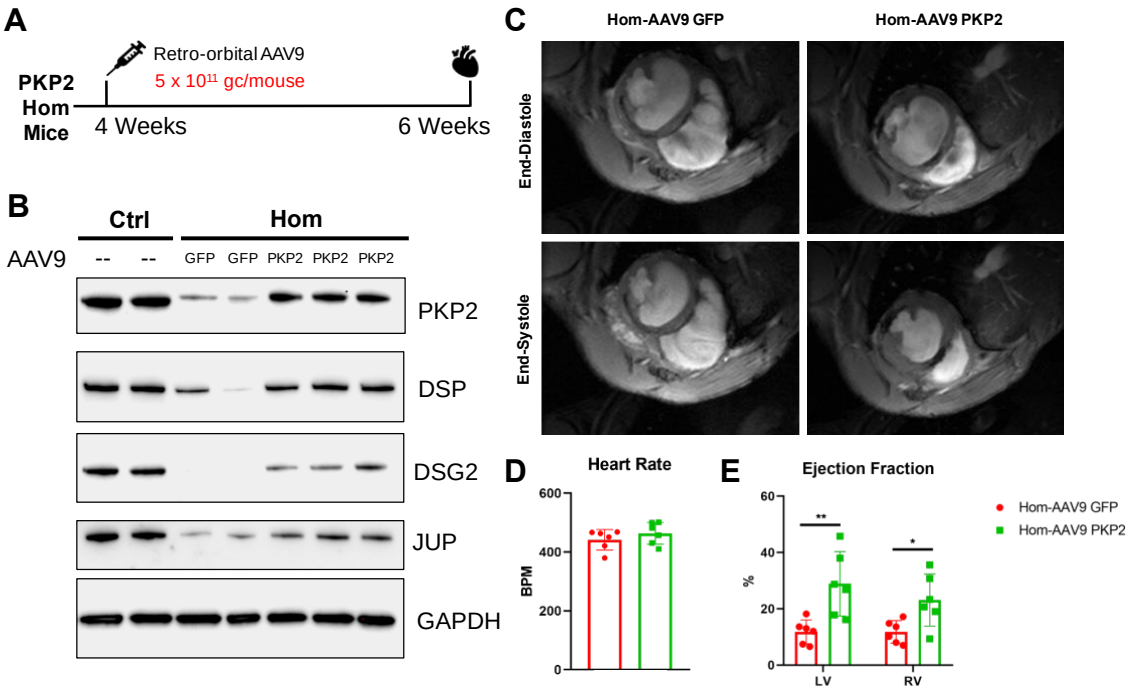

Figure 5.11: Late-stage AAV9 PKP2 treatment prevents desmosomal protein dissolution and improves cardiac mechanical function. A. Schemata for late-stage AAV9 delivery and analysis. **B.** Western blot analysis of desmosomal proteins in untreated wild-type control (Ctrl) and PKP2 Hom mice treated with either AAV9 GFP or AAV9 PKP2 at two weeks post-injection. GAPDH is the loading control. **C.** Representative short axis cardiac MRI for PKP2 Hom mice treated with either AAV9 GFP or AAV9 PKP2 at both end-diastole and end-systole. **D.** Quantification of heart rate for PKP2 Hom mice treated with either AAV9 GFP or AAV9 PKP2 at two weeks post-injection (n = 6 per group). Unpaired t-test. **E.** Quantification of ejection fraction for PKP2 Hom mice treated with either AAV9 GFP or AAV9 PKP2 at two weeks post-injection (n = 6 per group). Two-way ANOVA with Tukey's multiple comparison test. **, $p<0.01$. *, $p<0.05$.

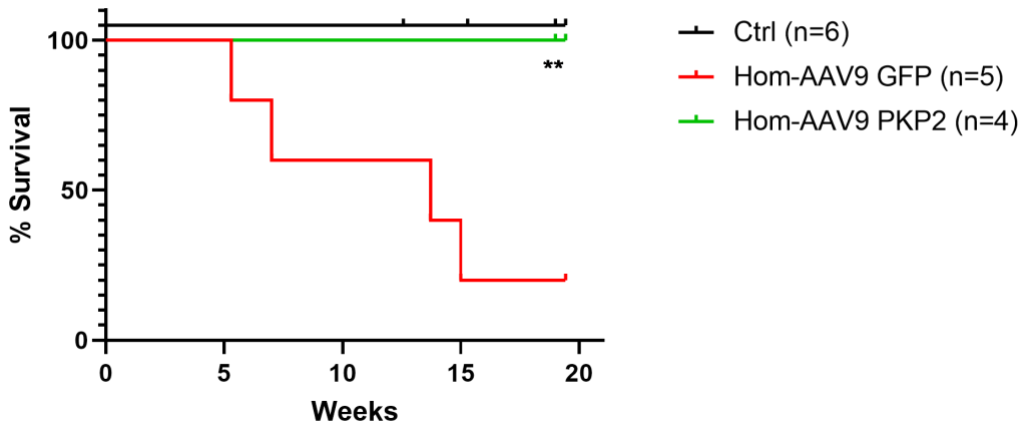

Figure 5.12: Late-stage AAV9 PKP2 administration prevents mortality of PKP2 Hom mice. Kaplan-Meier survival curves of untreated Ctrl mice, PKP2 Hom mice treated with AAV9 GFP, and PKP2 Hom mice treated with AAV9 PKP2 at four weeks of age. **, p<0. 01.

Chapter 6

Discussion of the Dissertation

6.1 A PKP2 splice acceptor site mutation is sufficient to recapitulate ARVC disease features in mice

Characterization of PKP2 Hom mice demonstrates that RNA splicing mutations are sufficient to drive all classic ARVC disease features including SCD, arrhythmias, mechanical dysfunction, and fibro-fatty replacement of myocardium. Genetic studies of ARVC patient populations implicate RNA splicing mutations as causal for human ARVC (Gerull, Heuser et al. 2004, Groeneweg, Ummels et al. 2014), and my work provides the first *in vivo* confirmation of this concept in mice. These results are consistent with clinical reports for patients harboring the PKP2 IVS10-1 G>C splice acceptor site mutation (equivalent to mouse PKP2 IVS9-1 G>C), where SCD, arrhythmias, biventricular dysfunction, and fibro-fatty replacement of myocardium were observed (Svensson, Astrom-Aneq et al. 2016). This suggests the PKP2 Hom mouse model can phenocopy key characteristics of PKP2 IVS10-1 G>C mutant ARVC patients. While human ARVC patients are heterozygous for the PKP2 IVS10-1 G>C mutation, my rationale for studying PKP2 Hom mice is based on the ARVC two hit hypothesis. This postulates that one genetic mutation in a desmosomal gene may be insufficient to develop disease and that an additional pathogenic “hit” may be required through an additional genetic mutation (homozygous or second desmosomal gene) or physiological stimulus (exercise-induced stress) do drive disease development (Delmar and McKenna 2010, Marcus, Edson et al. 2013). My results suggest that a two hit hypothesis may be required to elicit ARVC disease features in mouse models, in order to emulate the impact of the PKP2 IVS10-1 G>C mutation in human populations.

6.2 Non-premature termination codon (PTC) associated intron retention causes a decrease in PKP2 transcript levels

My studies in PKP2 Hom hearts highlight that partial intron retention is the mechanism that underlies the appearance of the mutant PKP2 transcript and which is responsible for the reduction in total PKP2 RNA levels. Previous work suggests that intron retention mechanisms decrease transcript levels through introduction of a PTC (Attali, Warwar et al. 2009). PTCs are known to trigger rapid mRNA degradation through a quality control mechanism termed nonsense mediated decay (NMD), ultimately reducing mutant transcript levels to prevent translation of a potential toxic/gain of function (GOF) protein (Anna and Monika 2018, Lambert, Ashi et al. 2020). My data suggests that mutant PKP2 transcripts in PKP2 Hom hearts are PTC free, which suggests the possibility that non-PTC associated mechanisms decrease PKP2 transcript levels. One possibility of how this may function is that the alternative upstream splice acceptor site generates fewer splicing events (less efficient at splicing), which leads to lower levels of transcript production. A lack of *cis* splicing elements in close proximity to the alternative splice site may decrease this number of splicing events (Herzel, Ottoz et al. 2017, Anna and Monika 2018). Another possibility could be that the partial intron retention may influence RNA structure and post-processing during splicing, which can trigger transcript degradation (Houseley and Tollervey 2009).

6.3 Unique PKP2 protein consequences confer postnatal viability and ARVC disease features in PKP2 Hom mice

Evidence from human genetic studies and pediatric populations mechanistically highlight that desmosomal protein loss may be a critical driver of disease, based on mutations that lead to recessive forms of ARVC (Lyon, Mezzano et al. 2014, Kant, Holthofer et al. 2015, Cerrone, Montnach et al. 2017). However, the mechanisms underlying RNA splicing variants that drive autosomal dominant forms of ARVC remain unclear. My studies showcase that PKP2 protein loss and likely PKP2 haploinsufficiency (in humans) are a critical cause of PKP2 IVS9-1 G>C splice acceptor site mutation-driven ARVC, which include hallmarks, such as baseline arrhythmias, biventricular dysfunction and fibro-fatty replacement of myocardium. Cardiac mechanical dysfunction and fibrosis has been observed in a cardiac-inducible PKP2 KO mouse, where PKP2 was specifically ablated during adulthood (Cerrone, Montnach et al. 2017). However, unlike PKP2 Hom mice which displayed baseline arrhythmias *in vivo* (coinciding with onset of SCD) and fat deposition, no basal arrhythmias or fat deposition were observed in cardiac-inducible PKP2 KO mice (Cerrone, Montnach et al. 2017). These data suggest the early molecular consequences of the PKP2 IVS9-1 G>C splice acceptor site mutation on PKP2 protein levels during cardiac development may be a critical contributor to arrhythmogenic development and fatty replacement. Previous studies from our lab using a cardiac-specific homozygous DSP deficient mouse model that targets DSP loss throughout early cardiac development using ventricular myosin light chain-2 promoter could recapitulate all classic ARVC disease features, including the baseline

arrhythmias and fat deposition in the heart (Lyon, Mezzano et al. 2014). Mechanistic studies in DSP deficient mice with a Tomato Red reporter system also demonstrate that fat deposition in the subepicardium originates from a cardiac muscle lineage, further supporting a cardiac developmental contribution to fatty replacement (Lyon, Mezzano et al. 2014). These data are also in line with a growing number of studies that suggest haploinsufficiency as a common mechanism that may underlie ARVC associated with PKP2 variants of various subtypes (insertion/deletion, nonsense, missense) (Kirchner, Schuetz et al. 2012, Rasmussen, Nissen et al. 2014).

ARVC-related human mutations can also give rise to protein byproducts that include lower (truncated) and higher molecular weight proteins (Rasmussen, Nissen et al. 2014, Cruz, Sanz-Rosa et al. 2015, Zhang, Stroud et al. 2015, Moncayo-Arlandi, Guasch et al. 2016). However, the role of these protein byproducts in driving ARVC disease features and mortality remains poorly understood. My studies demonstrate that despite the global loss of endogenous PKP2 in PKP2 Hom mice, it is the presence of the higher molecular weight mutant PKP2 protein that conferred a survival advantage to PKP2 Hom mice as they were viable at birth. This is in line with studies performed in global PKP2 KO mice, which demonstrated an embryonic lethal phenotype (Grossmann, Grund et al. 2004), further demonstrating that global loss of PKP2 during early embryonic development is not sufficient to prevent mortality in mice. My data may also help explain the lack of mortality in transgenic mice expressing truncated mutant PKP2 (S329X) and AAV-mediated expression of truncated mutant PKP2 (R735X) (Cruz, Sanz-Rosa et al. 2015, Moncayo-Arlandi, Guasch et al. 2016), as the models retained the presence of endogenous PKP2,

which likely conferred a survival advantage to mice. Since mechanical and electrical dysfunction could be seen with advanced age and exercise training in these PKP2 mutant models (Cruz, Sanz-Rosa et al. 2015, Moncayo-Arlandi, Guasch et al. 2016), this would suggest that these mutant byproducts may play a detrimental role on cardiac mechanical and electrical function in the presence of a second “hit”, such as age and exercise (Delmar and McKenna 2010). Further examples of a desmosomal variant resulting in mutant byproducts that confer a survival and disease-free advantage was shown in a mouse model harboring a JUP variant that is associated with Naxos disease, which is an autosomal recessive form of ARVC (McKoy, Protonotarios et al. 2000, Zhang, Stroud et al. 2015). Characterization of JUP mutant mice revealed that they expressed a truncated mutant JUP protein at significantly reduced levels when compared to controls (Zhang, Stroud et al. 2015). More importantly, generation of a new model that increased levels of the truncated JUP protein to endogenous levels was sufficient to prevent disease development, further suggesting that the mutant JUP protein could function equivalent to the endogenous JUP protein in the heart (Zhang, Stroud et al. 2015). These data parallel my studies, which demonstrated that increasing the protein dose of mutant PKP2 to endogenous levels in PKP2 Hom neonatal cardiomyocytes could restore desmosomal protein homeostasis. These data altogether highlight how the molecular consequences of a PKP2 IVS9-1 G>C splice acceptor site may drive both postnatal survival and ARVC disease development.

6.4 PKP2 has affinity to selective desmosomal proteins at the cardiac intercalated disc

PKP2 is known to interact with the cytoplasmic tails of the transmembrane desmosomal cadherins (DSG2, DSC2), as well as the plakin protein DSP within the desmosomal complex (Sheikh, Ross et al. 2009, Lyon, Zanella et al. 2015). JUP, similar to PKP2, is an armadillo protein thought to also function in linking the desmosomal cadherins and DSP (Sheikh, Ross et al. 2009, Lyon, Zanella et al. 2015). There is limited insight into the specific individual interactions that define the functions of PKP2 within the cardiac desmosome *in vivo*. My analysis of PKP2 Hom hearts highlights an early and selective disruption of the desmosome (DSP, DSG2, JUP), though DSC2 was not assessed due to poor antibodies for western blot detection. Within the desmosomal complex, DSG2 represents the most dramatically reduced protein in PKP2 Hom hearts, suggesting PKP2 may have a strong affinity for DSG2 at the desmosome. This parallels observations from PKP2 global KO embryonic hearts, where DSG2 appears to be the most severely impacted desmosomal component after PKP2 loss (Grossmann, Grund et al. 2004). Interestingly, in cardiac-specific DSG2 KO mice loss of DSG2 does not impact PKP2, DSP, or JUP localization to the intercalated disc (Kant, Holthofer et al. 2015). This implies PKP2 is not dependent on DSG2 for proper desmosomal localization and thus PKP2 may function independently to tether these proximal interactions in the cardiac desmosome rather than DSG2. The partial intron retention within mutant PKP2 protein does not occur in any critical structural domains, and is located towards the C-terminus of PKP2. The N-terminal head domain is known to be essential for the

interaction of PKP2 with desmosomal components (Chen, Bonne et al. 2002, Bass-Zubek, Godsel et al. 2009), therefore it is unlikely that the mutant PKP2 protein directly disrupts desmosomal interactions, and thus, loss of interactions are likely due to the loss of PKP2 protein dose. This concept is further exemplified in global PKP2 KO mice (Grossmann, Grund et al. 2004), where PKP2 protein loss in this setting could recapitulate the key desmosomal protein deficits found in neonatal and adult PKP2 Hom hearts.

CX43 reduction is a hallmark of ARVC and observed in PKP2 Hom mice at four weeks of age, when all ARVC disease features are present. This is in line with previous studies from the Sheikh laboratory's cardiac-specific DSP deficient mouse model, which similarly displayed a loss of desmosomal and gap junction components at a time point where all disease features were present (Lyon, Mezzano et al. 2014). However, mechanistic studies in DSP deficient neonatal cardiomyocytes demonstrated that CX43 loss was a primary molecular consequence of DSP loss at a time point when other desmosome and fascia adherens junction proteins remained intact, suggesting a unique relationship between DSP and its ability to directly regulate CX43 levels (Lyon, Mezzano et al. 2014). Since PKP2 directly interacts with DSP (Chen, Bonne et al. 2002) and we show reduction of DSP protein levels in PKP2 Hom hearts, it is possible that the impact on CX43 loss may occur through a DSP-dependent pathway. This is further supported in PKP2 Hom neonatal cardiomyocytes, where a more dramatic reduction in DSP (when compared to DSP levels in the PKP2 Hom P1 heart where CX43 is not reduced) coincides with an early and significant loss of CX43 levels in the presence of baseline arrhythmias.

Interestingly, CX43 levels were not impacted and baseline arrhythmias were not observed in cardiac-inducible PKP2 KO mice that targeted PKP2 loss in adulthood (Cerrone, Montnach et al. 2017), suggesting that susceptibility to CX43 loss may depend on PKP2 and DSP loss during early postnatal cardiac intercalated disc maturation. Instead, recent studies in cardiac-inducible PKP2 KO mice suggested CX43 hemichannel function (activation of channel resulting in increased membrane permeability) and not loss of CX43 levels were associated with stress-induced arrhythmias as a result of calcium handling dysfunction (Kim, Perez-Hernandez et al. 2019). These mechanisms were not specifically tested in PKP2 Hom hearts; however, independent studies in the Sheikh laboratory suggest that restoration (increasing levels) of CX43 in the setting of mouse and human models of ARVC, positively impact cardiac electrical and mechanical function as well as prolong lifespan in these models (unpublished data). These data altogether highlight that CX43 loss is likely a critical mediator of the electrical and structural deficits associated with ARVC pathogenesis in PKP2 Hom hearts.

Fascia adherens junction disruption is likely a secondary consequence to the desmosomal and gap junction disruption in PKP2 Hom hearts and likely indicative of transition of the heart to failure. These data are consistent with previous studies in the ARVC field, that highlight the fascia adherens junction is initially spared in ARVC hearts (Rampazzo, Calore et al. 2014). Molecular analysis of DSP deficient hearts similarly highlighted the fascia adherens junction (by using N-Cad as a marker) is spared at early cardiac pathological stages (Lyon, Mezzano et al. 2014). However, late disease dissolution of the fascia adherens junction is exemplified in ultrastructure

studies using late-stage ARVC patient endomyocardial biopsies, which demonstrated significantly widened gaps in the fascia adherens junction structure when compared to control non-ARVC hearts (Basso, Czarnowska et al. 2006). This further implicates fascia adherens junction disruption as a marker of late-stage ARVC.

6.5 PKP2 restoration prevents dissolution of the cardiac intercalated disc

ARVC pathogenesis is driven by a single desmosomal gene mutation which has devastating “domino” effects on loss of expression of adjacent desmosomal proteins and neighboring gap junction proteins (Rampazzo, Calore et al. 2014, Wang, James et al. 2019), which eventually impacts fascia adherens junction proteins in late-stages of disease (Rampazzo, Calore et al. 2014). Thus, ARVC is considered a disease of desmosomal protein loss with consequences on multiple-gene targets. My *in vivo* studies show that PKP2 restoration is sufficient to prevent the multi-gene target consequences ensuing in cardiac intercalated disc dissolution in PKP2 Hom hearts. Although the mechanisms driving the restoration of the cardiac intercalated disc remain to be precisely dissected, one possible mechanism could relate to its interactions with constitutive photomorphogenesis 9 signalosome subunit 6 (CSN6). CSN6, which is a protein previously implicated in restricting protein degradation (Wei, Serino et al. 2008, Milic, Tian et al. 2019), can directly interact with PKP2 and DSP and is localized to the cardiac intercalated disc (Liang, Lyon et al. 2021). The Sheikh laboratory showed that CSN6 loss removes this protein degradation restriction to drive selective desmosomal protein degradation resulting in hyperaccumulation of ubiquitin and selective autophagy protein degradation

machinery at the cardiac desmosome, which triggered desmosomal structural dissolution and ARVC in mice (Liang, Lyon et al. 2021). The relevance of the cardiomyocyte CSN6-desmosomal complex and connection to PKP2 in human ARVC was illustrated in human ARVC myocardial tissue harboring PKP2 mutations, which displayed a reduction in CSN6 localization to the intercalated disc (Liang, Lyon et al. 2021). Restoration of CSN function via neddylation inhibitor (MLN4924) in CSN6 deficient cardiomyocytes could restore the entire desmosomal complex (Liang, Lyon et al. 2021), showcasing a desmosomal resident mechanism that could be targeted by PKP2 restoration to completely resurrect the desmosomal complex. Independent studies from the Sheikh laboratory demonstrated that hiPSC cardiomyocytes harboring another PKP2 splice site mutation exhibit reduction in CSN6 protein levels coincident with loss of additional desmosomal components DSP and DSG2 (unpublished data). My TEM analysis of PKP2 Hom hearts revealed hyperaccumulation of multi-membrane vesicles at the cardiac intercalated disc distinct from wild-type control mice, altogether highlighting CSN6 dysregulation in PKP2 splice acceptor site mutant models. These data present a potential mechanism through which PKP2 restoration could reassemble the desmosome and prevent dissolution of the cardiac intercalated disc.

A second possible mechanism by which PKP2 restoration could restore the cardiac intercalated disc is via its proximal interactions with desmosomal proteins, which may themselves have selective protein affinity for key desmosomal, fascia adherens junction and gap junction proteins in order to scaffold the complex. Yeast two hybrid assays suggest that PKP2 can directly interact with the DSP N-terminus,

JUP C-terminus, DSC2 intracellular domains, and DSG2 intracellular domains, likely via its N-terminal region (Chen, Bonne et al. 2002, Bass-Zubek, Godsel et al. 2009). Overexpression of PKP2 enhanced DSP staining at the cell border in COS cells (Chen, Bonne et al. 2002), which highlights an ability of PKP2 administration to at least recruit DSP to the proper cellular location. My analysis of PKP2 Hom hearts highlights an early and selective disruption of the desmosome (DSP, DSG2, JUP), though DSC2 was not assessed due to poor antibodies for western blot detection. Thus, it may be possible that PKP2 restoration can be sufficient on its own, in an *in vivo* setting, to directly reassemble desmosomal components at the natural stochiometry required to resurrect the desmosomal complex. While PKP2 has not been shown to directly interact with the gap junction component CX43, mechanistic studies in DSP deficient cardiomyocytes showed a primary effect of DSP loss on CX43 protein levels (Lyon, Mezzano et al. 2014). Thus, it is possible that DSP may be responsible for regulating and stabilizing CX43 following PKP2 restoration. Interestingly, recent studies in *Xenopus* and HeLa cell systems suggest that CX43 may function as a positive transcriptional regulator of N-Cad expression through nuclear translocation and direct binding to the N-Cad promoter (Kotini, Barriga et al. 2018). While this work indicates a non-canonical role for CX43, it also provides a mechanism through which PKP2 restoration (via CX43 stabilization) may function to regulate the fascia adherens junction.

6.6 PKP2 gene therapy represents a therapeutic strategy for ARVC

A diagnosis of ARVC results in an immediate alteration to an individual's lifestyle and increased risk of shortened lifespan, as there is a 40% mortality in ARVC patients 10-11 years after diagnosis. (Lemola, Brunckhorst et al. 2005, Wang, James et al. 2019). Asymptomatic family members of ARVC probands that test positive for a pathological mutation or variant of unknown significance are recommended to undergo repeated diagnostic testing at 1-3 year intervals and observe exercise restriction throughout their lifespan (Wang, James et al. 2019). My results highlight that PKP2 gene therapy can be administered in prophylactic and late-stage disease settings as a means to circumvent ARVC development and mortality. Growing understanding of mutations and mechanisms causal for ARVC, as well as the incorporation of genetic testing and counseling into the diagnosis of ARVC have made early identification of ARVC patients possible (Wang, James et al. 2019). This suggests there is a continuously expanding ARVC population that would benefit from prophylactic PKP2 gene therapy. While this is an appealing approach to prevent disease development, limited human clinical trials have evaluated prophylactic gene therapy (Mendell, Al-Zaidy et al. 2021). However, recent success in clinical trials utilizing AAV delivery of the survival motor neuron 1 (SMN1) gene (LOF is causal for disease) for symptomatic patients of the neurodegenerative disease spinal muscular atrophy (SMA) has set the stage for application of prophylactic gene therapy to SMA patient populations in a clinical trial (Mendell, Al-Zaidy et al. 2021). Initial work with SMN gene therapy in symptomatic infants demonstrated impressive benefits on survival and improved motor function compared to historical patient cohorts (Mendell, Al-Zaidy et al. 2017, Al-Zaidy, Pickard et al. 2019). These encouraging results

prompted a clinical trial for pre-symptomatic infants with genetically confirmed deletion of the SMN1 gene (ClinicalTrials.gov identifier: NCT03505099). This full trial has just completed with no reported adverse events, and hopefully data analysis will provide evidence for the safety and feasibility of prophylactic gene therapy to human populations.

ARVC patients are reliant upon palliative approaches (ICD, catheter ablation, heart failure pharmacological treatments) to provide symptomatic relief and prevent SCD (Idris, Shah et al. 2018, Wang, James et al. 2019). Most therapeutic approaches are directed at the electrical disease underlying ARVC. This is exemplified by an ongoing clinical trial that is currently evaluating flecainide treatment on ARVC patients most at risk for SCD that also harbor an implanted ICD (ClinicalTrials.gov identifier: NCT03685149), also highlighting the insufficiency of ICD approaches to prevent SCD. Flecainide functions to block the fast inward sodium current in cardiomyocytes, which results in conduction slowing and thereby may decrease the incidence of arrhythmias (Andrikopoulos, Pastromas et al. 2015). While the evaluation of flecainide has the possibility to target electrical dysfunction in ARVC populations, mechanical disease must also be considered to prevent classic heart failure in these populations (Idris, Shah et al. 2018, Wang, James et al. 2019). Studies of an ARVC patient cohort demonstrated that 49% presented with heart failure, which was defined by ventricular dysfunction (either the left or right ventricle), as well as exertional dyspnea and fatigue (Gilotra, Bhonsale et al. 2017). These are classic characteristics of heart failure that are found in a significant portion of ARVC populations, which must be considered in therapeutic design and evaluation. Factors

such as *de novo* or lack of an identifiable mutation and lack of family history can also prevent early identification of individuals/families at risk for ARVC (Wang, James et al. 2019, Mattesi, Zorzi et al. 2020). Thus, this would necessitate therapeutic strategies that would function in the presence of disease and in particular, in the setting of mechanical dysfunction. My studies demonstrate the ability of PKP2 gene therapy to prevent mortality and improve cardiac mechanical function at a time point after ARVC has developed. PKP2 gene therapy represents an appealing approach as it targets the cardiac desmosome as the primary driver of both electrical and mechanical disease of ARVC, which also accounts for mutations associated within 30-60% of ARVC populations (Marcus, Edson et al. 2013). Thus, PKP2 restoration provides the ability to impact the full spectrum of ARVC disease features as well as prevent premature mortality.

6.7 PKP2 gene therapy may be applicable to many forms of cardiac disease

Studies of PKP2 ARVC populations demonstrate diverse mutation types (insertion/deletions, nonsense, missense), which are thought to lead to PKP2 protein haploinsufficiency (Gerull, Heuser et al. 2004, Kirchner, Schuetz et al. 2012, Rasmussen, Nissen et al. 2014). My work suggests PKP2 gene therapy has the potential to target a broad population of ARVC patients harboring mutations in PKP2, which represents the most frequently mutated gene in ARVC (Marcus, Edson et al. 2013, Wang, James et al. 2019). A subset of PKP2 mutations have been implicated in Brugada syndrome (Cerrone, Lin et al. 2014), which is an electrical disorder characterized by ST elevations in the absence of structural disease than can

predispose patients to ventricular fibrillation and SCD (Mizusawa and Wilde 2012). Brugada syndrome is thought to be triggered through abnormal sodium channel activity, which can occur through mutations which directly impact the cardiac sodium channel Nav1.5 (SCN5A gene) or regulators of Nav1.5 activity (Mizusawa and Wilde 2012). PKP2 is a known regulator of the cardiac sodium channel Nav1.5 activity (Cerrone, Lin et al. 2014), which suggests PKP2 gene therapy may also be a viable therapeutic in electrical diseases, such as Brugada syndrome. Desmosomal and ultimately intercalated disc dissolution is a hallmark of ARVC, and thus, may underlie all desmosomal mutations associated with ARVC (Marcus, Edson et al. 2013, Wang, James et al. 2019, Mattesi, Zorzi et al. 2020). Therefore, PKP2 gene therapy may also have therapeutic value in targeting ARVC populations harboring mutations in other desmosomal genes (DSP, DSG2, DSC2, JUP). Mutations in non-desmosomal components such as phosholamban (PLN) and alpha T-catenin have also been implicated in ARVC (Wang, James et al. 2019). Interestingly, analysis of endomyocardial biopsies from ARVC patients harboring a PLN mutation demonstrated a reduction in JUP staining, suggesting that the desmosome may also be a target of other ARVC forms (van der Zwaag, van Rijsingen et al. 2012). Studies of alpha T-catenin mutations in ARVC populations revealed an impact on JUP protein binding with an N-terminus missense mutation, as well as the formation of protein aggregates resulting from a C-terminus deletion mutation *in vitro* (van Hengel, Calore et al. 2013). This suggests alpha T-catenin mutations may both directly influence desmosomal interactions and disrupt protein degradation homeostasis. PKP2 gene therapy may also have therapeutic value as it could target the reassembly of

desmosomal components and/or restrict protein degradation via CSN6 restoration. These studies suggest PKP2 gene therapy could provide therapeutic value to other cardiac diseases associated with PKP2 mutations, as well as more broadly to target underlying pathways (represent a mutation-independent approach) that may be common to other forms of ARVC.

6.8 Conclusions

In conclusion, the PKP2 IVS9-1 G>C splice acceptor site mutation is sufficient to recapitulate premature death and disease features associated with a biventricular form of ARVC in mice, which include baseline arrhythmias, biventricular dysfunction, and fibro-fatty replacement of myocardium. The unique PKP2 protein consequences from the PKP2 IVS9-1 G>C splice acceptor site mutation confer embryonic viability as well as ARVC disease features and postnatal death in PKP2 Hom mice. Mechanistically the PKP2 IVS9-1 G>C splice acceptor site mutation impacts both PKP2 mRNA and protein products resulting in the absence of endogenous PKP2 mRNA and protein levels as well as the appearance of a mutant PKP2 byproduct caused by a partial intron retention that is localized at reduced levels at the cardiac intercalated disc. *In vitro* expression of mutant PKP2 in PKP2 Hom neonatal cardiomyocytes reveals that mutant PKP2 is functional and capable of restoring desmosomal protein levels, thus, likely accounts for the viability of PKP2 Hom mice during embryonic development. Desmosomal disruption in PKP2 Hom cardiomyocytes is driven by loss of function (dose/amount of PKP2) mechanism, since restoration of either wild-type or mutant PKP2 protein was sufficient to increase

desmosomal protein levels in PKP2 neonatal cardiomyocytes. This sustained desmosomal protein disruption subsequently impacts gap junction protein, CX43, levels to drive the baseline arrhythmias in PKP2 Hom neonatal cardiomyocytes and onset of SCD in adult PKP2 Hom hearts. These data further set the stage to exploit PKP2 restoration strategies as a means to circumvent desmosomal disruption in ARVC settings. PKP2 restoration is sufficient to prevent the multi-gene target consequences ensuing in cardiac intercalated disc dissolution in PKP2 Hom hearts. Although the mechanisms driving the restoration of the cardiac intercalated disc remain to be precisely dissected, possible mechanisms could include PKP2 interactions to desmosomal resident proteins that are associated with restricting protein degradation (based on hyperaccumulation of multi-membrane vesicles at the cardiac intercalated disc in PKP2 Hom hearts), such as CSN6 or proximal interactions to high affinity desmosomal protein interacting proteins, DSG2, DSP and JUP, which could act as a scaffold to other complexes at the cardiac intercalated disc. These data set the stage for PKP2 gene therapy to be administered in prophylactic and late-stage disease settings as a means to circumvent ARVC development and mortality. PKP2 gene therapy represents an appealing approach as it targets the cardiac desmosome, which is the primary driver of both electrical as well as mechanical/structural disease in ARVC, the latter of which has not been an immediate target for ARVC therapeutic interventions. PKP2 gene therapy may be applicable as a therapeutic to other forms of cardiac disease associated with PKP2 mutations, as PKP2 haploinsufficiency may underlie diverse PKP2 mutation types underlying ARVC and other cardiac arrhythmias (Brugada syndrome). In addition,

PKP2 gene therapy may also have therapeutic value in targeting ARVC populations harboring mutations in other desmosomal genes (DSP, DSG2, DSC2, JUP) as well as other ARVC forms (mutations in non-desmosomal components) as they may harbor common underlying desmosomal and protein degradation deficits. Altogether, these findings suggest that RNA splicing mutations are sufficient to trigger ARVC pathogenesis likely through PKP2 protein loss, and that PKP2 restoration represents an appealing therapeutic approach which may address a broad ARVC patient population with an unmet clinical need.

6.9 Future Studies

My studies have defined a mechanism of how the PKP2 IVS9-1 G>C mutation impacts RNA splicing by determining the molecular consequences on PKP2 RNA and protein byproducts, which ultimately drives ARVC disease development and premature mortality. However, the precise mechanisms influencing the splicing outcome of the PKP2 IVS9-1 G>C splice acceptor site mutation remain unknown. RNA-binding proteins, which function as *trans* acting splicing elements are critical in the regulation of splicing (van den Hoogenhof, Pinto et al. 2016), and may play an important role in determining the diverse potential outcomes resulting from splice acceptor site mutations. Future studies utilizing pulldown assays with RNA probes for both wild-type and mutant PKP2 splice junction sites and subsequent mass spec proteomics analysis would help define the canonical RNA-binding proteins involved in the regulation of PKP2, and provide insights into how PKP2 splice acceptor mutations alter the RNA-binding protein landscape to influence splicing in disease.

There is limited knowledge of RNA-binding proteins which may be specific to cardiac disease (van den Hoogenhof, Pinto et al. 2016), so these studies would help further understand pathological splicing mechanisms in the heart.

Although my studies were performed in mice, sequence alignment between the human and mouse genome at the PKP2 mutation locus suggest utilization of an alternative upstream splice acceptor site and resulting partial intron retention could be conserved between species. Future studies should be focused on more precisely determining the relevance of intron retention as a mechanism underlying PKP2 splice site mutations in humans. This would serve as an important confirmation of mouse models as approximations for human disease, particularly for mechanistic insights. Human induced pluripotent stems cells (iPSCs) are increasingly used as a platform to both model and understand the molecular mechanisms underlying human ARVC (Padron-Barthe, Villalba-Orero et al. 2019, Pan, Ebert et al. 2021). Thus, additional studies should be performed in PKP2 IVS10-1 G>C mutant (equivalent to PKP2 IVS9-1 G>C in mouse) human iPSCs to determine the consequences on PKP2 splicing at the RNA and protein level, as well as functional assays (xCELLigence RTCA CardioECR field potential measurements) to determine the impact on ARVC disease features such as arrhythmias. This platform would additionally enable evaluation of human PKP2 protein restoration (via adenovirus transduction) on cardiac intercalated disc proteins and cardiomyocyte electrophysiology in PKP2 IVS10-1 G>C mutant human iPSCs. These studies would be important to further validate the underlying mechanisms and physiological consequences of PKP2 splice site mutations in human ARVC settings.

PKP2 gene therapy represents an appealing therapeutic approach, which could be applicable to a majority of ARVC patients with PKP2 mutations as previous studies report that PKP2 variants of multiple subtypes (insertions/deletion, nonsense, missense) may also result in LOF mechanisms (Gerull, Heuser et al. 2004, Kirchner, Schuetz et al. 2012, Rasmussen, Nissen et al. 2014). My *in vivo* studies demonstrate that PKP2 restoration can reassemble desmosomal proteins and prevent dissolution of the cardiac intercalated disc, however, the precise mechanisms mediating this process remain unclear. Restoration of CSN-specific protein degradation pathways (via MLN4924 neddylation inhibitor) has been shown to resurrect desmosomal protein levels *in vitro* and may be a driving mechanism following PKP2 restoration (Liang, Lyon et al. 2021). Future studies could determine if CSN6-driven processes mediate desmosomal protein restoration in PKP2 Hom neonatal cardiomyocytes. Following wild-type PKP2 restoration in PKP2 Hom neonatal cardiomyocytes, treatment with either a CSN6 shRNA or scramble shRNA and then evaluation of cardiac intercalated disc proteins would determine the role for CSN6 in desmosomal restoration. This could further confirm the relevance of protein degradation processes in PKP2 Hom cardiomyocytes and provide mechanistic insights into regulation of desmosomal homeostasis at the intercalated disc.

It would be interesting to apply PKP2 gene therapy to independent ARVC models that harbor loss/mutations in distinct desmosomal components (DSP, DSG2, DSC2, JUP), as they have also been shown to trigger intercalated disc dissolution. The Sheikh laboratory developed a DSP-deficient mouse model, which similarly recapitulates all human ARVC disease features and demonstrates desmosomal and

gap junction disruption during disease progression (Lyon, Mezzano et al. 2014). Future studies would utilize late-stage delivery of AAV9 PKP2 to DSP deficient mice and assess the impact on survival, cardiac function, and the cardiac intercalated disc. These studies would have the potential to define if PKP2 can reassemble desmosomal components independent of DSP and whether this would be sufficient to prevent mortality and circumvent ARVC disease features. This would also help in broadening the scope of PKP2 gene therapy to recessive forms of ARVC harboring complete desmosomal deficiency.

My studies set the stage to exploit PKP2 gene therapy in ARVC populations. ARVC represents a devastating and fatal disease with no therapeutics (Elias Neto, Tonet et al. 2019, Wang, James et al. 2019), so clinical trials are imperative to evaluate emerging approaches for ARVC. Future studies would focus on the evaluation of PKP2 gene therapy in clinical trials, which should initially address ARVC patients with existing disease features that meet the 2010 Revised ARVC Task Force Criteria, which encompasses >200 PVCs in 24 hours of Holter monitor recordings for electrical disease and a right ventricle EF ≤40% as measured by cardiac MRI for mechanical dysfunction (Marcus, McKenna et al. 2010). Left ventricle involvement is not considered a major criteria for ARVC diagnosis, however, it would not be grounds for exclusion (Marcus, McKenna et al. 2010). Patients would be excluded if there was no evidence of functional or viable myocardium, as the absence of cardiomyocytes would prevent AAV9 transduction. Patients would also be excluded if anti-AAV9 neutralizing antibodies were detected, as neutralizing antibodies can prevent virus delivery to the heart (Rapti, Louis-Jeune et al. 2012).

This study would begin with a Phase I clinical trial which could simultaneously evaluate the safety and efficacy of AAV9 PKP2 administration to ARVC patients with existing electrical and mechanical disease. Within the trial design, multiple AAV9 PKP2 doses could be evaluated to determine the optimal dose that minimizes AAV-associated toxicity, while achieving a clinical benefit. Primary outcomes that could be measured could include the number of treatment-related adverse events (measure AAV toxicity), number of PVCs in a seven day period (electrical disease), and change in both left and right ventricular EF from baseline measurement (mechanical disease). These studies would represent the first clinical trial capable of addressing both electrical and mechanical dysfunction as a means to treat ARVC populations.

References

Al-Zaidy, S., A. S. Pickard, K. Kotha, L. N. Alfano, L. Lowes, G. Paul, K. Church, K. Lehman, D. M. Sproule, O. Dabbous, B. Maru, K. Berry, W. D. Arnold, J. T. Kissel, J. R. Mendell and R. Shell (2019). "Health outcomes in spinal muscular atrophy type 1 following AVXS-101 gene replacement therapy." Pediatr Pulmonol **54**(2): 179-185.

Andrikopoulos, G. K., S. Pastromas and S. Tzeis (2015). "Flecainide: Current status and perspectives in arrhythmia management." World J Cardiol **7**(2): 76-85.

Anna, A. and G. Monika (2018). "Splicing mutations in human genetic disorders: examples, detection, and confirmation." J Appl Genet **59**(3): 253-268.

Aponte-Ubillus, J. J., D. Barajas, J. Peltier, C. Bardliving, P. Shamlou and D. Gold (2018). "Molecular design for recombinant adeno-associated virus (rAAV) vector production." Appl Microbiol Biotechnol **102**(3): 1045-1054.

Attali, R., N. Warwar, A. Israel, I. Gurt, E. McNally, M. Puckelwartz, B. Glick, Y. Nevo, Z. Ben-Neriah and J. Melki (2009). "Mutation of SYNE-1, encoding an essential component of the nuclear lamina, is responsible for autosomal recessive arthrogryposis." Hum Mol Genet **18**(18): 3462-3469.

Baralle, D. and E. Buratti (2017). "RNA splicing in human disease and in the clinic." Clin Sci (Lond) **131**(5): 355-368.

Bass-Zubek, A. E., L. M. Godsel, M. Delmar and K. J. Green (2009). "Plakophilins: multifunctional scaffolds for adhesion and signaling." Curr Opin Cell Biol **21**(5): 708-716.

Basso, C., E. Czarnowska, M. Della Barbera, B. Bauce, G. Beffagna, E. K. Wlodarska, K. Pilichou, A. Ramondo, A. Lorenzon, O. Wozniek, D. Corrado, L. Daliento, G. A. Danieli, M. Valente, A. Nava, G. Thiene and A. Rampazzo (2006). "Ultrastructural evidence of intercalated disc remodelling in arrhythmogenic right ventricular cardiomyopathy: an electron microscopy investigation on endomyocardial biopsies." Eur Heart J **27**(15): 1847-1854.

Basso, C. and G. Thiene (2005). "Adipositas cordis, fatty infiltration of the right ventricle, and arrhythmogenic right ventricular cardiomyopathy. Just a matter of fat?" Cardiovasc Pathol **14**(1): 37-41.

Bezzerides, V. J., A. Caballero, S. Wang, Y. Ai, R. J. Hylind, F. Lu, D. A. Heims-Waldron, K. D. Chambers, D. Zhang, D. J. Abrams and W. T. Pu (2019). "Gene Therapy for Catecholaminergic Polymorphic Ventricular Tachycardia by Inhibition of Ca(2+)/Calmodulin-Dependent Kinase II." Circulation **140**(5): 405-419.

Cerrone, M., X. Lin, M. Zhang, E. Agullo-Pascual, A. Pfenniger, H. Chkourko Gusky, V. Novelli, C. Kim, T. Tirasawadichai, D. P. Judge, E. Rothenberg, H. S. Chen, C.

Napolitano, S. G. Priori and M. Delmar (2014). "Missense mutations in plakophilin-2 cause sodium current deficit and associate with a Brugada syndrome phenotype." Circulation **129**(10): 1092-1103.

Cerrone, M., J. Montnach, X. Lin, Y. T. Zhao, M. Zhang, E. Agullo-Pascual, A. Leo-Macias, F. J. Alvarado, I. Dolgalev, T. V. Karathanos, K. Malkani, C. J. M. Van Opbergen, J. J. A. van Bavel, H. Q. Yang, C. Vasquez, D. Tester, S. Fowler, F. Liang, E. Rothenberg, A. Heguy, G. E. Morley, W. A. Coetzee, N. A. Trayanova, M. J. Ackerman, T. A. B. van Veen, H. H. Valdivia and M. Delmar (2017). "Plakophilin-2 is required for transcription of genes that control calcium cycling and cardiac rhythm." Nat Commun **8**(1): 106.

Cerrone, M., M. Noorman, X. Lin, H. Chkourko, F. X. Liang, R. van der Nagel, T. Hund, W. Birchmeier, P. Mohler, T. A. van Veen, H. V. van Rijen and M. Delmar (2012). "Sodium current deficit and arrhythmogenesis in a murine model of plakophilin-2 haploinsufficiency." Cardiovasc Res **95**(4): 460-468.

Chen, X., S. Bonne, M. Hatzfeld, F. van Roy and K. J. Green (2002). "Protein binding and functional characterization of plakophilin 2. Evidence for its diverse roles in desmosomes and beta -catenin signaling." J Biol Chem **277**(12): 10512-10522.

Cruz, F. M., D. Sanz-Rosa, M. Roche-Molina, J. Garcia-Prieto, J. M. Garcia-Ruiz, G. Pizarro, L. J. Jimenez-Borreguero, M. Torres, A. Bernad, J. Ruiz-Cabello, V. Fuster, B. Ibanez and J. A. Bernal (2015). "Exercise triggers ARVC phenotype in mice expressing a disease-causing mutated version of human plakophilin-2." J Am Coll Cardiol **65**(14): 1438-1450.

Daya, S. and K. I. Berns (2008). "Gene therapy using adeno-associated virus vectors." Clin Microbiol Rev **21**(4): 583-593.

Delmar, M. and W. J. McKenna (2010). "The cardiac desmosome and arrhythmogenic cardiomyopathies: from gene to disease." Circ Res **107**(6): 700-714.

Elias Neto, J., J. Tonet, R. Frank and G. Fontaine (2019). "Arrhythmogenic Right Ventricular Cardiomyopathy/Dysplasia (ARVC/D) - What We Have Learned after 40 Years of the Diagnosis of This Clinical Entity." Arq Bras Cardiol **112**(1): 91-103.

Gerull, B., A. Heuser, T. Wichter, M. Paul, C. T. Basson, D. A. McDermott, B. B. Lerman, S. M. Markowitz, P. T. Ellinor, C. A. MacRae, S. Peters, K. S. Grossmann, J. Drenckhahn, B. Michely, S. Sasse-Klaassen, W. Birchmeier, R. Dietz, G. Breithardt, E. Schulze-Bahr and L. Thierfelder (2004). "Mutations in the desmosomal protein plakophilin-2 are common in arrhythmogenic right ventricular cardiomyopathy." Nat Genet **36**(11): 1162-1164.

Gilotra, N. A., A. Bhonsale, C. A. James, A. S. J. Te Riele, B. Murray, C. Tichnell, A. Sawant, C. S. Ong, D. P. Judge, S. D. Russell, H. Calkins and R. J. Tedford (2017). "Heart Failure Is Common and Under-Recognized in Patients With Arrhythmogenic Right Ventricular Cardiomyopathy/Dysplasia." Circ Heart Fail **10**(9).

Groeneweg, J. A., A. Ummels, M. Mulder, H. Bikker, J. J. van der Smagt, A. M. van Mil, T. Homfray, J. G. Post, A. Elvan, J. F. van der Heijden, A. C. Houweling, J. D. Jongbloed, A. A. Wilde, J. P. van Tintelen, R. N. Hauer and D. Dooijes (2014). "Functional assessment of potential splice site variants in arrhythmogenic right ventricular dysplasia/cardiomyopathy." Heart Rhythm **11**(11): 2010-2017.

Grossmann, K. S., C. Grund, J. Huelsken, M. Behrend, B. Erdmann, W. W. Franke and W. Birchmeier (2004). "Requirement of plakophilin 2 for heart morphogenesis and cardiac junction formation." J Cell Biol **167**(1): 149-160.

Guernsey, D. L., H. Jiang, K. Bedard, S. C. Evans, M. Ferguson, M. Matsuoka, C. Macgillivray, M. Nightingale, S. Perry, A. L. Rideout, A. Orr, M. Ludman, D. L. Skidmore, T. Benstead and M. E. Samuels (2010). "Mutation in the gene encoding ubiquitin ligase LRSAM1 in patients with Charcot-Marie-Tooth disease." PLoS Genet **6**(8).

Herzel, L., D. S. M. Ottoz, T. Alpert and K. M. Neugebauer (2017). "Splicing and transcription touch base: co-transcriptional spliceosome assembly and function." Nat Rev Mol Cell Biol **18**(10): 637-650.

Hinderer, C., N. Katz, E. L. Buza, C. Dyer, T. Goode, P. Bell, L. K. Richman and J. M. Wilson (2018). "Severe Toxicity in Nonhuman Primates and Piglets Following High-Dose Intravenous Administration of an Adeno-Associated Virus Vector Expressing Human SMN." Hum Gene Ther **29**(3): 285-298.

Ho, S. Y. and P. Nihoyannopoulos (2006). "Anatomy, echocardiography, and normal right ventricular dimensions." Heart **92 Suppl 1**: i2-13.

Houseley, J. and D. Tollervey (2009). "The many pathways of RNA degradation." Cell **136**(4): 763-776.

Idris, A., S. R. Shah and K. Park (2018). "Right ventricular dysplasia: management and treatment in light of current evidence." J Community Hosp Intern Med Perspect **8**(3): 101-106.

Ishikawa, K., T. Weber and R. J. Hajjar (2018). "Human Cardiac Gene Therapy." Circ Res **123**(5): 601-613.

Kant, S., B. Holthofer, T. M. Magin, C. A. Krusche and R. E. Leube (2015). "Desmoglein 2-Dependent Arrhythmogenic Cardiomyopathy Is Caused by a Loss of Adhesive Function." Circ Cardiovasc Genet **8**(4): 553-563.

Kim, J. C., M. Perez-Hernandez, F. J. Alvarado, S. R. Maurya, J. Montnach, Y. Yin, M. Zhang, X. Lin, C. Vasquez, A. Heguy, F. X. Liang, S. H. Woo, G. E. Morley, E. Rothenberg, A. Lundby, H. H. Valdivia, M. Cerrone and M. Delmar (2019). "Disruption of Ca(2+)i Homeostasis and Connexin 43 Hemichannel Function in the Right Ventricle Precedes Overt Arrhythmogenic Cardiomyopathy in Plakophilin-2-Deficient Mice." Circulation **140**(12): 1015-1030.

Kirchner, F., A. Schuetz, L. H. Boldt, K. Martens, G. Dittmar, W. Haverkamp, L. Thierfelder, U. Heinemann and B. Gerull (2012). "Molecular insights into arrhythmogenic right ventricular cardiomyopathy caused by plakophilin-2 missense mutations." Circ Cardiovasc Genet **5**(4): 400-411.

Kotini, M., E. H. Barriga, J. Leslie, M. Gentzel, V. Rauschenberger, A. Schambony and R. Mayor (2018). "Gap junction protein Connexin-43 is a direct transcriptional regulator of N-cadherin in vivo." Nat Commun **9**(1): 3846.

Lambert, J. M., M. O. Ashi, N. Srour, L. Delpy and J. Sauliere (2020). "Mechanisms and Regulation of Nonsense-Mediated mRNA Decay and Nonsense-Associated Altered Splicing in Lymphocytes." Int J Mol Sci **21**(4).

Lek, M., K. J. Karczewski, E. V. Minikel, K. E. Samocha, E. Banks, T. Fennell, A. H. O'Donnell-Luria, J. S. Ware, A. J. Hill, B. B. Cummings, T. Tukiainen, D. P. Birnbaum, J. A. Kosmicki, L. E. Duncan, K. Estrada, F. Zhao, J. Zou, E. Pierce-Hoffman, J. Berghout, D. N. Cooper, N. Deflaux, M. DePristo, R. Do, J. Flannick, M. Fromer, L. Gauthier, J. Goldstein, N. Gupta, D. Howrigan, A. Kiezun, M. I. Kurki, A. L. Moonshine, P. Natarajan, L. Orozco, G. M. Peloso, R. Poplin, M. A. Rivas, V. Ruano-Rubio, S. A. Rose, D. M. Ruderfer, K. Shakir, P. D. Stenson, C. Stevens, B. P. Thomas, G. Tiao, M. T. Tusie-Luna, B. Weisburd, H. H. Won, D. Yu, D. M. Altshuler, D. Ardissino, M. Boehnke, J. Danesh, S. Donnelly, R. Elosua, J. C. Florez, S. B. Gabriel, G. Getz, S. J. Glatt, C. M. Hultman, S. Kathiresan, M. Laakso, S. McCarroll, M. I. McCarthy, D. McGovern, R. McPherson, B. M. Neale, A. Palotie, S. M. Purcell, D. Saleheen, J. M. Scharf, P. Sklar, P. F. Sullivan, J. Tuomilehto, M. T. Tsuang, H. C. Watkins, J. G. Wilson, M. J. Daly, D. G. MacArthur and C. Exome Aggregation (2016). "Analysis of protein-coding genetic variation in 60,706 humans." Nature **536**(7616): 285-291.

Lemola, K., C. Brunckhorst, U. Helfenstein, E. Oechslin, R. Jenni and F. Duru (2005). "Predictors of adverse outcome in patients with arrhythmogenic right ventricular dysplasia/cardiomyopathy: long term experience of a tertiary care centre." Heart **91**(9): 1167-1172.

Liang, Y., R. C. Lyon, J. Pellman, W. H. Bradford, S. Lange, J. Bogomolovas, N. D. Dalton, Y. Gu, M. Bobar, M. H. Lee, T. Iwakuma, V. Nigam, A. Asimaki, M. Scheinman, K. L. Peterson and F. Sheikh (2021). "Desmosomal COP9 regulates proteome degradation in arrhythmogenic right ventricular dysplasia/cardiomyopathy." J Clin Invest.

Lim, K. H., L. Ferraris, M. E. Filloux, B. J. Raphael and W. G. Fairbrother (2011). "Using positional distribution to identify splicing elements and predict pre-mRNA processing defects in human genes." Proc Natl Acad Sci U S A **108**(27): 11093-11098.

Lyon, R. C., V. Mezzano, A. T. Wright, E. Pfeiffer, J. Chuang, K. Banares, A. Castaneda, K. Ouyang, L. Cui, R. Contu, Y. Gu, S. M. Evans, J. H. Omens, K. L. Peterson, A. D. McCulloch and F. Sheikh (2014). "Connexin defects underlie arrhythmogenic right ventricular cardiomyopathy in a novel mouse model." Hum Mol Genet **23**(5): 1134-1150.

Lyon, R. C., F. Zanella, J. H. Omens and F. Sheikh (2015). "Mechanotransduction in cardiac hypertrophy and failure." Circ Res **116**(8): 1462-1476.

Ma, X., C. Chen, J. Veevers, X. Zhou, R. S. Ross, W. Feng and J. Chen (2017). "CRISPR/Cas9-mediated gene manipulation to create single-amino-acid-substituted and floxed mice with a cloning-free method." Sci Rep **7**: 42244.

Manso, A. M., S. I. Hashem, B. C. Nelson, E. Gault, A. Soto-Hermida, E. Villarruel, M. Brambatti, J. Bogomolovas, P. J. Bushway, C. Chen, P. Battiprolu, A. Keravala, J. D. Schwartz, G. Shah, Y. Gu, N. D. Dalton, K. Hammond, K. Peterson, P. Saftig and E. D. Adler (2020). "Systemic AAV9.LAMP2B injection reverses metabolic and physiologic multiorgan dysfunction in a murine model of Danon disease." Sci Transl Med **12**(535).

Marcus, F. I., S. Edson and J. A. Towbin (2013). "Genetics of arrhythmogenic right ventricular cardiomyopathy: a practical guide for physicians." J Am Coll Cardiol **61**(19): 1945-1948.

Marcus, F. I., W. J. McKenna, D. Sherrill, C. Basso, B. Bauce, D. A. Bluemke, H. Calkins, D. Corrado, M. G. Cox, J. P. Daubert, G. Fontaine, K. Gear, R. Hauer, A. Nava, M. H. Picard, N. Protonotarios, J. E. Saffitz, D. M. Sanborn, J. S. Steinberg, H. Tandri, G. Thiene, J. A. Towbin, A. Tsatsopoulou, T. Wichter and W. Zareba (2010). "Diagnosis of arrhythmogenic right ventricular cardiomyopathy/dysplasia: proposed modification of the task force criteria." Circulation **121**(13): 1533-1541.

Mattesi, G., A. Zorzi, D. Corrado and A. Cipriani (2020). "Natural History of Arrhythmogenic Cardiomyopathy." J Clin Med **9**(3).

McKoy, G., N. Protonotarios, A. Crosby, A. Tsatsopoulou, A. Anastasakis, A. Coonar, M. Norman, C. Baboonian, S. Jeffery and W. J. McKenna (2000). "Identification of a deletion in plakoglobin in arrhythmogenic right ventricular cardiomyopathy with palmoplantar keratoderma and woolly hair (Naxos disease)." Lancet **355**(9221): 2119-2124.

Mendell, J. R., S. Al-Zaidy, R. Shell, W. D. Arnold, L. R. Rodino-Klapac, T. W. Prior, L. Lowes, L. Alfano, K. Berry, K. Church, J. T. Kissel, S. Nagendran, J. L'Italien, D. M. Sproule, C. Wells, J. A. Cardenas, M. D. Heitzer, A. Kaspar, S. Corcoran, L. Braun, S. Likhite, C. Miranda, K. Meyer, K. D. Foust, A. H. M. Burghes and B. K. Kaspar (2017). "Single-Dose Gene-Replacement Therapy for Spinal Muscular Atrophy." N Engl J Med **377**(18): 1713-1722.

Mendell, J. R., S. A. Al-Zaidy, L. R. Rodino-Klapac, K. Goodspeed, S. J. Gray, C. N. Kay, S. L. Boye, S. E. Boye, L. A. George, S. Salabarria, M. Corti, B. J. Byrne and J. P. Tremblay (2021). "Current Clinical Applications of In Vivo Gene Therapy with AAVs." Mol Ther **29**(2): 464-488.

Milic, J., Y. Tian and J. Bernhagen (2019). "Role of the COP9 Signalosome (CSN) in Cardiovascular Diseases." Biomolecules **9**(6).

Mizusawa, Y. and A. A. Wilde (2012). "Brugada syndrome." Circ Arrhythm Electrophysiol **5**(3): 606-616.

Moncayo-Arlandi, J., E. Guasch, M. Sanz-de la Garza, M. Casado, N. A. Garcia, L. Mont, M. Sitges, R. Knoll, B. Buyandelger, O. Campuzano, A. Diez-Juan and R. Brugada (2016). "Molecular disturbance underlies to arrhythmogenic cardiomyopathy induced by transgene content, age and exercise in a truncated PKP2 mouse model." Hum Mol Genet **25**(17): 3676-3688.

Pachon, R. E., B. A. Scharf, D. E. Vatner and S. F. Vatner (2015). "Best anesthetics for assessing left ventricular systolic function by echocardiography in mice." Am J Physiol Heart Circ Physiol **308**(12): H1525-1529.

Padron-Barthe, L., M. Villalba-Orero, J. M. Gomez-Salinero, F. Dominguez, M. Roman, J. Larrasa-Alonso, P. Ortiz-Sanchez, F. Martinez, M. Lopez-Olaneta, E. Bonzon-Kulichenko, J. Vazquez, C. Marti-Gomez, D. J. Santiago, B. Prados, G. Giovinazzo, M. V. Gomez-Gaviro, S. Priori, P. Garcia-Pavia and E. Lara-Pezzi (2019). "Severe Cardiac Dysfunction and Death Caused by Arrhythmogenic Right Ventricular Cardiomyopathy Type 5 Are Improved by Inhibition of Glycogen Synthase Kinase-3beta." Circulation **140**(14): 1188-1204.

Pan, Z., A. Ebert and P. Liang (2021). "Human-induced pluripotent stem cells as models for rare cardiovascular diseases: from evidence-based medicine to precision medicine." Pflugers Arch **473**(7): 1151-1165.

Rampazzo, A., M. Calore, J. van Hengel and F. van Roy (2014). "Intercalated discs and arrhythmogenic cardiomyopathy." Circ Cardiovasc Genet **7**(6): 930-940.

Rapti, K., V. Louis-Jeune, E. Kohlbrenner, K. Ishikawa, D. Ladage, S. Zolotukhin, R. J. Hajjar and T. Weber (2012). "Neutralizing antibodies against AAV serotypes 1, 2, 6, and 9 in sera of commonly used animal models." Mol Ther **20**(1): 73-83.

Rasmussen, T. B., P. H. Nissen, J. Palmfeldt, K. Gehmlich, S. Dalager, U. B. Jensen, W. Y. Kim, L. Heickendorff, H. Molgaard, H. K. Jensen, U. T. Baandrup, P. Bross and J. Mogensen (2014). "Truncating plakophilin-2 mutations in arrhythmogenic cardiomyopathy are associated with protein haploinsufficiency in both myocardium and epidermis." Circ Cardiovasc Genet **7**(3): 230-240.

Sen-Chowdhry, S., R. D. Morgan, J. C. Chambers and W. J. McKenna (2010). "Arrhythmogenic cardiomyopathy: etiology, diagnosis, and treatment." Annu Rev Med **61**: 233-253.

Sheikh, F., R. S. Ross and J. Chen (2009). "Cell-cell connection to cardiac disease." Trends Cardiovasc Med **19**(6): 182-190.

Srivastava, A. (2016). "In vivo tissue-tropism of adeno-associated viral vectors." Curr Opin Virol **21**: 75-80.

Svensson, A., M. Astrom-Aneq, K. F. Widlund, C. Fluur, A. Green, M. Rehnberg and C. Gunnarsson (2016). "Arrhythmogenic Right Ventricular Cardiomyopathy - 4 Swedish families with an associated PKP2 c.2146-1G>C variant." Am J Cardiovasc Dis **6**(2): 55-65.

Syrris, P., D. Ward, A. Asimaki, S. Sen-Chowdhry, H. Y. Ebrahim, A. Evans, N. Hitomi, M. Norman, A. Pantazis, A. L. Shaw, P. M. Elliott and W. J. McKenna (2006). "Clinical expression of plakophilin-2 mutations in familial arrhythmogenic right ventricular cardiomyopathy." Circulation **113**(3): 356-364.

Te Riele, A. S., C. A. James, B. Philips, N. Rastegar, A. Bhonsale, J. A. Groeneweg, B. Murray, C. Tichnell, D. P. Judge, J. F. Van Der Heijden, M. J. Cramer, B. K. Velthuis, D. A. Bluemke, S. L. Zimmerman, I. R. Kamel, R. N. Hauer, H. Calkins and H. Tandri (2013). "Mutation-positive arrhythmogenic right ventricular dysplasia/cardiomyopathy: the triangle of dysplasia displaced." J Cardiovasc Electrophysiol **24**(12): 1311-1320.

Thiene, G., D. Corrado and C. Basso (2007). "Arrhythmogenic right ventricular cardiomyopathy/dysplasia." Orphanet J Rare Dis **2**: 45.

van den Hoogenhof, M. M., Y. M. Pinto and E. E. Creemers (2016). "RNA Splicing: Regulation and Dysregulation in the Heart." Circ Res **118**(3): 454-468.

van der Zwaag, P. A., I. A. van Rijsingen, A. Asimaki, J. D. Jongbloed, D. J. van Veldhuisen, A. C. Wiesfeld, M. G. Cox, L. T. van Lochem, R. A. de Boer, R. M. Hofstra, I. Christiaans, K. Y. van Spaendonck-Zwarts, R. H. Lekanne dit Deprez, D. P. Judge, H. Calkins, A. J. Suurmeijer, R. N. Hauer, J. E. Saffitz, A. A. Wilde, M. P. van den Berg and J. P. van Tintelen (2012). "Phospholamban R14del mutation in patients diagnosed with dilated cardiomyopathy or arrhythmogenic right ventricular cardiomyopathy: evidence supporting the concept of arrhythmogenic cardiomyopathy." Eur J Heart Fail **14**(11): 1199-1207.

van Hengel, J., M. Calore, B. Bauce, E. Dazzo, E. Mazzotti, M. De Bortoli, A. Lorenzon, I. E. Li Mura, G. Beffagna, I. Rigato, M. Vleeschouwers, K. Tyberghein, P. Hulpiau, E. van Hamme, T. Zaglia, D. Corrado, C. Basso, G. Thiene, L. Daliento, A. Nava, F. van Roy and A. Rampazzo (2013). "Mutations in the area composita protein alphaT-catenin are associated with arrhythmogenic right ventricular cardiomyopathy." Eur Heart J **34**(3): 201-210.

Wang, S., Y. Li, Y. Xu, Q. Ma, Z. Lin, M. Schlame, V. J. Bezzerides, D. Strathdee and W. T. Pu (2020). "AAV Gene Therapy Prevents and Reverses Heart Failure in a Murine Knockout Model of Barth Syndrome." Circ Res **126**(8): 1024-1039.

Wang, W., C. A. James and H. Calkins (2019). "Diagnostic and therapeutic strategies for arrhythmogenic right ventricular dysplasia/cardiomyopathy patient." Europace **21**(1): 9-21.

Watanabe, T., H. Hanawa, T. Suzuki, S. Jiao, K. Yoshida, M. Ogura, Y. Ohno, Y. Hayashi, M. Ito, T. Kashimura, H. Obata, A. Sato, T. Ozawa, M. Kodama, H. Sakuraba and T. Minamino (2013). "A mutant mRNA expression in an endomyocardial biopsy sample obtained from a patient with a cardiac variant of Fabry disease caused by a novel acceptor splice site mutation in the invariant AG of intron 5 of the alpha-galactosidase A gene." Intern Med **52**(7): 777-780.

Wei, N., G. Serino and X. W. Deng (2008). "The COP9 signalosome: more than a protease." Trends Biochem Sci **33**(12): 592-600.

Zhang, Z., M. J. Stroud, J. Zhang, X. Fang, K. Ouyang, K. Kimura, Y. Mu, N. D. Dalton, Y. Gu, W. H. Bradford, K. L. Peterson, H. Cheng, X. Zhou and J. Chen (2015). "Normalization of Naxos plakoglobin levels restores cardiac function in mice." J Clin Invest **125**(4): 1708-1712.

Zhao, G., Y. Qiu, H. M. Zhang and D. Yang (2019). "Intercalated discs: cellular adhesion and signaling in heart health and diseases." Heart Fail Rev **24**(1): 115-132.

Zincarelli, C., S. Soltys, G. Rengo and J. E. Rabinowitz (2008). "Analysis of AAV serotypes 1-9 mediated gene expression and tropism in mice after systemic injection." Mol Ther **16**(6): 1073-1080.